MINERALOGY AND PETROLOGY OF TWO KIMBERLITES AT DUTOITSPAN MINE, KIMBERLEY

by

D.V. SNOWDEN, B.Sc. (Hons.)

Thesis presented for the degree of Master of Science in the Department of Geology, Rhodes University, Grahamstown.

January, 1981

DECLARATION

All work in this thesis is the original work of the author except where specific acknowledgement is made to the work of others.

SIGNED 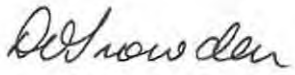

D.V. Snowden
Department of Geology,
Rhodes University
Grahamstown.

January, 1981.

ABSTRACT

The mineralogy and petrology of two kimberlites, a peripheral monticellite kimberlite, and its core of phlogopite kimberlite, from the West Auxiliary Pipe at Dutoitspan Mine are described. The mineralogy of the two kimberlites differs mainly in the presence of phlogopite macrocrysts, greater abundance of angular crustal inclusions, more heavy minerals and higher diamond grade in the phlogopite type.

Microprobe analyses of olivine, phlogopite, monticellite, oxide minerals and garnet are presented. Silicate compositions are comparable in both kimberlites and zoning of olivine grains is typically towards a rim of Fo_{89-90}, irrespective of whether cores are more Fe-rich or more Mg-rich. This is caused by re-equilibration after fluidised emplacement in the earth's crust of macrocryst-bearing kimberlite magma. Olivine aggregates were derived from sheared mantle lherzolite and single-crystal macrocrysts were formed at higher mantle levels from a kimberlitic crystal-mush magma. This was emplaced in the crust by rapid gas streaming. The post-fluidisation phenocrysts of olivine and phlogopite which formed then are in general more Fe-rich than macrocrysts. Re-equilibration of ilmenite results in the formation of complex perovskite and titanomagnetite mantles. Phlogopite macrocrysts are preserved in the monticellite contact rock where rapid quenching prevented their resorption and allowed separation of an immiscible carbonate melt, giving the abundant groundmass calcite. Atoll-textured spinels are found in the contact rock.

Major and minor trace-element analyses of whole rock samples are presented and discussed, bringing into account the problem of contamination by crustal inclusions. Whole rock chemistry supports derivation of the kimberlites as partial melts of mantle material in the presence of a lithophile-element-enriched fluid.

The monticellite contact rock is highly enriched in REE, Nb, and Sr due to rapid freezing of this perovskite-

enriched phase. The monticellite type is more enriched in lithophile elements than the phlogopite type, which supports derivation of the monticellite type by a small degree of partial melting, further melting reducing the relative concentrations of lithophile elements to give the phlogopite kimberlite chemistry.

ACKNOWLEDGEMENTS

I wish to express my sincere gratitude to Professor H.V. Eales for his guidance and support, and I am also most grateful to I.R. Reynolds and J.S. Marsh for their advice. Rhodes University is thanked for financial assistance. The de Beers Geology Department in Kimberley is thanked for access to the mine and help in sampling, and for their financial support. I am grateful to J.B. Hawthorne, S.R. Shee, E.M.W. Skinner and C.R. Clement for information, their suggestions and helpful discussions. The technical assistance of D.A. Gouws is greatly appreciated. Miss D. Carr is thanked for the typing and my husband for assistance with the diagrams and his unfailing support throughout.

CONTENTS

I. INTRODUCTION

1. The Scope of the Present Study

The Dutoitspan mine is one of the three major diamond-producing kimberlite pipes in the Kimberley area. These pipes represent deeply eroded roots of the original diatremes (Hawthorne, 1975) and the present-day surface intersects agglomerate/tuff kimberlite roughly oval in outcrop and approximately 500m x 150m in dimension. The pipes taper downwards and become irregular in morphology, grading into intrusive breccias at about 300m below surface (Hawthorne, 1975). Archaean Basement Complex gneisses and schists, Ventersdorp Supergroup lavas and quartzites and Karoo dolerite, Dwyka shales and Tillite are intersected by the kimberlites and inclusions of these rocks are found in the pipes.

The Dutoitspan pipe comprises several discrete units of different kimberlite types which have been intruded into each other within the confines of the pipe. Two units, the D2 and D5 kimberlites (Fig. 1), from the West Auxiliary pipe of the Dutoitspan Mine, form the subject of study in this thesis.

The objectives of this study are to:

a) Establish the detailed petrography of the D2 and D5 kimberlites.

b) Define criteria for recognition of the distinct types.

c) Describe the mineralogy and mineral chemistry of the phases olivine, phlogopite, monticellite, ilmenite,perovskite and garnet.

d) Use the mineral chemistry to formalise differences between the two kimberlite types and variations within types.

e) Compare the kimberlite mineralogy represented by the D2 and D5 kimberlites with that of other rock types with particular reference to olivine, phlogopite, monticellite, ilmenite and perovskite.

f) Determine the major - and trace - element content of the D2 and D5 kimberlites, taking the problem of contamination into account.

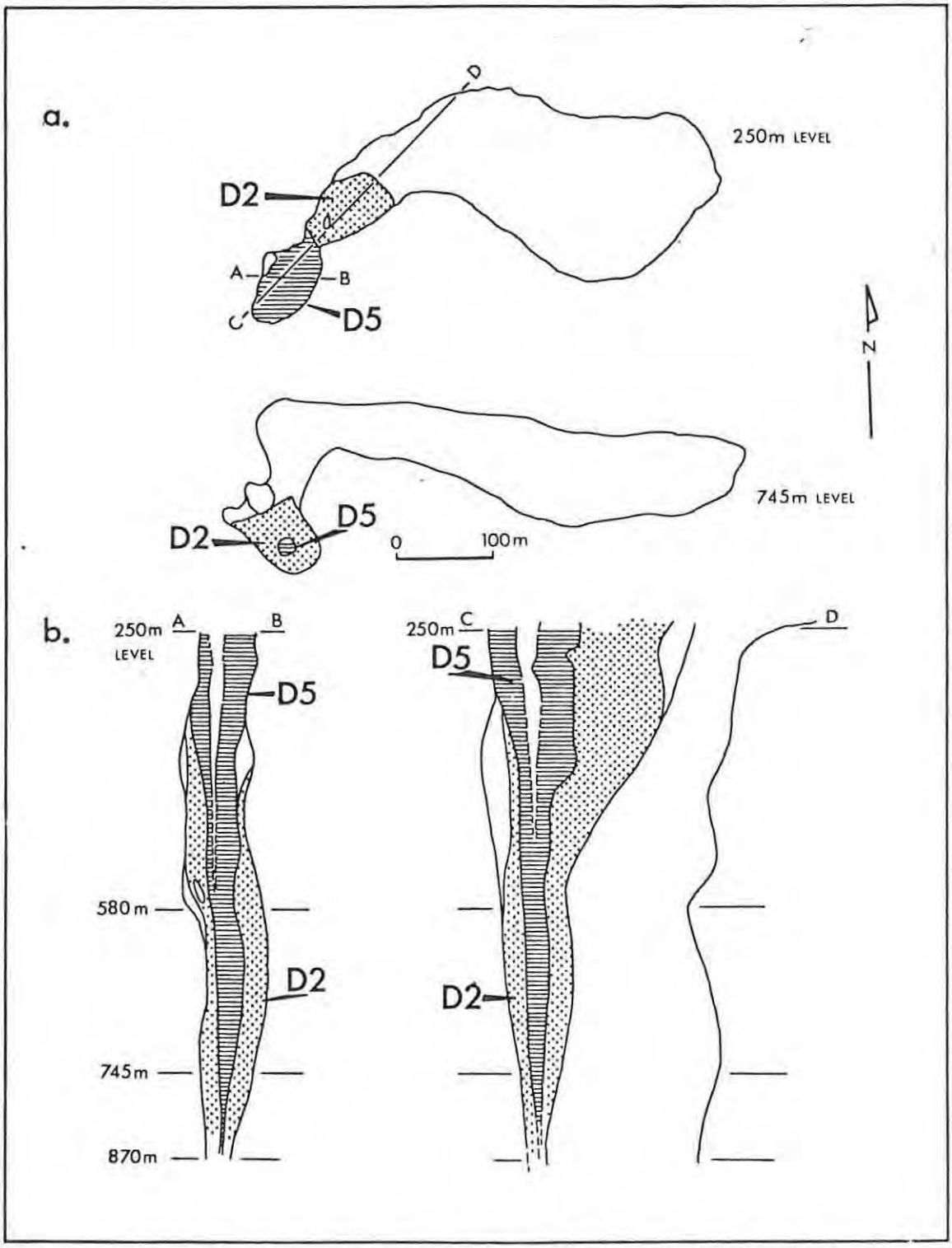

Fig. 1 Relationship between the D2 and D5 kimberlites in the West Auxiliary pipe of the Dutoitspan diatreme.

a) 250 m and 745 m level plans

b) Sections A-B and C-D marked in a).

g) Compare the whole-rock chemistry of these with data from other Kimberley area kimberlites.

h) Discuss observed trends in the light of available information on diamond and heavy mineral content.

2. Nomenclature

The textural-genetic classification of kimberlite rocks, proposed by Clement and Skinner (1979), contains three broad groups termed crater-facies, diatreme-facies and hypabyssal-facies kimberlites which correspond to the major depth zones of kimberlite pipes, namely the crater, diatreme and root zones (Clement, 1979). The Dutoitspan 580m and 745m levels intersect the root zone of the pipe, and hypabyssal facies rocks were sampled at these levels. The rock types at these sites are, according to the classification of Clement and Skinner (1979), kimberlites (sensu stricto) or (if they contain upwards of 15 volume per cent of fragments of country rock larger than 4 mm in size) kimberlite breccias. The major textural subdivision of kimberlites and kimberlite breccias is into aphanitic and macroporphyritic varieties and, according to groundmass texture, a further subdivision into uniform or segregationary (globular textured) types is possible.

Skinner and Clement (1979) propose a mineralogical classification based on quantitative modal analysis whereby five basic subdivisions of kimberlite, depending on the volumetric abundance of diopside, monticellite, phlogopite, calcite and serpentine are made. They accept, for further subdivision, characterisation by accessories present to the extent of two thirds or more of the abundance of the dominant mineral. The proportion of olivine is not used in this classification mainly because of ambiguity in distinguishing between different generations of olivine. Some coarse (over 1 mm) rounded grains, particularly those that are strained, may be xenocrysts derived from disaggregated material carried up from elsewhere (Boyd and Clement, 1977), possibly from the mantle, whereas other coarse grains could, as argued by Mitchell (1973b) be phenocrysts. It is believed (for example by Boyd and Clement, 1977, Mitchell, 1973b and Clement et al., 1977) that the smaller (0,1 - 1 mm)

euhedral to subhedral olivine phenocrysts.

Clement et al. (1977) define kimberlite as a "volatile-rich, potassic, ultrabasic, igneous rock which has a distinctively inequigranular texture resulting from the presence of macrocrysts set in an essentially microporphyritic matrix". This definition is taken to imply that the magma, rather than the crystalline product, is volatile-rich. Volatiles are lost during de-gassing of the magma and the resultant kimberlite, though possibly exhibiting effects attributed to the original presence of volatiles, for example carbonatisation of inclusions and serpentinisation of olivine, no longer contains the original volatile content.

Kimberlite matrix consists of phenocrysts in a finer grained groundmass and represents essentially the composition of the kimberlite magma, whereas macrocrysts (defined by Clement et al.(1977) as "crystals visible to the unaided eye and significantly larger than the surrounding matrix") represent a suite of ferro-magnesian minerals, generally anhedral in shape and cryptogenic (that is material of unknown or hidden origin). In addition there may be present contaminatory xenolithic material, such as rounded inclusions of a variety of ultramafic rocks (nodules) including mantle-derived peridotites, eclogites and pyroxenites as well as crustal xenoliths and xenocrysts.

Using the terminology outlined above, the coarse (over 1mm) rounded olivine grains will be called macrocrysts and the smaller euhedral to subhedral grains phenocrysts. Similarly, phlogopite will be qualified as macrocrystic, phenocrystic or groundmass material. The use of the terms macro- or (for larger grains) megacryst avoids a genetic implication and is recommended by Hawthorne (personal communication).

Alteration effects may be deuteric (partial or complete pseudomorphous replacement of original minerals) or caused by metasomatic or weathering processes giving rise to clay,

chlorite or carbonate minerals (Skinner and Clement, 1979). Highly weathered kimberlites may be named according to the dominant alteration process, for example carbonatised kimberlite. Skinner and Clement (1979) have not encountered any classification problems with respect to deuteric alteration, which is a direct consequence of consolidation of the magma.

3. Approaches to kimberlite research

Since the discovery of diamondiferous kimberlite at Jagersfontein in 1870, much attention has been focussed on the description, classification and thoughts on the genesis of kimberlite and diamonds (in particular the works of Wagner, 1914 and Williams, 1932). The Russian deposits of Yakutia kimberlite province were described by Bobrievich et al. (1957, 1959). Since then the interest in kimberlite has shown several specific trends as outlined below.

a) The Study of kimberlite nodules as indicators of the nature of the upper mantle environment

Kimberlite has been exploited extensively in the search for an understanding of the composition, mineralogy and processes occurring within the upper mantle (for example Boyd and Nixon, 1978; Mitchell, 1977b; Basu and MacGregor, proof print; Smith and Zientek, 1979; Boyd, 1975; Nixon and Boyd, 1973a and b and 1975; Smith and Dawson, 1975; Dawson and Smith, 1977; O'Hara et al., 1975 and Meyer, 1977). As kimberlite has been emplaced by rapid gas streaming at relatively low temperatures, which minimises the risk of modifying transported xenoliths, ostensibly it affords a unique opportunity to study little altered materials from the upper mantle (O'Hara et al., 1975). According to O'Hara et al. (1975), who support a residual hypothesis for the origin of kimberlite (fractionation of bimineralic eclogite from an initial picritic partial melt of garnet peridotite, thus providing the alkaline residual liquids required), representative xenoliths of the source mantle (garnet-lherzolite), residual mantle (garnet-harzburgite and harzburgite), primary magma (ultrabasic) and high-pressure cumulates (eclogite) are all present in kimberlite. The phlogopite xenocrysts in kimberlite tend to support

an "incipient melting" hypothesis (Dawson, 1971).

Minor trace element distribution in the upper mantle has been estimated using high-precision microprobe techniques (Bishop et al., 1978). The mineralogy of various types of nodules is described, for example, by Nixon and Boyd (1973), working on Northern Lesothoan ultrabasic nodules, by Mitchell (1977b and 1978) on ultramafic xenoliths and garnet lherzolite nodules, by Danchin (1979) and Boyd and Nixon (1978) on garnet lherzolite and harzburgite xenoliths, by Smith and Zientek (1979) on eclogites and by Dawson and Smith (1977) on MARID (mica-amphibole-rutile-ilmenite-diopside) xenoliths. Such studies on nodules have reflected three main mantle processes, listed by Nixon and Boyd (1978) as chemical depletion (accumulation of "incompatible elements"), structural changes (mantle deformation) and temperature changes (configuration of the palaeogeotherm). Boyd (1973) presents a kinked pyroxene geotherm showing temperature/depth relationships for sheared and coarse lherzolite as well as for diopside discrete nodules. Inflections are interpreted by Boyd (1976) as probably due to slow upwelling of partially melted mantle.

An important objective of the study of nodules is the determination of the source of diamonds, by matching up the mineralogy of diamond inclusions with that of nodules, for example the harzburgite-dunite paragenesis described by Pokhilenko et al. (1979). Peridotitic inclusions predominate over eclogitic inclusions by about 3:1 in southern African diamonds (Gurney et al., 1979). Cohen and Rosenfeld (1979) have found that some diamond, containing garnet of the kind found in eclogite, originates within the mantle (145-300km beneath surface).

Chromite spinels from ultramafic xenoliths have a wide range in chemistry and, because of the sensitivity of their composition to factors such as P,T and fO_2, they are considered by Basu and MacGregor (1974) as particularly important minerals in examining the environmental conditions of

the upper mantle.

b) The study of the petrogenesis of kimberlite

Kimberlites have unique geochemical and petrologic features, for example the common occurrence of Mg-rich olivine and characteristically high abundances of both compatible and incompatible trace elements (Frey et al., 1977). For any given mantle source, workers have tested various petrogenetic models to account for the petrologic features observed. Frey et al. (1977) studied major and trace element data for kimberlitic and associated rock suites (melilites, carbonatites and peridotites). Fesq et al. (1975) consider that the REE enrichment and fractionation patterns exhibited by South African kimberlites imply a close genetic relationship with carbonatites but Mitchell (1979a) produces strong arguments against the hypothesis of such a relationship. He draws a distinction between carbonatite and the end-product of kimberlite differentiation, namely calcite-kimberlite, and suggests that the so called "central complex kimberlites" found in alkaline complexes are in fact not true kimberlites but should be termed lamprophyres.

Mitchell and Brunfelt (1975) attribute high REE contents to the presence of apatite, perovskite and carbonate, and Eu anomalies to perovskite or mica. According to Kable et al. (1975), the high concentration of incompatible elements in kimberlite can only in part be accounted for by phlogopite in the source rock, minor phases such as apatite and rutile possibly being of significance in determining inter-element relationships.

Experimental phase relationships presented by Wyllie (1979) indicate that the "variation of temperature and oxygen fugacity as a function of depth, place, and time is critical for understanding kimberlite generation". Carbonate involvement appears a pre-requisite if low-SiO_2 magmas are to transport diamond to surface and there precipitate carbonate (Wyllie, 1979). A recent study by Rogers (1979) of trace elements in South African kimberlites and ultrabasic xenoliths,

led him to conclude that REE abundance patterns reflect a real feature of the mantle and that fundamentally different processes operate during kimberlite, as opposed to basalt, petrogenesis. Local differences in composition are explained in terms of mantle heterogeneity - varying contributions of ilmenite-bearing mantle rocks and deep seated K-rich fluids are thought by Gurney and Ebrahim (1973) to be responsible for the higher TiO_2 and lower K_2O content of Lesothoan kimberlites compared with the average values for South African kimberlites.

c) The study of the mineralogy of kimberlite

In 1977 Boyd and Clement recognised the need for more detailed study of kimberlite minerals to obtain a better understanding of the petrographic nature of kimberlites and their relationship (if any) with mantle xenoliths. Much of the most recent work published on kimberlites has involved the detailed mineralogy of the common phases found as macrocrysts or as matrix material. The Proceedings of the second International Kimberlite Conference published in 1979, together with the abstracts from the second Kimberlite Symposium held in Cambridge in 1979 contain descriptive mineralogy and mineral chemistry for oxides (spinels, ilmenite, rutile and perovskite) and silicates (olivine, phlogopite, garnets and pyroxenes), with the greatest emphasis on oxide mineral chemistry.

Haggerty (1973) found that the reaction mantles surrounding picroilmenites are sensitive markers of changes in redox potential and can thus be usefully employed to determine the environmental conditions that prevail during groundmass crystallisation of kimberlites. This has been followed up by many workers including Wyatt (1979), Boyd and Pasteris (1977), Boctor and Meyer (1979), Elthon and Ridley (1979) and Shee (1979a and b). Great interest has also been shown in spinels (Pasteris, 1979; McMahon et al., 1979; Mitchell and Clarke, 1976; Haggerty, 1975 and 1976; Shee, 1979a and b). According to Haggerty (1976) spinels from kimberlites show extremely complex zonal trends (pp. Hg-142) which reflect the interaction of early formed crystals with liquid as the

temperature decreases and/or as fO_2 changes.

Compositional zoning has been described in olivine, the most abundant mineral in the modes of most kimberlites (Dawson and Hawthorne, 1973; Emeleus and Andrews, 1975; Boyd and Clement, 1977 and Moore and Erlank, in press). Detailed microprobe studies by Boyd and Clement (1977) led them to interpret olivine zoning from a De Beers pipe kimberlite as marginal zoning of metasomatic origin, rather than growth zoning. The distribution of minor elements (Ca, Mn, Ni, Na, K, P and Ti) in olivine has been studied in depth by workers such as Simkin and Smith (1970), Stormer (1973), Stephenson (1974), Arndt (1977), Finnerty and Boyd (1977) Hart and Davis (1978), Ferguson (1978) and Watson (1979), but Bishop et al. (1978) are among the few who have investigated minor elements in olivine specifically from kimberlite (and they used peridotite xenoliths, not kimberlite matrix).

Experimental work on phlogopites has included tests on melting (Modreski, 1977), compressibility (Hazen and Finger, 1978) and phase relations (Forbes and Flower, 1974). Kimberlite phlogopites have featured in K-Ar dating of pipes (Allsopp and Kramers, 1977 and Allsopp et al., 1979) and their mineral chemistry and mineralogy have been studied by Clarke and Mitchell (1975), Smith et al. (1978 and 1979), Skinner and Scott (1979) and Mitchell (1979). Interest has also been shown in the composition of phlogopite from the so-called MARID xenoliths (Dawson and Smith, 1977).

Dawson and Stephens (1975) and Stephens and Dawson (1976) have applied statistical cluster analysis to the compositions of garnets and pyroxenes respectively, in order to classify them and compare kimberlite constituents with those of their associated xenoliths. Minor elements (Na, K, Ti and P) in garnets and pyroxenes have been analysed by Bishop et al. (1978) and Reid et al. (1976), but again from xenolithic material in both cases.

The common groundmass mineral, monticellite, has been

analysed by Clement et al. (1975) but has otherwise been neglected beyond the step of identification.

This study, as sketched by the stated objectives, is focussed on the mineralogy and mineral chemistry of the silicates olivine, monticellite, phlogopite and garnet, and the oxides ilmenite and perovskite. These are described within the context of petrographic and petrochemical differences between the two kimberlites (D2 and D5), and in comparison with other rock types, leading in turn to a consideration of possible environmental conditions at the time of intrusion and the probable factors influencing diamond grade. It is thus designed to help achieve an understanding of kimberlite magma by researching aspects which have, except for studies by a few 'matrix' workers, received relatively little attention compared with the vast amount learnt since kimberlite was first discovered.

II. PROCEDURES

1. Sampling

The two kimberlites investigated from the Dutoitspan Mine form the core (D5) and periphery (D2) of the West Auxilliary pipe intrusive into Archaean granites and gneisses at both the 580-metre and 745-metre levels from which samples were taken. Approximately 2 kg of fresh material was taken at positions 2 metres apart along the conveyance level at 580 metres depth (580/1 - 580/28 inclusive, Fig. 2a). A three-metre zone incorporating a 1-metre wide 'flow zone', or area showing vertical fine grained bands devoid of inclusions, thought to represent the contact between the D2 and D5 units was sampled at about 30 cm intervals. The 745 metre level was sampled at 4-metre intervals (740/1 - 740/15 inclusive) along the main development drive and at closer intervals along a crosscut (740/16 - 740/20). The wallrock contact was also sampled (740/C). These sites are marked on Fig. 2b.

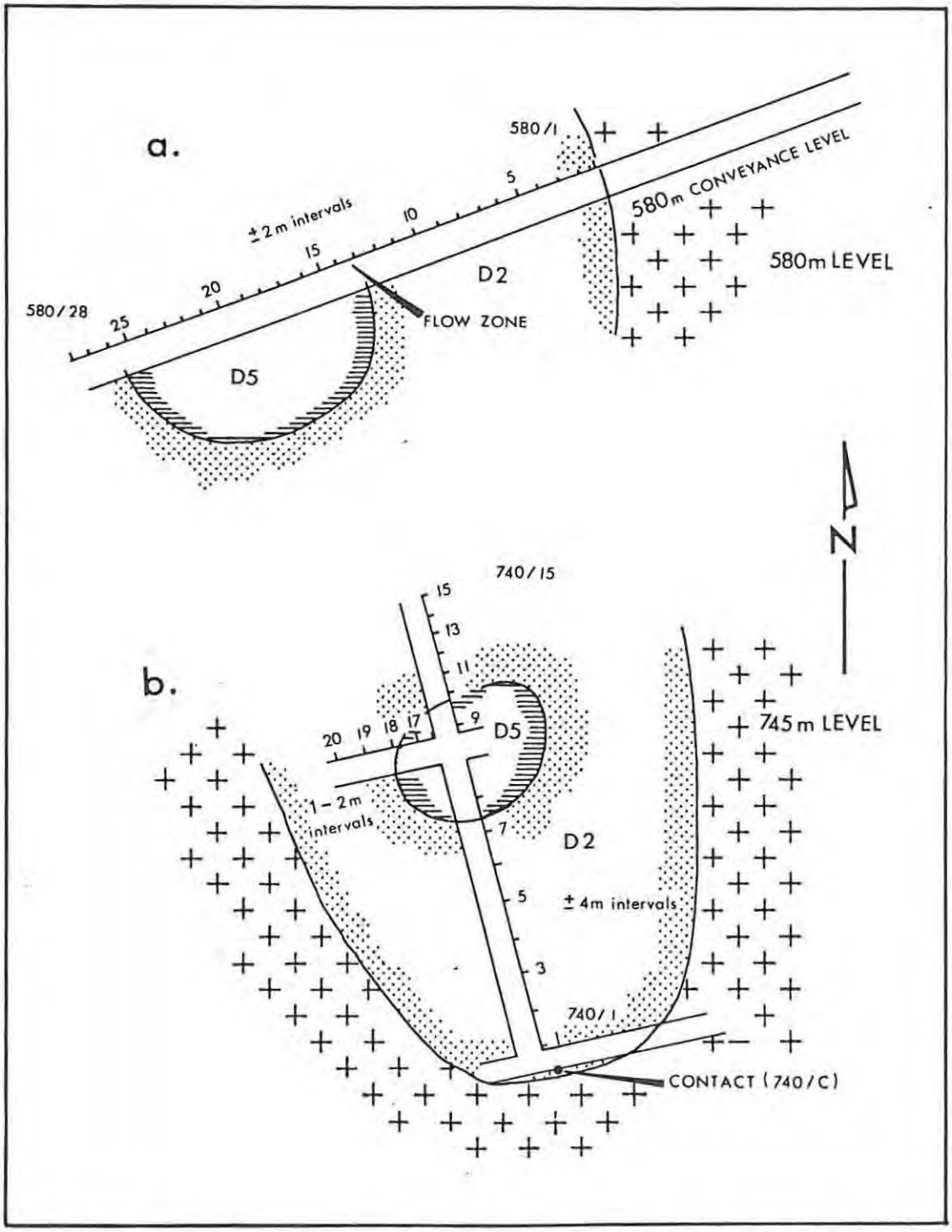

Fig. 2 Diagram illustrating the sample sites at the

a) 580 m level

b) 745 m level

2. Polished Sections

All section cutting was done in paraffin to avoid undue serpentinisation of the kimberlite, as recommended by Skinner (personal communication). A full suite of thin sections was prepared using a special paraffin-lubricated grinding machine (constructed by Mr. D. Cawood). These sections were examined briefly and representative samples containing fresh olivine or any other particular features requiring detailed examination were chosen for the preparation of doubly polished probe sections, using the following method:

a) A thick section (about 1 mm) is mounted in Canada balsam on a slide sized to fit the microprobe holder.

b) The section is cleaned ultrasonically in paraffin.

c) The section is polished on an automatic polishing machine using Struers diamond aerosol spray and machine oil for lubrication.

d) Polishing procedure is as follows:

Grade (microns)	Disc	Weight	r.p.m.	oil	time (minutes)
15	petrodisc	no	100	generous amount	20
6	petrodisc	yes	100	sparing amount	60
1	paper	no	300	few drops	10

e) Methanol is used to clean the slides at intervals during the polishing. Thorough ultrasonic cleaning in paraffin, not only of polished sections but also all the slide holders, rubber feet and plastic fittings, is essential when changing to a finer grade disc.

f) The slide is heated to melt the Canada balsam and the section is remounted, polished side down, in epoxy resin.

g) The section is ground and polished to the thickness of normal thin sections.

The De Beers polishing laboratory is thanked for undertaking the polishing of 20 of the 35 sections prepared.

3. Preparation of mounts for X-ray diffraction

The following method was employed in the preparation

of powder diffraction mounts:

a) The crystal to be analysed is crushed between two clean glass slides and ground as finely as possible.

b) A small drop of rubber solution is applied to one side of the powder and worked into the powder using a pin. The mixture is rolled into a ball between the two slides.

c) Straight human hair cut into 1 cm lengths is secured by means of plasticine in the cylindrical brass holders. The end of the hair is dipped in benzene and touched to the powder ball which immediately adheres to it.

4. Electron Microprobe Analysis

Analyses were performed using Rhodes University's Microscan V Electron Probe Microanalyser. Polished sections were thoroughly cleaned using petroleum ether and then carbon-coated by arcing under vacuum. A maximum thickness of 25 nM was deposited.

Standards were run at approximately 2-hour intervals or after about every 5 grain analyses (4 elements). The specimen current (30 nA) was monitored after each grain analysis by checking the Faraday cage. The accelerating potential was 20 kV and flow counters were used throughout.

The operating system employs an automatic display of all count rates on a video display screen, an editing sub-program, and uses a program written by Prof. H.V. Eales (HVE MARK 3.) This corrects for dead-time counting losses and then corrects nominal concentrations according to the Bence-Albee correction routine (Bence and Albee, 1968), using the alpha factors of Albee and Ray (1970). An oxygen corrected concentration is automatically presented in case it is relevant (as for example in phlogopite analyses).

Analytical conditions are presented in Appendix 1. Mineral formulae were computed for olivine and calculated by hand for phlogopite and ilmenite.

5. Mineral Formulae

a) Calculation of olivine formula

The oxide data for olivine was processed using a program 'FORM' (see Appendix 2) written in BASIC to calculate the mineral formula on a basis of 4 oxygens according to the method of Deer et al. (1967). An example of the output from the program 'FORM' is given in the Appendix.

b) Calculation of phlogopite formula

The idealised phlogopite formula, according to Deer et al. (1967), is

$K_2(Mg,Fe^{+2})_6(Si_6Al_2O_{20})(OH,F)_4$ - (trioctahedral layered structure)

Common replacements in octahedral sites include Fe^{+3}, Ti, Al and Li. The interlayer K cations may be substituted by Na. In Mg - rich phlogopites, such as those analysed here, there may be insufficient Al to satisfy the tetrahedral site requirement (Si_6Al_2) and the methods of Deer et al. (1962) and Foster (1960) allow Ti, Fe^{+3} and Fe^{+2} to fill the tetrahedral sites to the required 8 cations per unit cell and the rest is allocated to the octahedral sites. Deer et al. (1962) use a basis of 24 O, OH and F anions in their method of calculation of the formula. This method was not used here as the fluorine composition of the phlogopites analysed was not determined. Foster (1950) uses a basis of 44 cationic + 44 anionic valencies per unit cell. Czamanske et al. (1977) report a method proposed by Ludington (1974) (in Czamanske et al., 1977) who recommends using a basis of 7 octahedral and tetrahedral cations per unit half cell, that is Σ (tetrahedral + octahedral sites) = 14, when a complete analysis is unavailable.

The method used in this thesis is a modification of the method used by Ludington. It assumes 8 tetrahedral and 6 octahedral cations, that is full site occupancy. Ti and Fe^{+3} are allocated to tetrahedral sites as necessary. The remaining Fe^{+2}, Al and Ti (as well as Cr and Ni if present) are allocated to octahedral sites. Tetrahedral-site Fe^{+3} is estimated as though it was Fe^{+2} and no adjustment is made for its actual

molecular weight. Very small amounts of Fe^{+3} are involved and the simplification in calculation is considered to outweigh any danger of misrepresentation.

The effect of adopting the method outlined is a tendency to increase the Si occupancy relative to the methods of Foster (1960) and Deer et al. (1962) but the number of cations is standardised and thus allows meaningful comparisons to be made between analyses.

Sample calculations of the same analysis by the method adopted, and by the method of Foster (1960), are presented below for comparison.

Calculation by the modification of Ludington's method

Oxide	Weight per cent	Molecular Proportion	Atomic Proportion of Cations	Number of Cations (At. Prop. x F)	
SiO_2	42,00	0,699	0,699	Si^{+4}: 6,018	8,00 (tetrahedral)
TiO_2	0,82	0,010	0,010	Ti^{+4}: 0,086	
Al_2O_3	11,19	0,110	0,220	Al^{+3}: 1,894	
FeO_{total}	4,28	0,060	0,060	Fe^{+2}: 0,517	6,00 (octahedral)
MgO	25,68	0,637	0,637	Mg^{+2}: 5,485	
			1,626	14,00	
Na_2O	0,12	0,002	0,004	Na^{+1}: 0,034	
K_2O	10,43	0,111	0,222	K^{+1}: 1,911	
				1,945	(interlayer)

F = 14/1,626 = 8,6101

Calculation by Foster's Method

Oxide	Weight per cent	A_i	B_i	C_i			
SiO_2	42,00	2,796	24,061	Si^{+4}: 6,015			
TiO_2	0,82	0,041	0,353	Ti^{+4}: 0,088			8,00 (tetra-
Al_2O_3	11,19	0,658	5,662	Al^{+3}: 1,887			hedral)
				Fe^{+3}:	0,010		
FeO_{total}	4,28	0,119	1,024	0,512			
				Fe^{+2}:	0,502		5,98 (octa-
MgO	25,68	1,274	10,963	Mg^{+2}: 5,482			hedral)
Na_2O	0,12	0,004	0,034	Na^{+1}: 0,034			
K_2O	10,43	0,221	1,902	K^{+1}: 1,902			
		5,113		1,936	(inner layer)		

A_i = Gram equivalent of cationic constituents
= Molecular weight divided by the number of cationic valencies per oxide

B_i = Cationic valencies per unit cell
= $A_i \div F$ where $F = \Sigma A_i \div 44 = 5,113 \div 44 = 0,1162$

C_i = Number of cations
= $B_i \div$ Valency

c) Recalculation of FeO to ($FeO + Fe_2O_3$) in ilmenite analyses

A modification of the method described by Carmichael (1967) is used here. The steps are outlined below:

a) Convert oxide weight percentages to moles.

b) Allocate the bivalent elements (MgO, CaO, MnO) plus sufficient FeO to ($TiO_2 + SiO_2$) in the proportion 1:1 to form ilmenite. The remaining FeO goes to form spinel and haematite.

c) Allocate ($Cr_2O_3 + Al_2O_3$) and the same amount of FeO to spinel - $FeO.(Cr,Al)_2O_3$.

d) Allocate the remaining FeO to Fe_2O_3, the number of moles of which is found by dividing by 2.

e) FeO per cent is found by adding up the number of

of moles of FeO in ilmenite and spinel and multiplying this by its molecular weight, 71,85.

f) Fe_2O_3 per cent is found by multiplying the number of moles by its molecular weight, 159,7.

g) The total is adjusted accordingly.

A worked calculation is presented below:

Sample 580/26 Grain 2	Oxide	Molecular Proportion	Ilmenite $2FeTiO_3$	Spinel $FeO.R_2O_3$	Haematite Fe_2O_3
TiO_2	53,10	0,6646	0,6646		
Cr_2O_3	2,51	0,0165		0,0165	
Al_2O_3	0,40	0,0039		0,0039	
FeO_{total}	32,03	0,4458	0,3718	0,0204	0,0536
MnO	11,57	0,2870	0,2870		
.	100,02				

FeO = (0,3718 + 0,0204) x 71,85 = 28,18%

Fe_2O_3 = (0,0536/2) x 159,7 = 4,28%

Adjusted total = 100,60%

The ilmenite cationic formula is calculated on the basis of 6 oxygens according to the method of Deer et al. (1967).

d) Recalculation of FeO to ($FeO+Fe_2O_3$) in spinel analyses

Some of the spinels exhibit somewhat unusual compositions, setting them apart from typical spinel-group minerals of basaltic rocks. A method was devised to recalculate FeO to $FeO+Fe_2O_3$ in those spinels which have ($FeO - 2TiO_2$) less than 2MgO (in moles). On calculation of TiO_2 as $2FeO.TiO_2$, the residual FeO is less than the MgO. Accordingly, MgO has to be assigned to the magnesioferrite molecule $MgO.Fe_2O_3$. Therefore a hypothetical ulvospinel molecule $2(Fe,Mg)O.TiO_2$ has been formed in conjunction with magnesioferrite. A worked example follows:

Sample 740/C, Grain 4

Oxide	Mol. Prop.	Usp.	Sp.	Mg-Chromite	Rem.	$MgO.Fe_2O_3$
TiO_2	19,77	0,2474	0,2474		-	
Al_2O_3	6,08	0,0596	0,0596		-	
FeO	57,44	0,7994	0,3351*		0,4643	
MgO	15,35	0,3808	0,1597	0,0596	0,0005	0,1610	0,1610
Cr_2O_3	0,08	0,0005			0,0005	-	
	98,72						
Fe_2O_3							0,1610

Sample 740/C, Grain 4 - continued

	Rem.	Mt.	Total	Wt. per cent
TiO_2	-			
Al_2O_3	-			
FeO	0,1423**	0,0474†	0,3825	27,48
MgO	-			
Cr_2O_3				
Fe_2O_3		0,0474	0,2084	33,28
				60,76
Recalculated total = 102,04%				

* (0,7994/(0,7994 + 0,3808)) x 0,2474 x 2 = 0,3351

** 0,4643 - 2(0,1610) = 0,1423

† 0,1423/3 = 0,0474

The spinel cationic formula is calculated on the basis of 32 oxygens:

$$(Al,Cr,Fe^3(FeTi))_{16}O_{24}(Fe,Mg)_8O_8$$

6. Modal Analyses

The mineral proportions of two samples from both kimberlite types were estimated by point counting. Each thin section was scanned in full on a 0,5 x 1,0 mm grid (about 750 counts) to obtain the proportions of macrocrysts and phenocrysts present. The matrix groundmass was then scanned on a 0,1 x 0,2 mm grid (about 1500 counts) to obtain the

proportions of the finer grained material.

The modal analyses (see Table 1) are presented in the following format:

Macrocrysts and phenocrysts - mineral per cent
Groundmass - mineral per cent

7. X-Ray Fluorescence Spectrometry

Major elements were determined on duplicate fusion discs, prepared after the method of Norrish and Hutton (1969). Trace elements were determined by the author on pressed powder briquettes prepared from inclusion-free material obtained as follows. Approximately 1,5 kg of material was passed through the jaw crusher or cut into 0,5 cm slices on a diamond saw. Inclusions were carefully removed, leaving about 0,75 - 1 kg for crushing in a swing mill.

Fe was determined as Fe_2O_3 and FeO was not separately determined. Standard computer programs for data reduction included corrections for position factors, dead-time, background, drift and spectral line interferences. Mass absorption coefficients were calculated by the Mo K_α Compton Peak. In Appendix 3 are given the values for the trace element standards, analytical conditions for major and trace element runs and the lower limits of detection and absolute error for trace elements.

8. Heavy Mineral Identification and Separation

A heavy mineral concentrate from a sample of monticellite kimberlite was examined to determine the phases present. Once the phases were identified a procedure for heavy mineral separation could be designed to assess quantitatively garnet, ilmenite, chrome diopside and spinel abudances in the monticellite and phlogopite kimberlite types.

A test sample was crushed in a roller mill and a 30 g portion of it was washed, de-slimed, dried, and sieved into several size fractions. Fractions -90+53μ, -125+90μ and

-250+125μ were panned on a superpanner, and the heavy-tail concentrate was demagnetised by removing magnetic material with a hand magnet. The residue was separated into several portions by means of an electomagnetic separator. The main heavy minerals in the concentrates included olivine, ilmenite, orange-red and mauve garnets, perovskite and bright green chrome diopside. Much of the ilmenite was sufficiently magnetic to be removed with a hand magnet. Appendix 4 gives the results of X-ray diffraction of samples of olivine and ilmenite.

The method of Neuerburg (1975), a procedure using hydrofluoric acid for quantitative mineral separations, was used to derive a heavy concentrate, devoid of olivine, from a 100 g slab sample. The great advantage of the acid dissolution method is that ilmenite and garnet grains are left intact and they can be sorted into meaningful size categories. Dissolution of a 100 g sample took about 4 weeks, and prohibitively large amounts of hydrofluoric acid were required. Furthermore it was estimated that about 2 kg samples were needed in order to be left with sufficient ilmenite and garnet grains for a statistically significant assessment of relative abundances between samples (Skinner, personal communication).

The outcome of the trial was the decision that the De Beers laboratory would process 5 kg samples from the D2 and D5 Dutoitspan kimberlites using acid dissolution and the residues would be examined and classified there. Their subsequent sampling unfortunately included only a few sites from the D2 and D5 kimberlites. This reduced the value of the data in terms of correlation with the detailed mineralogy of these specific units but the results, as presented in Appendix 5, allow a comparison to be made between the two kimberlite types.

III. PETROGRAPHY AND DESCRIPTIVE MINERALOGY OF KIMBERLITES

1. Monticellite - Kimberlite Type (D2)

Modal analyses for two samples of the D2 kimberlite are given in Table 1. Sample 740/11 is, according to the classification of Skinner and Clement (1979), a monticellite kimberlite and there are sufficient opaque minerals in this rock for its name to be modified to 'opaque-mineral rich monticellite kimberlite'. The modal proportions of sample 580/9 suggest classification as a monticellite-serpentine kimberlite. The D2 kimberlite is characterised by and distinguished from the D5 kimberlite by the presence of monticellite and, for the sake of brevity, will be referred to simply as monticellite kimberlite. The contact phase (740/C 740/1, 580/1 and 580/2) is substantially different in groundmass mineral proportions from those coarser grained samples that were modally analysed, being very rich in carbonate minerals and having only small patches of fine grained monticellite. As seen from the modal data in Table 1, the monticellite type is olivine- and serpentine-rich (primary and secondary). It contains little phlogopite and few crustal, ultramafic or other altered inclusions. Opaque minerals feature in abundance and include spinels, perovskite and ilmenite. Calcite (primary and secondary) and cebollite are other accessory minerals.

Olivine is colourless and devoid of inclusions, except for rare spinel octahedra. It occurs as rounded macrocrysts (1-5 mm) and smaller euhedral phenocrysts (0,5 mm), as shown in Plate 1, set in a fine-grained granular groundmass of monticellite (20-50μm) with phlogopite, spinel, perovskite, calcite and serpentine. Olivine is preserved in some samples, for example those modally analysed, but in others it is totally serpentinised. The phenocrysts may be rimmed by serpentine or altered at crystal terminations (as illustrated in Plate 1) or extensively altered (to serpentine, calcite/dolomite and, in the contact rock, to titanomagnetite (580/1) or phlogopite (740/1)). Macrocrysts tend to be well preserved,

TABLE 1

MODAL ANALYSES

Sample Number	580/9	740/11	580/26	580/21
Macrocrysts and Phenocrysts				
Olivine	34	50	23	20
Serpentine	50	27	33	32
Phlogopite	-	9	10	14
Inclusions*	16	9	28	34
Chrome diopside	-	-	5	-
Garnet	-	-	1	-
Calcite	-	4	-	-
Ilmenite	-	1	-	-
Groundmass				
Monticellite	21	45	-	-
Serpentine	37	14	25	30
Phlogopite	15	5	43	32
Perovskite	5	5	7	13
Opaques**	8	23	1	1
Apatite	-	trace	4	8
Cebollite	9+	-	16	15
Calcite	5+	7	-	-
Diopsidic pyroxene	-	-	4	-

* Includes crustal inclusions (altered, carbonatised), ultramafic rocks and other altered fragments.

** Spinels - primary and secondary.

\+ Secondary.

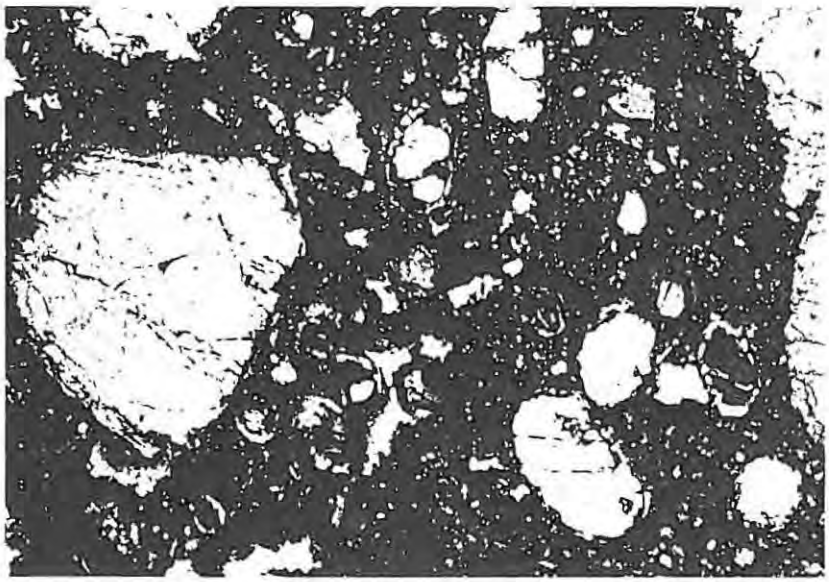

Plate 1 Monticellite kimberlite. Rounded olivine macrocryst (left) and euhedral to subhedral olivine phenocrysts (rimmed by serpentine) set in a dark fine grained matrix.
Width of field = 4 mm (crossed nicols).

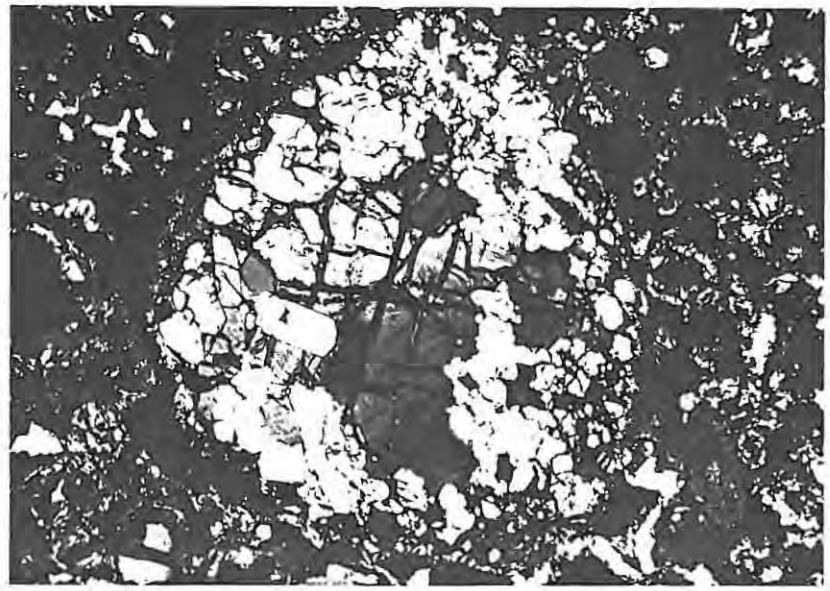

Plate 2 Monticellite kimberlite. Rounded granular aggregate of olivine. The central area (dark green) has strain shadows, and fine deformation lamellae are faintly visible at the top right. The outer area shows a recrystallisation texture, in parts fine grained granular (top and bottom right), and elsewhere good crystal form is obvious (left of centre).
Width of field = 1 mm (crossed nicols).

exhibiting rims of serpentine or alteration along cracks but seldom being totally pseudomorphed. Some olivine macrocrysts are granular aggregates of smaller grains (Plates 2 and 3), some are large strained grains or are centrally strained but, have recrystallised margins where individual grains are unstrained, as in Plate 2 and others are unstrained. Stages in recrystallisation are evident because of the presence of fine-grained, obviously granulated, margins which grade into areas where crystal growth has advanced and larger well formed euhedral grains are present (Plate 2). An unusual macrocryst exhibiting an aggregate of grains with sutured or cuspate margins (Plate 4) from the contact sample 740/1 is unlike any of the other macrocrysts observed. It has inclusions of small olivine(?) crystals .

. The phenocrysts show neither granular aggregate textures nor evidence of strain. They are mostly euhedral, this form being preserved despite serpentinisation (Plates 1 to 4) but others are subhedral or rounded. Plate 3 shows well preserved euhedral phenocrysts of olivine and subhedral grains which contrast with the rounded form of the central large granular aggregate of olivine. The broken phenocryst (bottom left) is indicative of brittle deformation.

Phlogopite is found as macrocrysts only in the contact phases (580/1). It occurs here as large rounded plates or semi-angular laths (2-5 mm). Matrix phenocrysts up to 1 mm across form a second population and smaller groundmass laths a third. Away from the contact there are no macrocrysts and only occasional phenocrysts are preserved, but fine grained pale yellow, faintly pleochroic laths (0,01-0,5 mm) are ubiquitous (Plates 5 and 6), forming 5 - 15% of the groundmass.

The contact-phase phlogopite macrocrysts are dark brown and pleochroic. Some have narrow bleached rims with reverse pleochroism. The macrocrysts are strained and some have deformation lamellae. One rounded macrocryst contains inclusions of strained phlogopite (out of optical continuity) with deformation lamellae orientated nearly parallel to

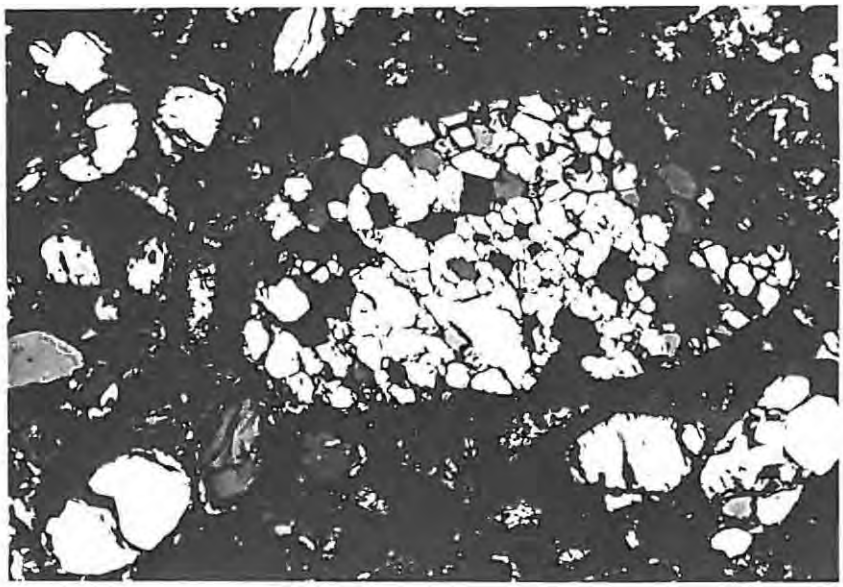

Plate 3 Monticellite kimberlite. Fully recrystallised, rounded aggregate of olivine in the contact phase, 740/1.
Width of field = 4 mm (crossed nicols).

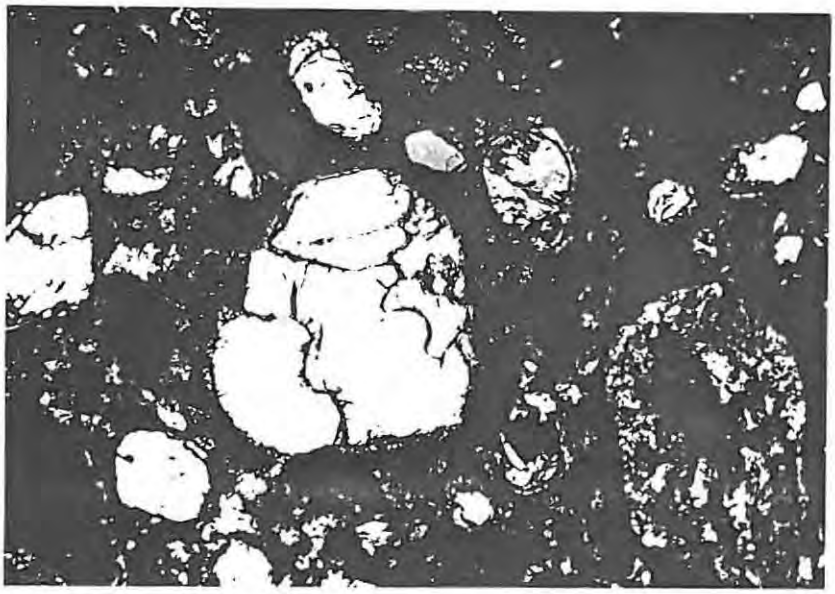

Plate 4 Monticellite kimberlite. Olivine macrocryst made up of grains with cuspate margins.
Width of field = 4 mm (crossed nicols).

Plate 5 Monticellite kimberlite matrix. Large euhedral perovskite grain (bottom), euhedral magnetite (black) and colourless monticellite, with good orthorhombic crystal form and high relief, set in serpentine (low relief). A plate of phlogopite extends from the top right of the perovskite grain parallel to and left of the two monticellite grains at top right.
Width of field = 0,3 mm (plane light).

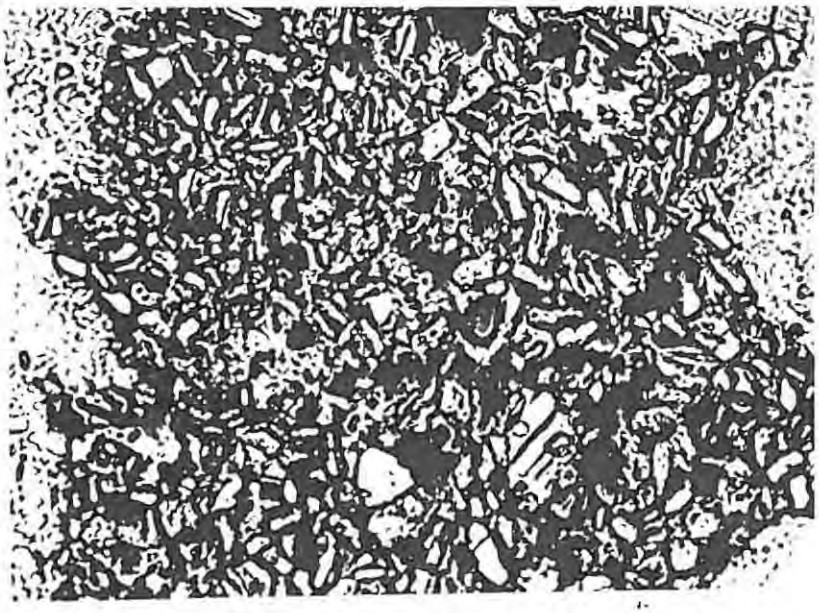

Plate 6 Monticellite kimberlite. Colourless, fine-grained monticellite with perovskite (larger subhedral to euhedral dark grey crystals), opaque spinels and phlogopite (elongate or stubby laths, e.g. grain A) set in serpentine.
Width of field = 0,44 mm (plane light)

deformation lamellae in the host grain. The phenocrysts are also dark brown and pleochroic. They are invariably altered around the rims to magnetite and some grains have bleached cores. Strained phenocrysts have been noted. The groundmass phlogopite is fine grained (0,1 - 0,5 mm) with pale yellow pleochroism. In sample 740/C and 740/1 there is an association of groundmass phlogopite with primary calcite which frequently encloses phlogopite laths (Plates 7 and 8). Secondary phlogopite and calcite/dolomite replacement of olivine phenocrysts is seen in 740/C.

Monticellite forms 21% and 45% of the groundmass in the samples modally analysed. It is strikingly characteristic as an important component among all the D2 samples except in the contact phase, where it is accessory and very fine grained (less than 0,01 mm).

Plate 6 shows the granular texture of the groundmass (monticellite, spinel, perovskite and phlogopite). Monticellite grains (0,2 - 0,5 mm) have high relief, low first order grey birefringence, and larger crystals (0,05 mm) exhibit perfect orthorhombic shape (Plate 5). The monticellite grains commonly appear to have a blemished texture under crossed nicols and this could be the expression of the process of alteration.

Plates 7 and 8 illustrate the texture of the contact phase where monticellite is absent and calcite dominates the groundmass. Plates 9 and 10 show the typical groundmass of the monticellite kimberlite.

Perovskite occurs as primary microphenocrysts in the groundmass. As shown in Plates 7 and 9, it forms discrete, euhedral to subhedral crystals with corroded margins, or rounded crystals (in the size range 0,01 - 0,05 mm). In polished thin sections perovskite is yellow to brown in plane polarised transmitted light and is either isotropic or shows anomalous grey birefringence between crossed nicols. Cross-hatched twinning is observed between crossed nicols in some

Plate 7 Monticellite kimberlite, contact phase (plane light). Olivine macrocrysts (colourless, high relief) are extensively serpentinised. Olivine phenocrysts are totally serpentinised, for example top right, where a serpentine pseudomorph is outlined by perovskite (yellow brown) and magnetite (black). The central macrocryst lacks this association.

Plate 8 As above (crossed nicols). Olivine (plus serpentine pseudomorphs) and laths of phlogopite are set in a groundmass rich in calcite (anomalous high interference colours), with perovskite and magnetite (opaques). Compare with Plate 10 (away from contact) where phlogopite phenocrysts are absent and there is no calcite in the groundmass. Note the phlogopite lath (blue) enclosed in calcite (top).

Width of field = 1 mm

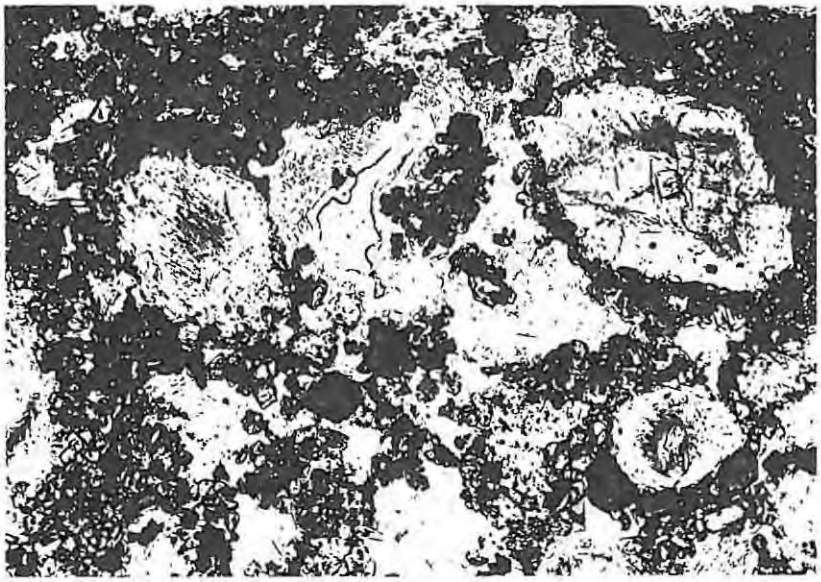

Plate 9 Monticellite kimberlite (plane light). Microphenocrysts of perovskite (yellow brown) and magnetite clustered around serpentinised phenocrysts of olivine. A central pool of primary serpentine encloses primary anhedral calcite (colourless, high relief). The groundmass contains abundant fine grained monticellite (high relief, euhedral), phlogopite, magnetite and perovskite.

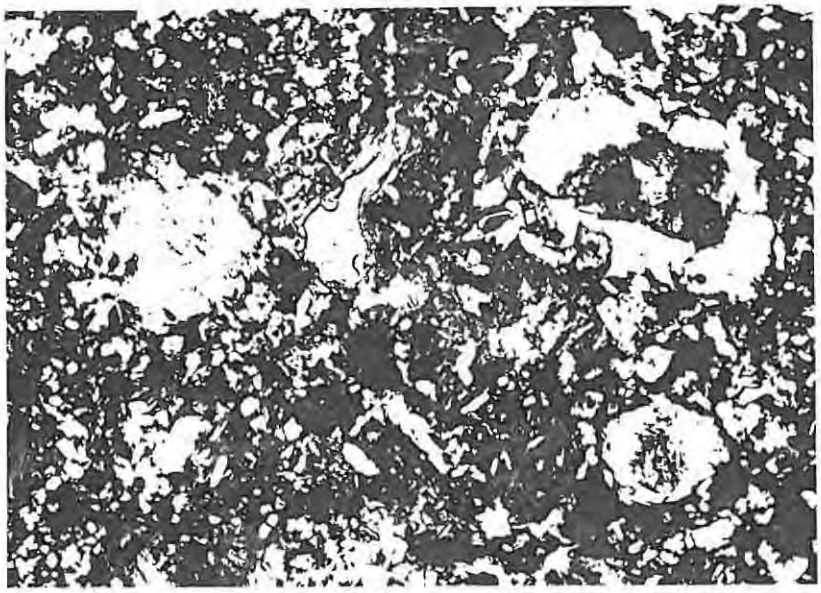

Plate 10 As above (crossed nicols). Monticellite (white), primary serpentine (brown), secondary serpentine (blue-grey), calcite (green), perovskite (dark brown) and magnetite.

Width of field = 1 mm.

of the larger grains. In reflected light this mineral is creamy white with a pinkish tinge and has higher refectivity than magnetite which appears grey by contrast. Between crossed nicols it is isotropic with grey internal reflections in reflected light.

In reflected light some of the perovskite grains are seen to be composite. A central rounded core of perovskite is often surrounded by a darker phase, possibly a spinel, which, in turn, is sometimes rimmed by a thin, bright overgrowth of perovskite. Some of the larger perovskite grains are rounded but have evidence of a break along one edge, the characteristic overgrowth being absent along this edge. This indicates that the grains were subjected to 'impact' after rounding, reaction (to give the spinel rim) and epitaxial overgrowth or reaction to give the perovskite mantle. Further evidence for brittle deformation is provided by the presence of rounded grains which have been shattered into several fragments remaining in situ.

Perovskite is closely associated with spinels which occur as small euhedral inclusions and as clusters of euhedral grains hugging the edges of perovskite grains. Alteration of perovskite to spinel is indicated where irregular areas of spinel (probably titanomagnetite) enclose anhedral grains of perovskite.

A second generation of perovskite occurs as an alteration or re-equilibration product rimming ilmenite macrocrysts. It forms a reaction intergrowth with ilmenite, which is in turn rimmed by an overgrowth of euhedral perovskite associated with titanomagnetite. A detailed description of the resulting texture is given with the description of ilmenite below.

Clusters of perovskite and spinels are commonly found around the edges of serpentinised olivine phenocrysts. The density of opaque grains encircling altered olivine appears to be a function of the degree of serpentinisation. Unaltered olivine phenocrysts lack this feature as do olivine

macrocrysts, whether altered or not. Plates 7 and 8 illustrate the texture in the contact phase 740/1. The finer size of perovskite grains at the contact is apparent by comparison of these plates with Plates 9 and 10.

Ilmenite occurs as anhedral macrocrysts, some composite, ranging in maximum intercept from 0,5 to 5 mm. Plate 11 shows part of an ilmenite macrocryst (from sample 580/6) which consists of an aggregate of 3 grains (with irregular grain margins) rimmed by a complex, fine-grained intergrowth of ilmenite (patchy grey), perovskite and titanomagnetite, with an overgrowth of clear perovskite (light grey) and associated titanomagnetite (dark grey).

In transmitted light the ilmenite, which is opaque, may be distinguished by colour and form from the angular, yellow-brown perovskite overgrowth, but not from the intervening intergrowth area which also appears black. The higher reflectivity and anisotropism of the ilmenite (Table 2) serve, however, to highlight this contact in reflected light. The intergrowth area consists of fine grained lamellae and patches, and is isotropic with patches of grey internal reflections, while the perovskite overgrowth is isotropic with characteristic orange internal reflections. The polished surface of the intergrowth area is noticeably pitted in comparison with both the ilmenite and perovskite. Reflectivity measurements from the three zones are summarised in Table 2.

Coarse, dark grey alteration/exsolution lamellae (titanomagnetite) are seen extending from the ilmenite/intergrowth contact, into the ilmenite parallel to its basal plane (Plate 11) and there is preferential alteration to titanomagnetite along cracks. Another alteration product (which could not be positively identified) is intergrown with the titanomagnetite in places and forms alteration lamellae within the ilmenite (darker grey than titanomagnetite, Plate 11, along crack). This phase is pinkish grey and isotropic.

Sample 580/10 contains a rounded black grain with a

Plate 11 Ilmenite in monticellite kimberlite. Part of an anhedral macrocryst formed by an aggregate of 3 grains. The central pale grey area of ilmenite is mantled by an intergrowth (patchy grey) of ilmenite, perovskite and titanomagnetite, with an overgrowth of clear perovskite (grey) and associated titanomagnetite (dark grey). Alteration/ exsolution lamellae of titanomagnetite are parallel to the basal plane of the ilmenite. Along the large crack is a patchy alteration product which, in places, is intergrown with the titanomagnetite and forms lamellae into the ilmenite.
Width of field = 0,6 mm (reflected light, oil immersion).

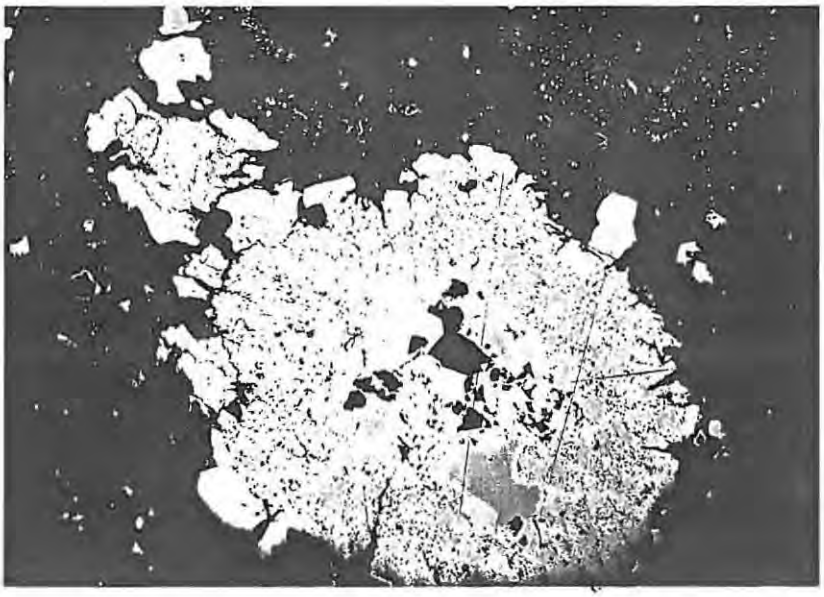

Plate 12 Secondary perovskite in monticellite kimberlite. Central area of fine scale intergrowth (perovskite/ titanomagnetite?) surrounded by pitted border similar to that shown in Plate 11 and rimmed by clear subhedral perovskite.
Width of grain = 0,4 mm (reflected light, oil immersion).

TABLE 2

SUMMARY OF REFLECTIVITY MEASUREMENTS

Type	Sample Number	Reflectance Values (Number of readings in brackets)			
		Ilmenite		Intergrowth	Perovskite
		R1	R2		
Monticellite	580/10	-	-	16,3 (8)	16,5 (2)
	580/6	17,5 (3)	14,4	15,1 (4)	15,1 (4)
Phlogopite	740/16*	17,1 (3)	16,3	-	16,5 (4)
	580/26	16,6 (3)	14,9	-	-
	580/21	17,0 (2)	15,1	-	15,4 (2)

* Oxidation/exsolution patches (see Plate 24) have reflectance R = 24,0 (n=3).

Note: Reflectance measured at 546 nm against Zeiss Sika Standard Number 110.

yellow-brown overgrowth of clear subhedral perovskite. The central portion of the grain has reflectivity (Table 2) equal to that of perovskite but is composite, as shown in Plate 12. A core of fine-scale intergrowths and patches of darker material (possibly titanomagnetite) are surrounded by a pitted fine-scale intergrowth, which forms a border similar to that in Plate 11, and is in turn rimmed by the perovskite. The petrographic evidence indicates that the grain described may be secondary perovskite, with titanomagnetite having played a part in the alteration process, and, indeed, this is confirmed by chemical analysis as described later. A comparison of the textures shown in Plates 11 and 12 supports progressive breakdown of ilmenite and its reaction with the magma to form perovskite, titanomagnetite and, possibly, silicate alteration products (resulting in the pitted texture of the polished surface) as described by Mitchell (1972). Further nucleation and growth of perovskite then occurred on the rim of the crystal preventing further breakdown of the ilmenite as in Plate 11. Large perovskite grains as in Plate 12 may represent an advanced stage of such a process, where the overgrowth of perovskite nucleated too late to preserve any ilmenite. The secondary perovskite grain (Plate 12) is smaller than the macrocryst of ilmenite (Plate 11) and could thus feasibly be the product of total breakdown, whereas the larger grain still has a core of ilmenite preserved.

The opaque minerals of the groundmass in the monticellite kimberlite appear not to include ilmenite.

Spinels are abundant in the groundmass and are also found as inclusions in perovskite and olivine. Both spinel and perovskite are found as inclusions in phlogopite which is thus a later crystallising phase. Fine grained euhedral to subhedral magnetite is disseminated throughout the groundmass but a second generation is particularly abundant, together with perovskite, in clusters around the margins of altered olivine phenocrysts and in the reaction mantles around ilmenite macrocrysts. Rare larger euhedral and rounded grains of chromite are found.

In the contact phase some euhedral to subhedral composite grains are found to exhibit a texture of 'spinel core-gap-thin opaque rim.' The cores, in reflected light are white and isotropic and are titaniferous, moderate Mg- low Al-magnetites in composition. The "gap" is a grey area of transparent silicate material. The crystal form is delineated by a patchy bright rim, which is possibly rutile, titaniferous magnetite or magnetite, but is too thin to determine positively. These spinels are spatially related with perovskite and could possibly represent the result of reaction of ilmenite with the melt to produce perovskite plus magnetite. If the rim is rutile it could represent residual material previously enclosed in ilmenite and not completely replaced during reaction with the melt, as described by Elthon and Ridley (1979). Alternately, if the rim is titanomagnetite, it could represent growth zoning, especially as the intervening silicate is idiomorphic (as in Boctor and Meyer, 1979). A third possibility, if the rim is Ti-free magnetite, is that these spinels represent the atoll texture described by Pasteris (1979) which will be more fully discussed in section IV. Textural evidence in support of this possibility includes the fact that the titanomagnetite cores are often irregular and fragmented, as if partially resorbed.

Serpentine is an important primary groundmass constituent, pools of which often enclose primary anhedral calcite (plates 9 and 10). Plates 5 and 6 show monticellite, perovskite, magnetite and phlogopite set in serpentine.

Cebollite, a rare hydrous aluminium silicate $Ca_5Al_2(OH)_4Si_3O_{12}$, is found in 580/9 as a secondary alteration product associated with a vein of calcite. The characteristics of cebollite will be discussed in the following section as it is more common as a primary accessory mineral in the phlogophite kimberlite.

2. Phlogopite - Kimberlite Type (D5)

The modal analyses of two samples (580/26 and 580/21) are given in Table 1. About a third of the coarse grained

material is xenolithic and a comparison of the hand specimens in Plates 13 and 14 shows the greater extent to which the phlogopite type is dominated by inclusions. These include crustal fragments (usually carbonatised), ultramafic and other altered fragments. Xenocrysts of chrome diopside and garnet are found and ilmenite is also seen in hand specimens.

As seen from Table 1, the main kimberlitic constituent of the coarse grained rock is serpentine (about 30 per cent) derived by alteration of both olivine and phlogopite. Fresh olivine (20-23 per cent) and phlogopite (10-14 per cent) is present in these samples but complete alteration of both components is found where weathering has been more severe. The groundmass is mainly phlogopite (32-43 per cent) but primary serpentine is an important phase (forming 25-30 per cent) which according to Skinner and Clement (1979), calls for classification of this rock as a phlogopite-serpentine kimberlite. Perovskite, cebollite and apatite are important accessory minerals. Minor amounts of opaques are found and diopsidic pyroxene was noted in sample 580/26.

Olivine has been extensively serpentinised and is preserved mainly in the central parts of large macrocrysts. Serpentine pseudomorphs of olivine phenocrysts are scattered throughout the matrix. Plate 15, a photomicrograph of a section from a relatively little weathered sample (580/21), illustrates the presence of both macrocrystic and phenocrystic olivine. The large olivine grain (right) is typical of the macrocrysts which, like those of the monticellite kimberlite, are rounded and fall into a size range of 1-5 mm. The euhedral outlines of the smaller (0,5-1 mm) phenocrysts are well portrayed by their serpentine rims, as illustrated by the three largest grains adjacent to the central phlogopite lath in Plate 15. Totally serpentinised olivine phenocrysts tend to be rounded in shape and are rimmed by perovskite and spinels. In Plate 16 the perovskite grains (top left) partially encircle a small serpentinised olivine phenocryst.

Phlogopite falls into three grain-size populations.

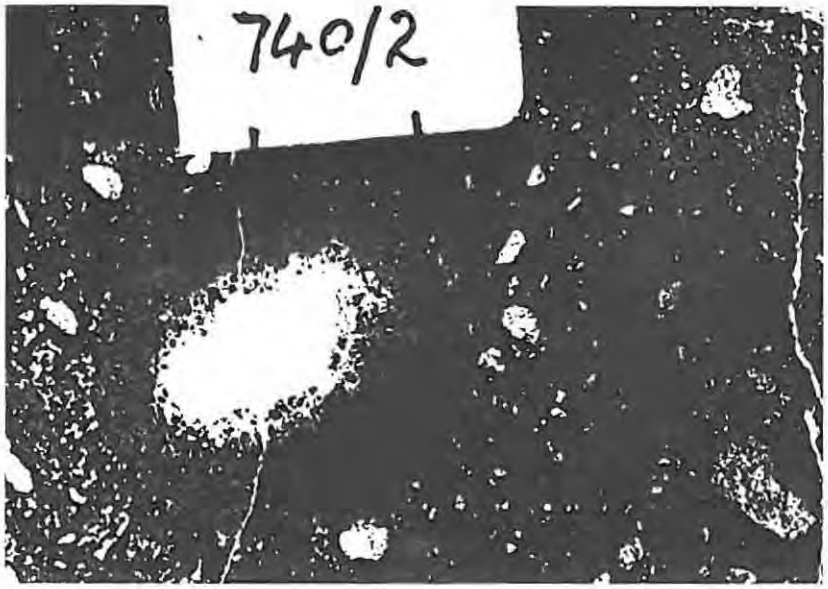

Plate 13 Monticellite kimberlite, hand specimen. Rounded and sub-rounded olivine macrocrysts and olivine phenocrysts set in a dark fine grained groundmass of monticellite, perovskite, spinels, phlogopite, and serpentine. Large white carbonatised inclusions are seen (top right and left of centre)
Scale marks 1 cm.

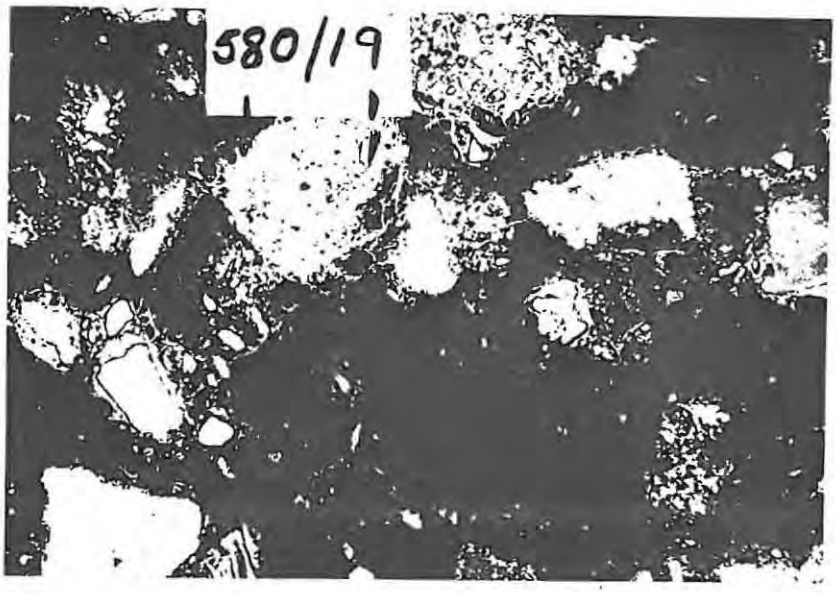

Plate 14 Phlogopite kimberlite, hand specimen. Angular carbonatised crustal inclusions dominate the texture. Rounded serpentinised olivine macrocrysts (grey) and phlogopite laths (dark grey) are set in a fine grained groundmass of serpentine and phlogopite.
Scale marks 1 cm.

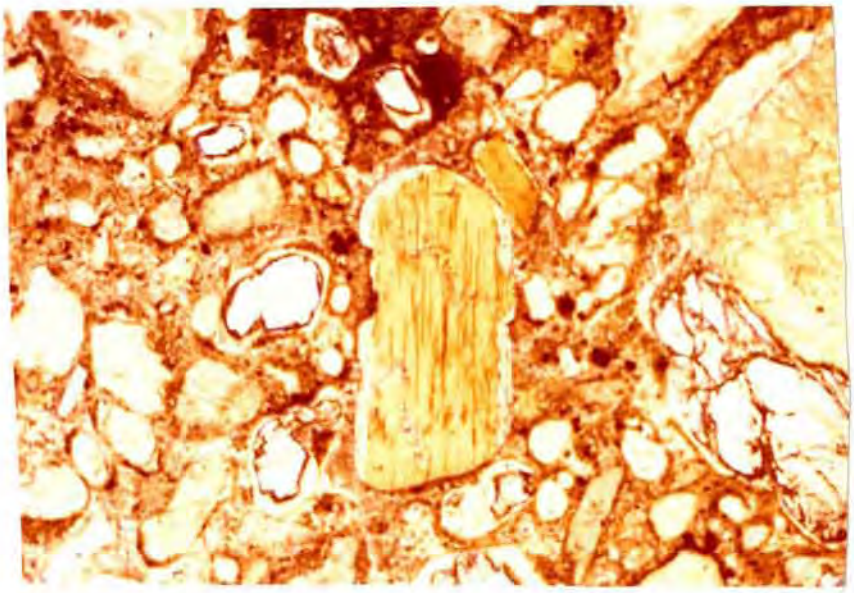

Plate 15 Phlogopite kimberlite. Large and small yellow-brown phlogopite laths, both with narrow bleached rims. Olivine (clear white with high relief) is rimmed by serpentine. Serpentine pseudomorphs (white and pale brown) of both olivine and phlogopite with perovskite and spinel micro-phenocrysts are set in a groundmass of serpentine and phlogopite. The angular fragment (top right) is an altered crustal inclusion and the large rounded grain on the right is part of an extensively serpentinised olivine macrocryst.

Width of field = 4 mm (plane light).

Large subhedral laths or rounded plates (2-5 mm across) are termed macrocrysts; these are dark brown or yellow brown and pleochroic (α = yellow, $\beta = \gamma$ = brown). Smaller phenocryst laths of similar colour are about 1 mm long and often extensively altered along margins to magnetite. Core-margin colour zoning is common and is usually as shown in Plate 15, where the cores of the grains are dark and the margins are paler. The margins have reverse pleochroism. Groundmass phlogopite is finer grained (0,01-0,5 mm) and occurs as pale-yellow, faintly pleochroic stubby laths (Plates 16 and 17).

Deformation features are seen in both the macrocrystic and phenocrystic phlogopite grains. Plate 18 features a phlogopite macrocryst with N-S kink bands, diagonal deformation lamellae and E-W cleavage traces. The macrocryst in Plate 19 shows strain shadows and the cleavages are bent while Plate 20 shows herring-bone deformation lamellae in a phenocryst or macrocryst of phlogopite. Some phenocrysts in 580/18 were seen to have broad twin lamellae with parallel fine deformation lamellae apparent within alternate twins.

Clusters of phlogopite laths are found around rounded pinkish-mauve garnets in samples 740/6 and 580/18. The phlogopite in this association is similar in colour to the rest of the macrocrysts and phenocrysts but shows no sign of deformation. It could be a small mantle nodule, particularly as the cluster is rounded in outline.

Perovskite forms about 10 per cent of the groundmass. It occurs as microphenocrysts up to 0,1 mm across. As shown in Plate 16, the grains are subhedral or rounded, brown and have high relief. Plate 17 shows the appearance of perovskite under crossed nicols when it appears either isotropic or weakly birefringent. The birefringence is usually shown when the grains are twinned. Complex lamellar twinning is common.

Euhedral spinel inclusions are found as shown in the large perovskite grains in Plate 16. There is a tendency for perovskite grains to rim serpentinised olivine phenocrysts

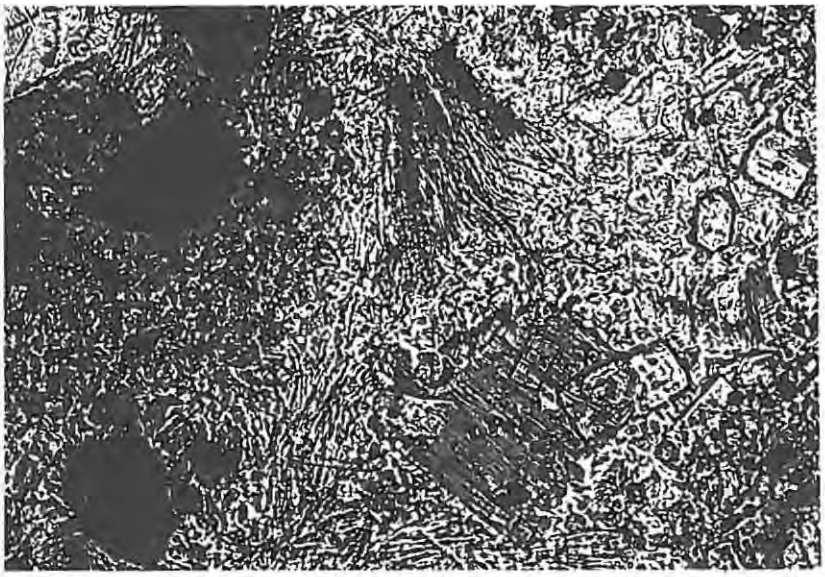

Plate 16 Phlogopite kimberlite matrix (plane light). Subhedral to rounded brown perovskite grains encircling serpentinised olivine (top left). Pale brown phlogopite (centre) is set in greenish serpentine and associated with colourless apatite (high relief) and fibrous cebollite (brownish). Spinels are rare in comparison with the monticellite kimberlite matrix (Plates 5 and 6). Tiny rounded grains are thought to be rutile.

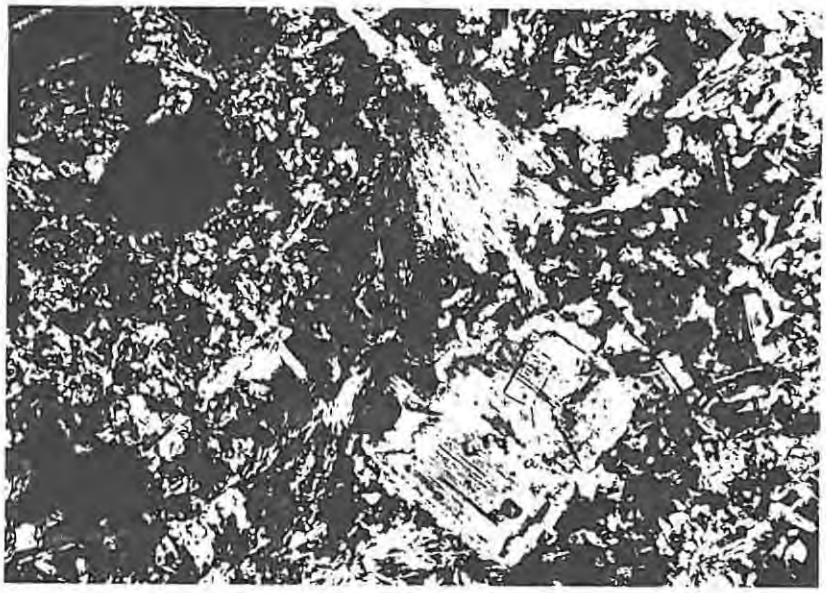

Plate 17 As above (crossed nicols). Cebollite (top and bottom centre) has yellow first order interference colours. Serpentine has anomalous grey interference colours.

Width of field = 0,4 mm.

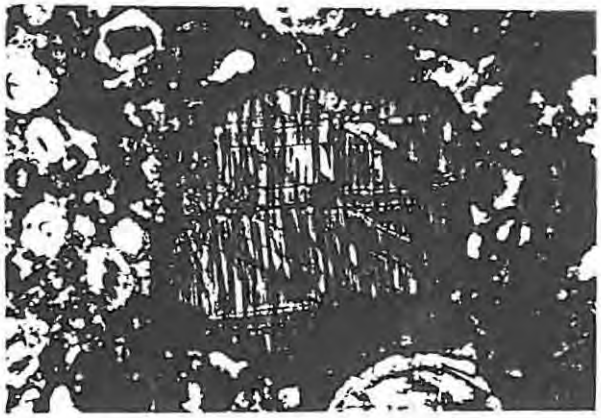

Plate 18 Phlogopite kimberlite. Phlogopite macrocryst with kink bands (NW-SE) and deformation lamellae (E-W).

Width of field = 4 mm (plane light).

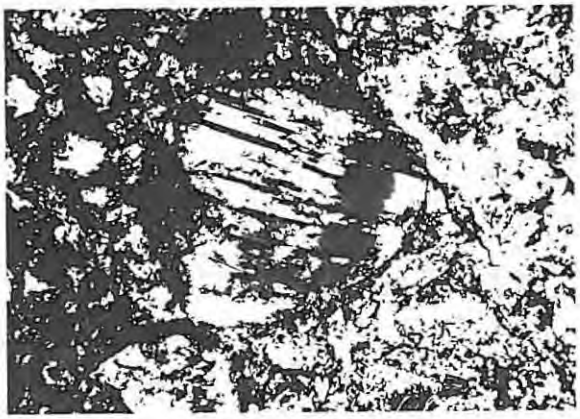

Plate 19 Phlogopite kimberlite. Strained phlogopite with bent cleavages.

Width of field = 4 mm (crossed nicols).

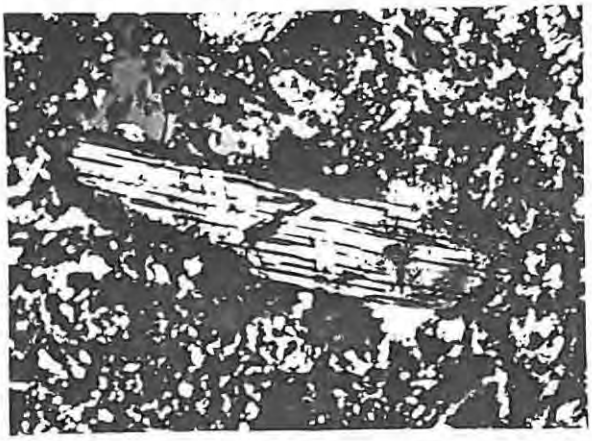

Plate 20 Phlogopite kimberlite. Phlogopite lath exhibiting herringbone deformation lamellae.

Width of field = 1,5 mm (crossed nicols).

in the same manner as described for the monticellite kimberlite and perovskite also occurs in reaction mantles around ilmenite in the phlogopite-kimberlite type.

Ilmenite occurs as large macrocrysts (up to 5 mm long) or aggregates. Plates 21 and 22 illustrate a rounded remnant of an aggregate of ilmenite. The ilmenite has high reflectivity (see Table 2) and is anisotropic (grey to blue grey). The altered part of the nodule illustrated consists of phlogopite, calcite, serpentine and spinels, that is, it is kimberlitic in composition. There is no perovskite associated with this particular occurrence. However, other aggregates, for example that illustrated in Plate 23, exhibit an alteration rim of perovskite. The aggregates typically feature triple junctions at grain boundaries as is shown in Plates 21, 22 and 23. Plate 24 shows part of a large single grain macrocryst of ilmenite which exhibits irregular patches of a highly reflective exsolution/oxidation product, possibly haematite. An average reflectivity of 24 per cent was measured at 3 sites (see Table 2). The euhedral grains around the rim of the macrocryst represent an overgrowth perovskite while a perfectly euhedral groundmass perovskite grain is seen (top right). The unusual exsolution/oxidation product is also associated with the overgrowth perovskite and with the 'free' grains adjacent to the ilmenite macrocryst. The reflectivity of the perovskite rim and ilmenite are very similar and the phases are distinguished with confidence only between crossed nicols (when the internal reflections in perovskite are obvious) or in transmitted light (when a brown rim is seen around a central opaque core).

Spinels form only 1 per cent of the groundmass. They occur as small euhedral magnetite grains scattered in the groundmass. Secondary magnetite is the usual alteration product found around the margins of phlogopite, especially the matrix phenocrysts.

Apatite occurs as fine grained hexagonal or prismatic sections (0,01 mm long) associated with primary serpentine

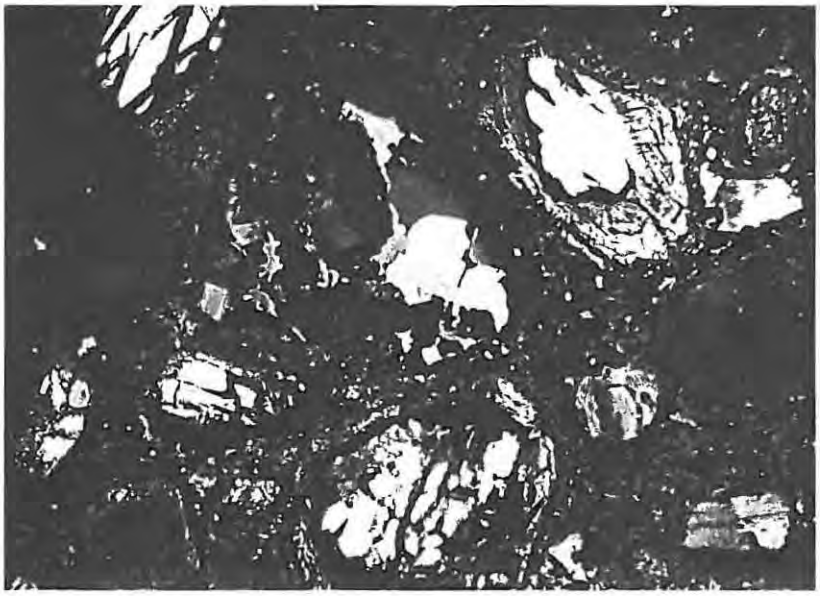

Plate 21 Ilmenite in phlogopite kimberlite. Remnant of nodule containing relict rounded ilmenite aggregate (centre). Note the triple junctions at grain boundaries. There is no rim of perovskite.

Width of field = 2,5 mm.

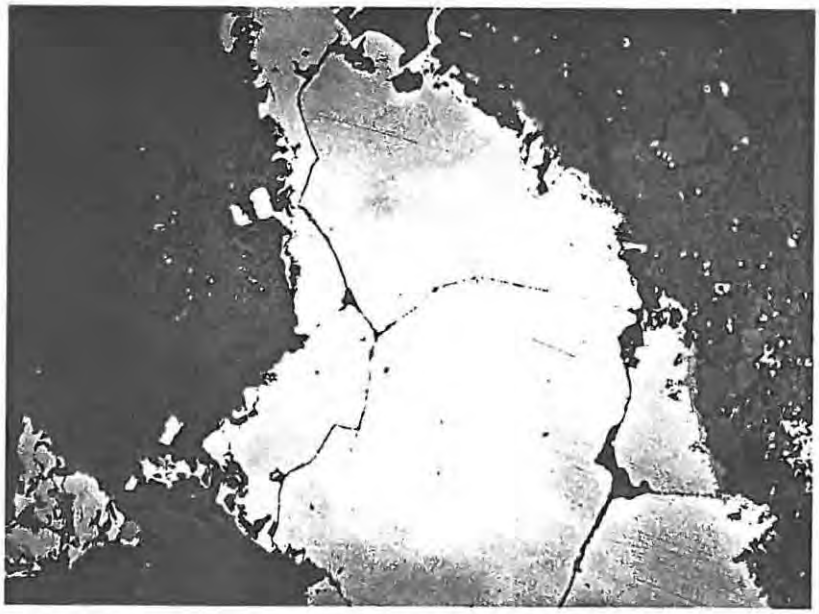

Plate 22 Enlarged view of the ilmenite aggregate above.

Width of field = 0,6 mm

(reflected light, oil immersion)

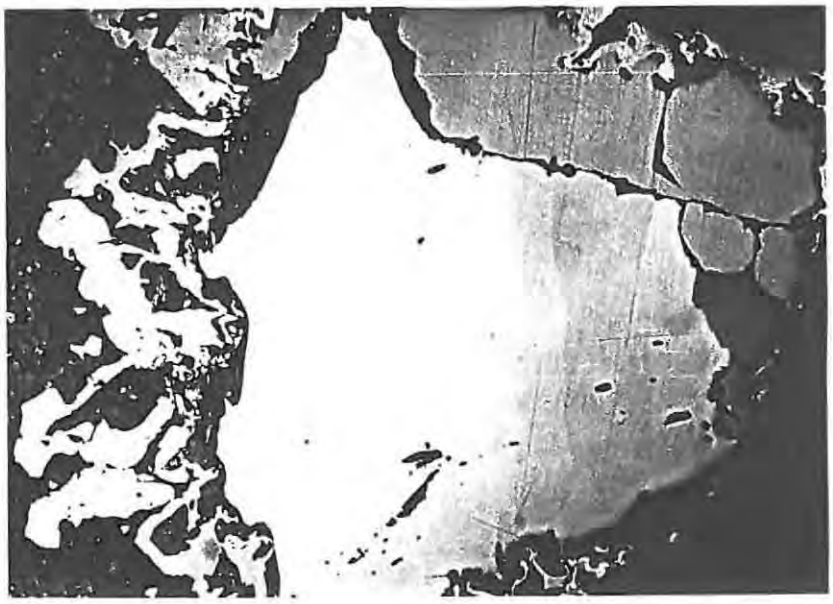

Plate 23 Ilmenite in phlogopite kimberlite. Aggregate of ilmenite exhibiting a mantle of perovskite (left).

Width of field = 0,6 mm (reflected light, oil immersion)

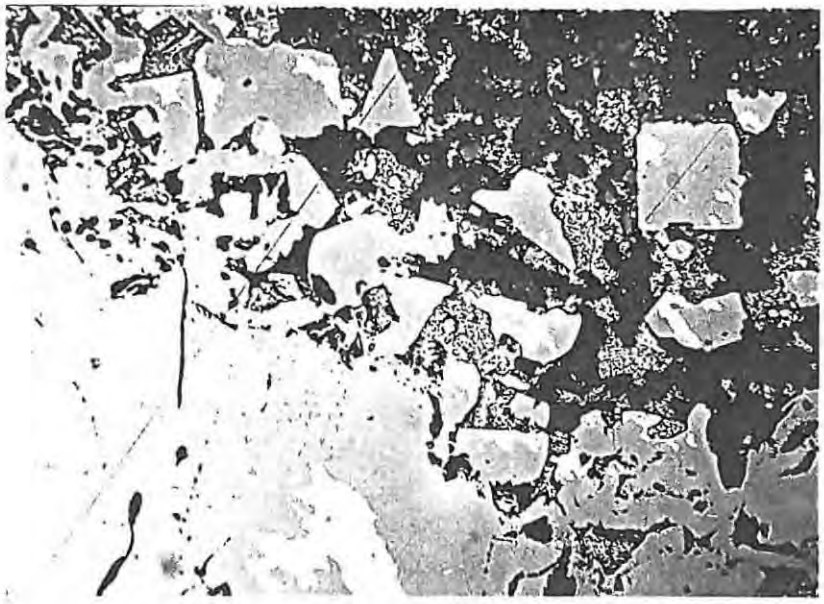

Plate 24 Ilmenite in phlogopite kimberlite. Dark grey ilmenite has light grey oxidation/exsolution patches of haematite (?). The perovskite overgrowth (subhedral to euhedral grey grains at the right) and discrete matrix perovskite grains also contain patches of the same highly reflective material.

Width of Field = 0,6 mm (reflected light oil immersion).

pools and phlogopite in the groundmass. Plates 16 and 17 illustrate high-relief, weakly birefringent apatite grains in this association. The section is very thin and the apatite grains are not believed to be enclosed in the phlogopite but rather to lie above and below it.

Cebollite forms about 15 per cent of the groundmass. It occurs in distinctive, fibrous, sheaf-like aggregates commonly associated with phlogopite and anhedral primary calcite. It appears to be a late-stage primary mineral similar in paragenesis to the cebollite described by Kruger (1978) from the De Beers Mine kimberlite. Plate 16 shows a brownish cluster of cebollite fibres intergrown with primary serpentine (greenish) and associated with a pale brown phlogopite grain. Between crossed nicols (Plate 17) the cebollite is easily distinguished by the first-order-yellow interference colours.

Serpentine is an important interstitial primary groundmass mineral. It is slightly greenish in colour as shown in Plate 16. Plate 17 illustrates fine-grained anhedral serpentine.

IV. MINERAL CHEMISTRY

The emphasis in this section is placed on the chemistry of the silicates olivine, phlogopite and monticellite because they have undergone relatively little post-emplacement alteration in the Dutoitspan kimberlites, unlike many kimberlites in which total serpentinisation of these phases or, in the case of monticellite, its fine grain size, precludes chemical analysis. Opaque minerals are preserved in abundance in all kimberlites and have formed the subject of thorough investigation elsewhere (Haggerty, 1976; Pasteris, 1979; Wyatt, 1979; Boyd and Pasteris, 1977; Shee, 1979a and b; Boctor and Meyer, 1979; Mitchell and Clarke, 1976; Mitchell, 1979 and others). Accordingly, only a limited number of analyses of ilmenite, perovskite and spinel are presented for comparative purposes. A single analysis of a relict mauve

garnet grain in a nodule is given.

1. Olivine

a) Variations in composition of Crystal Cores

The two types of olivine grains, namely phenocrysts and macrocrysts, which have been identified in both the monticellite (Tables 3 and 4) and phlogopite kimberlites (Table 5) fall into two overlapping chemical populations. Fig. 3 shows the variation of NiO, MnO and CaO plotted against MgO in phenocryst and macrocryst cores from both the monticellite and phlogopite kimberlites. Macrocrysts include large rounded strained or unstrained grains as well as granular aggregates of smaller grains and grains with recrystallised margins (Section III, Plates 2 and 3).

Monticellite kimberlite. There is a marked correlation between NiO and MgO among phenocrysts in the monticellite kimberlite (Fig. 3a). NiO increases from 0,1 per cent at 44 per cent MgO (grain 19A, not plotted) to 0,44 per cent at 50,8 per cent MgO. This trend is, to some extent, followed (at MgO contents below 51,5 per cent) by the macrocrysts but on the whole they have lower NiO levels. The two most magnesian macrocrysts show a sharp drop in nickel content. There is an overlap in MgO between the two types of olivine but the macrocrysts reach higher levels of MgO and the phenocrysts are generally less magnesian. There is a narrow range in manganese content but, in general, phenocrysts have slightly more MnO than macrocrysts (Fig. 3b). The two high-MgO macrocrysts have the lowest manganese contents (both less than 0,1 per cent). Grains 16 and 19 (not plotted) have anomalously high MnO contents (0,52 and 0,27 per cent, Tables 3 and 4). There is a marked trend of Ca depletion from high-Ca phenocrysts (0,15 - 0,05 per cent) towards magnesium-rich low-Ca macrocrysts (0,10 - 0,01 per cent). Grain 19 is, once again different with a low CaO content of 0,01 per cent (at MgO = 44 per cent).

Phlogopite kimberlite. The data for the phlogopite

Table 3 Microprobe Analyses of Olivine Phenocrysts from Monticellite Kimberlite

Oxides	1A	1B	1C	2A	2B	3A	3B	3C	4A	4B	4C	5A	5B	5C	5D
SiO_2	41,14	40,65	40,95	40,75	41,01	40,81	41,16	41,12	40,90	40,97	41,11	41,37	41,08	41,12	41,20
TiO_2	0,04	0,05	0,03	0,01	0,01	0,03	0,03	0,02	0,04	0,03	0,04	0,02	0,02	n.d.	0,03
FeO_{total}	8,83	9,50	10,32	11,23	10,88	10,24	10,34	9,97	11,26	11,21	9,43	11,20	10,93	10,87	11,03
MnO	0,11	0,13	0,12	0,14	0,13	0,13	0,13	0,09	0,11	0,12	0,10	0,16	0,09	n.d.	0,11
MgO	50,77	49,63	49,15	48,43	48,81	48,96	49,52	49,83	48,20	48,31	48,61	49,27	49,68	49,37	49,20
CaO	0,04	0,13	0,16	0,10	0,12	0,09	0,10	0,57	0,09	0,09	0,18	0,15	0,10	n.d.	0,12
NiO	0,40	0,38	0,34	0,42	0,16	0,40	0,46	0,50	0,37	0,40	0,41	0,38	0,36	0,25	0,21
Total	101,32	100,46	101,07	101,07	101,12	100,66	101,73	102,10	100,97	101,13	99,88	102,54	102,26	101,60	101,89
Cations															
Si	0,99	0,99	1,00	1,00	1,00	1,00	1,00	0,99	1,00	1,00	1,01	1,00	0,99	1,00	1,00
Ti	0,00	0,00	0,00	0,00	0,00	0,00	0,00	0,00	0,00	0,00	0,00	0,00	0,00	-	0,00
Fe	0,18	0,19	0,21	0,23	0,22	0,21	0,21	0,20	0,23	0,23	0,19	0,22	0,22	0,22	0,22
Mn	0,00	0,00	0,00	0,00	0,00	0,00	0,00	0,00	0,00	0,00	0,00	0,00	0,00	-	0,00
Mg	1,82	1,81	1,78	1,76	1,77	1,78	1,78	1,79	1,75	1,76	1,78	1,77	1,79	1,78	1,77
Ca	0,00	0,00	0,00	0,00	0,00	0,00	0,00	0,01	0,00	0,00	0,00	0,00	0,00	-	0,00
Ni	0,01	0,01	0,01	0,01	0,00	0,01	0,01	0,01	0,01	0,01	0,01	0,01	0,01	0,00	0,00
Total	3,00	3,00	3,00	3,00	2,99	3,00	3,00	3,00	2,99	3,00	2,99	3,00	3,01	3,00	2,99
Fo %	91,11	90,30	89,46	88,48	88,88	89,50	89,51	89,90	88,41	88,48	90,18	88,69	89,01	89,00	88,83

Note: A,B,C and D denote analyses from core(A) outwards to rim. Grains 1-6 are from sample 740/11, 12-17 from 580/5, 22-26 from 740/1 (contact phase), 37-39 from sample 580/1 (contact phase) and 43 and 49 from 740/19.

Table 3 (continued) Microprobe Analyses of Olivine Phenocrysts from Monticellite Kimberlite

Oxides	6A	6B	12A	12B	13A	13B	14A	14B	15A	15B	16A	16B	17A	17B
SiO_2	41,18	40,78	40,12	40,45	40,61	40,50	40,47	40,29	40,60	40,26	40,35	40,13	40,04	39,83
TiO_2	0,05	0,04	0,02	0,02	0,05	0,05	0,03	0,04	0,05	0,04	0,06	0,04	0,03	0,04
FeO_{total}	10,47	10,53	11,86	10,64	10,31	10,28	11,10	11,32	8,95	9,93	10,24	10,20	10,64	9,75
MnO	0,16	0,19	0,17	0,13	0,14	0,13	0,16	0,13	0,15	0,10	0,52	0,85	0,11	0,13
MgO	49,02	48,72	46,64	47,34	48,23	48,02	47,25	46,93	49,52	47,91	48,44	47,80	47,42	48,01
CaO	0,09	0,27	0,09	0,10	0,06	0,07	0,10	0,10	0,08	0,12	0,09	0,11	0,09	0,06
NiO	0,43	0,41	0,32	0,35	0,39	0,38	0,40	0,32	0,43	0,39	0,36	0,41	0,34	0,36
Total	101,39	100,82	99,20	99,03	99,78	99,42	99,51	99,13	99,79	98,75	100,06	99,52	98,66	98,18
Cations														
Si	1,00	1,00	1,00	1,01	1,00	1,00	1,00	1,00	1,00	1,00	0,99	1,00	1,00	1,00
Ti	0,00	0,00	0,00	0,00	0,00	0,00	0,00	0,00	0,00	0,00	0,00	0,00	0,00	0,00
Fe	0,21	0,21	0,25	0,22	0,21	0,21	0,23	0,24	0,18	0,21	0,21	0,21	0,22	0,20
Mn	0,00	0,00	0,00	0,00	0,00	0,00	0,00	0,00	0,00	0,00	0,01	0,02	0,00	0,00
Mg	1,77	1,77	1,74	1,75	1,77	1,77	1,75	1,74	1,81	1,78	1,78	1,77	1,77	1,79
Ca	0,00	0,01	0,00	0,00	0,00	0,00	0,00	0,00	0,00	0,00	0,00	0,00	0,00	0,00
Ni	0,01	0,01	0,01	0,01	0,01	0,01	0,01	0,01	0,01	0,01	0,01	0,01	0,01	0,01
Total	2,99	3,00	3,00	2,99	2,99	2,99	2,99	2,99	3,00	3,00	3,00	3,01	3,00	3,00
Fo %	89,30	89,18	87,51	88,80	89,29	89,28	88,35	88,08	90,79	89,58	89,40	89,31	88,82	89,77

Table 3 (continued) Microprobe Analyses of Olivine Phenocrysts from Monticellite Kimberlite

Oxides	22A	22B	23A	23B	24A	25A	25B	26A	26B	37A	38A	39A	43A	49A
SiO_2	40,50	40,78	40,83	41,31	41,32	40,56	40,69	40,39	40,27	41,41	40,78	40,08	40,37	40,23
TiO_2	0,02	0,03	0,05	0,05	0,04	0,04	0,05	0,04	0,06	0,03	0,04	0,05	0,01	0,01
FeO_{total}	10,99	10,62	12,02	10,75	10,32	10,94	9,48	11,81	10,52	9,01	8,99	11,16	10,90	10,84
MnO	0,12	0,16	0,12	0,14	0,11	0,11	0,10	0,14	0,15	0,11	0,11	0,12	0,11	0,11
MgO	47,46	47,46	46,72	48,16	49,51	48,65	49,46	47,80	48,65	50,82	49,52	47,23	47,63	47,63
CaO	0,09	0,20	0,14	0,11	0,11	0,06	0,07	0,15	0,12	0,01	0,01	0,01	n.d.	n.d.
NiO	0,37	0,20	0,39	0,13	0,40	0,32	0,44	0,39	0,16	0,44	0,39	0,36	0,34	0,34
Total	99,55	99,44	100,27	100,65	101,81	100,66	100,27	100,70	99,92	101,82	99,84	99,02	99,36	99,16
Cations														
Si	1,00	1,01	1,01	1,01	1,00	0,99	0,99	0,99	0,99	0,99	1,00	1,00	1,00	1,00
Ti	0,00	0,00	0,00	0,00	0,00	0,00	0,00	0,00	0,00	0,00	0,00	0,00	0,00	0,00
Fe	0,23	0,22	0,25	0,22	0,21	0,22	0,19	0,24	0,22	0,18	0,18	0,23	0,23	0,23
Mn	0,00	0,00	0,00	0,00	0,00	0,00	0,00	0,00	0,00	0,00	0,00	0,00	0,00	0,00
Mg	1,75	1,75	1,72	1,75	1,78	1,78	1,80	1,75	1,79	1,82	1,81	1,76	1,76	1,76
Ca	0,00	0,01	0,00	0,00	0,00	0,00	0,00	0,00	0,00	0,00	0,00	0,00	n.d.	n.d.
Ni	0,01	0,00	0,01	0,01	0,01	0,01	0,01	0,01	0,01	0,01	0,01	0,01	0,01	0,01
Total	2,99	2,99	2,99	2,99	3,00	3,00	2,99	2,99	3,01	3,00	3,00	3,00	3,00	3,00
Fo %	88,50	88,84	87,38	88,87	89,53	88,79	90,29	87,82	89,18	90,99	90,76	88,29	88,60	88,40

Table 4 Microprobe Analyses of Olivine Macrocrysts and Aggregates from Monticellite Kimberlite

Oxides	7A	7B	7C	7D	8A	8B	9C	9D	10A	10B	10C	10D	11A	11B
SiO_2	41,56	41,53	41,75	41,51	41,18	40,88	40,85	41,49	41,63	41,70	41,61	41,86	40,92	40,45
TiO_2	0,03	0,04	n.d.	0,06	0,05	n.d.	0,05	0,03	0,02	0,02	0,02	0,01	0,01	0,02
FeO_{total}	6,71	6,32	6,48	6,54	8,48	10,19	8,99	9,19	6,03	6,12	6,22	6,26	7,25	10,41
MnO	0,09	0,09	n.d.	0,11	0,11	n.d.	0,11	0,15	0,07	0,09	0,09	0,10	0,10	0,23
MgO	52,06	52,40	52,34	51,93	50,04	49,34	50,29	50,54	52,68	52,43	51,93	52,54	50,60	47,72
CaO	0,12	0,02	n.d.	0,11	0,06	n.d.	0,10	0,11	0,03	0,02	0,02	0,04	0,03	0,17
NiO	0,35	0,41	0,41	0,39	0,43	0,43	0,45	0,44	0,31	0,33	0,36	0,33	0,43	0,10
Total	100,90	100,80	100,99	100,65	100,35	101,05	100,84	101,93	100,77	100,71	100,26	101,13	99,34	99,10
Cations														
Si	1,00	1,00	1,00	1,00	1,00	1,00	0,99	1,00	1,00	1,00	1,00	1,00	1,00	1,00
Ti	0,00	0,00	-	0,00	0,00	-	0,00	0,00	0,00	0,00	0,00	0,00	0,00	0,00
Fe^{2+}	0,13	0,13	0,13	0,13	0,17	0,21	0,18	0,18	0,12	0,12	0,13	0,12	0,15	0,22
Mn	0,00	0,00	-	0,00	0,00	-	0,00	0,00	0,00	0,00	0,00	0,00	0,00	0,00
Mg	1,86	1,87	1,87	1,86	1,81	1,79	1,82	1,81	1,88	1,87	1,86	1,87	1,84	1,76
Ca	0,00	0,00	-	0,00	0,00	-	0,00	0,00	0,00	0,00	0,00	0,00	0,00	0,00
Ni	0,01	0,01	0,01	0,01	0,01	0,01	0,01	0,01	0,01	0,01	0,01	0,01	0,01	0,00
Total	3,00	3,01	3,01	3,00	2,99	2,99	3,00	3,00	3,01	3,00	3,00	3,00	3,00	2,98
Fo %	93,26	93,66	93,50	93,40	91,32	89,61	90,88	90,74	93,96	93,85	93,70	93,73	92,56	89,09

Note: A,B,C and D denote analyses from the core (A) outwards to the rim of a given grain. Grains 7-11 inclusive are from sample 740/11, grains 18-21 from 580/5, 28-30 from 740/1 (contact phase), grain 40 from 580/1A (contact phase), grains 44 and 45 from 740/19. Grains 28,29,30 and 44 are granular aggregates and subscripts represent sub-grains within the aggregate.

Table 4 (continued) Microprobe Analyses of Olivine Macrocrysts and Aggregates from Monticellite Kimberlite

Oxide	18A	18B	19A	19B	20A	20B	20D	21A	21B	21C	$28B_1$	$28A_2$	$28B_2$	$28A_3$	$28B_3$
SiO_2	40,41	39,87	39,46	39,45	41,64	41,02	41,17	40,64	41,25	40,38	40,35	40,90	40,84	41,06	40,90
TiO_2	0,04	0,05	0,01	0,01	0,03	0,03	0,04	0,02	0,00	0,03	0,01	0,02	0,01	0,03	0,03
FeO_{total}	8,90	10,58	15,44	15,48	7,84	7,70	7,82	8,53	8,66	8,53	8,56	7,73	8,95	7,87	9,52
MnO	0,11	0,79	0,27	0,26	0,11	0,11	0,11	0,12	0,11	0,14	0,10	0,10	0,11	0,11	0,10
MgO	48,92	47,22	44,04	44,10	50,21	50,00	50,34	49,43	49,56	49,14	49,89	50,00	49,02	49,47	48,43
CaO	0,04	0,13	0,01	0,02	0,03	0,03	0,06	0,06	0,05	0,06	0,09	0,06	0,09	0,08	0,11
NiO	0,32	0,15	0,10	0,11	0,35	0,36	0,37	0,39	0,35	0,38	0,38	0,34	0,39	0,39	0,30
Total	98,72	98,76	99,31	99,42	100,21	99,26	99,91	99,17	99,98	98,65	99,38	99,12	99,41	99,00	99,39
Cations															
Si	1,00	1,00	1,00	1,00	1,01	1,00	1,00	1,00	1,01	1,00	0,99	1,00	1,00	1,01	1,01
Ti	0,00	0,00	0,00	0,00	0,00	0,00	0,00	0,00	0,00	0,00	0,00	0,00	0,00	0,00	0,00
Fe^{2+}	0,18	0,22	0,33	0,33	0,16	0,16	0,16	0,18	0,18	0,18	0,18	0,16	0,18	0,16	0,20
Mn	0,00	0,02	0,01	0,01	0,00	0,00	0,00	0,00	0,00	0,00	0,00	0,00	0,00	0,00	0,00
Mg	1,80	1,76	1,66	1,66	1,81	1,82	1,83	1,81	1,80	1,81	1,83	1,83	1,80	1,81	1,78
Ca	0,00	0,00	0,00	0,00	0,00	0,00	0,00	0,00	0,00	0,00	0,00	0,00	0,00	0,00	0,00
Ni	0,01	0,00	0,00	0,00	0,01	0,01	0,01	0,01	0,01	0,01	0,01	0,01	0,01	0,01	0,01
Total	2,99	3,00	3,00	3,00	2,99	2,99	3,00	3,00	3,00	3,00	3,01	3,00	2,99	2,99	3,00
Fo %	90,74	88,83	83,56	83,54	91,94	92,05	91,98	91,17	91,07	91,12	91,22	92,02	90,71	91,80	90,06

Table 4 (continued) Microprobe Analyses of Olivine Macrocrysts and Aggregates from Monticellite Kimberlite

Oxide	$29A_1$	$29A_2$	$29B_2$	$30A_1$	$30B_1$	$30A_2$	$30B_2$	40A	$44A_1$	$44A_2$	$44A_3$	$44A_4$	45A
SiO_2	40,72	40,86	40,70	41,16	40,94	41,45	40,89	41,65	40,58	40,41	40,47	40,44	40,51
TiO_2	0,03	0,04	0,04	0,03	0,03	0,02	0,03	0,03	0,04	0,04	0,02	0,03	0,00
FeO_{total}	12,14	12,36	12,32	7,65	9,37	7,33	9,84	7,36	9,23	10,08	9,51	9,29	9,11
MnO	0,11	0,14	0,18	0,10	0,13	0,10	0,12	0,11	0,11	0,11	0,10	0,11	0,13
MgO	46,93	47,24	47,32	50,10	49,23	50,56	48,69	51,44	49,37	49,05	48,58	49,26	49,31
CaO	0,09	0,10	0,44	0,09	0,11	0,02	0,10	0,01	-	-	-	-	-
NiO	0,35	0,35	0,31	0,36	0,44	0,45	0,35	0,45	0,36	0,34	0,35	0,35	0,34
Total	100,37	101,08	101,30	99,49	100,24	99,93	100,02	101,04	99,69	100,03	99,02	99,48	99,38
Cations													
Si	1,01	1,00	1,00	1,00	1,00	1,01	1,00	1,00	1,00	0,99	1,00	1,00	1,00
Ti	0,00	0,00	0,00	0,00	0,00	0,00	0,00	0,00	0,00	0,00	0,00	0,00	0,00
Fe^{2+}	0,25	0,25	0,25	0,16	0,19	0,15	0,20	0,15	0,19	0,21	0,20	0,19	0,19
Mn	0,00	0,00	0,00	0,00	0,00	0,00	0,00	0,00	0,00	0,00	0,00	0,00	0,00
Mg	1,73	1,73	1,73	1,82	1,79	1,83	1,78	1,84	1,81	1,80	1,79	1,81	1,81
Ca	0,00	0,00	0,01	0,00	0,00	0,00	0,00	0,00	-	-	-	-	-
Ni	0,01	0,01	0,01	0,01	0,01	0,01	0,01	0,01	0,01	0,01	0,01	0,01	0,01
Total	3,00	2,99	3,00	2,99	3,00	3,00	2,99	3,00	3,01	3,01	3,00	3,01	3,01
Fo %	87,32	87,20	87,25	92,11	90,35	92,48	89,81	92,57	90,54	90,00	90,09	90,40	90,40

Table 5 Microprobe Analyses of Olivine from Phlogopite Kimberlite

	Phenocrysts			Macrocrysts and Aggregates						
Oxides	31A	32A	32B	33A	33B	34A	35A	36A	41A	42A
SiO_2	40,88	41,62	41,14	41,73	41,17	41,28	41,39	41,40	40,91	40,81
TiO_2	0,04	0,01	0,01	0,01	0,03	0,02	n.d.	n.d.	0,01	0,01
FeO_{total}	10,36	6,73	6,69	7,67	10,66	6,93	6,84	6,57	8,74	9,63
MnO	0,10	0,11	0,09	0,12	0,15	0,10	0,08	n.d.	0,41	0,36
MgO	48,13	50,81	50,66	49,76	48,43	49,95	51,07	50,33	49,65	49,56
CaO	0,09	0,03	0,02	0,03	0,09	0,03	0,02	n.d.	n.d.	n.d.
NiO	0,38	0,46	0,42	0,33	0,21	0,36	0,42	0,33	0,32	0,38
Total	99,98	99,76	99,02	99,65	100,73	98,67	99,82	98,63	100,04	100,75
Cations										
Si	1,01	1,01	1,00	1,02	1,00	1,01	1,00	1,01	1,00	1,00
Ti	0,00	0,00	0,00	0,00	0,00	0,00	-	-	0,00	0,00
Fe^{2+}	0,21	0,14	0,14	0,16	0,22	0,14	0,14	0,13	0,18	0,20
Mn	0,00	0,00	0,00	0,00	0,00	0,00	0,00	-	0,01	0,01
Mg	1,76	1,83	1,84	1,80	1,76	1,82	1,84	1,83	1,81	1,80
Ca	0,00	0,00	0,00	0,00	0,00	0,00	0,00	-	-	-
Ni	0,01	0,01	0,01	0,01	0,00	0,01	0,01	0,01	0,01	0,01
Total	2,99	2,99	2,99	2,99	2,98	2,98	2,99	2,98	3,01	3,02
Fo %	89,22	93,08	93,10	92,04	89,01	92,78	93,01	93,17	90,95	90,00

Note: A and B denote core and rim respectively. Grains 31-35 are from sample 580/18 (grain 33 being a granular aggregate), grain 36 is from sample 740/10 and grains 41 (aggregate) and 42 are from sample 580/22.

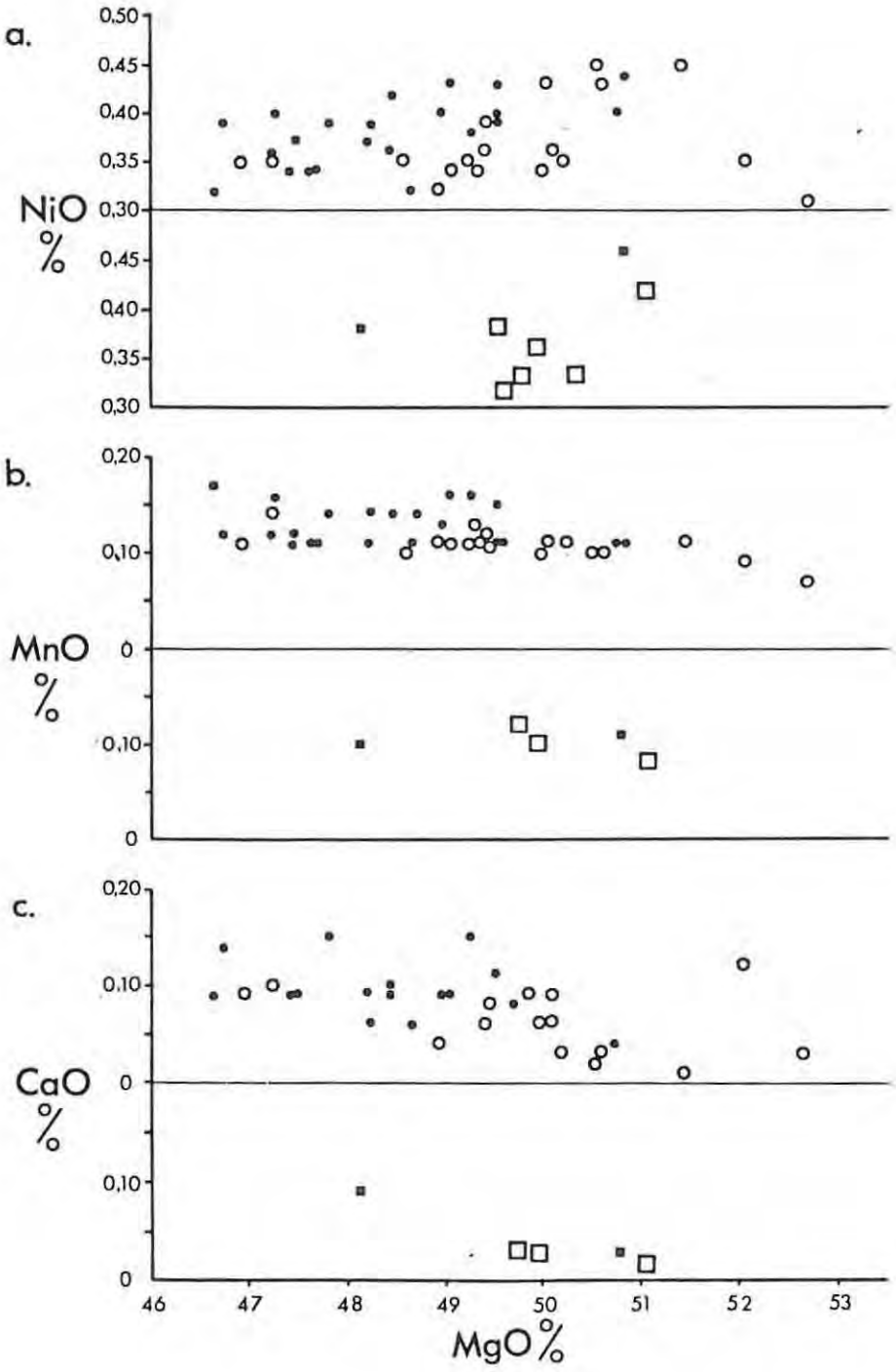

Fig. 3 Chemical variations of a) NiO, b) MnO and c) CaO against Mgo composition in phenocryst and macrocryst cores from monticellite and phlogopite kimberlites. Closed circles denote phenocrysts and open circles denote macrocrysts from the monticellite kimberlite. Closed squares denote phenocrysts and open squares denote macrocrysts from the phlogopite kimberlite.

Note: Grains 41 and 42 are not plotted on 3b.

type, plotted below corresponding diagrams for the monticellite type, indicate that there are no obvious differences between the olivines from the two kimberlites. It can be seen from the data that only 2 phenocrysts could be analysed and far fewer macrocrysts were preserved than in the monticellite type. Grains 41 and 42 (see Table 4) have unusually high MnO content (0,41 and 0,36 per cent and are not plotted on the MnO variation diagram.

b) Zoning

The microprobe data for traverses across the olivine grains from 3 monticellite type specimens - 740/11, 580/5 and 740/1 - are given in Tables 3 and 4. Phenocrysts have thin sharply zoned rims; macrocrysts are weakly zoned. The histograms of Fig. 4 summarise the distribution of Fo per cent between phenocryst cores and rims (Fig. 4a) and macrocryst cores and rims (Fig. 4b).

Phenocryst cores have an average composition of Fo_{89} with a standard deviation, (s), of 1,3 per cent. Analyses of rims are tightly clustered (s=0,8 per cent) around a mean of $Fo_{89,2}$. Macrocryst core compositions fall into a well defined normal distribution about a mean of $Fo_{91,5}$ and members of an iron-rich population (less than Fo_{88}) are identified on the left of the diagram (Fig. 4b). These include analyses from grains 19 (44 per cent MgO) and 29(46,9 and 47,2 per cent MgO) in Table 4. Macrocryst rims (excluding those of the Fe-rich grains) show a diffuse compositional distribution (about a mean of $Fo_{90,7}$). The tendency shown by zoning is thus towards Fo_{89-91} from mainly less magnesian phenocryst cores and mainly more magnesian macrocryst cores. Fig. 5a illustrates the convergence of rim compositions on a band of $Fo_{88,4-90,0}$ for phenocrysts (which have core compositions marked by the filled circles). Macrocrysts (Fig. 5b) show the band ($\pm$ 1 s. dev.) for rim compositions shifted to the left of core compositions but there is evidence of reverse and oscillatory zoning particularly among the most magnesian macrocrysts.

Figs 5a and b show that although there is a general

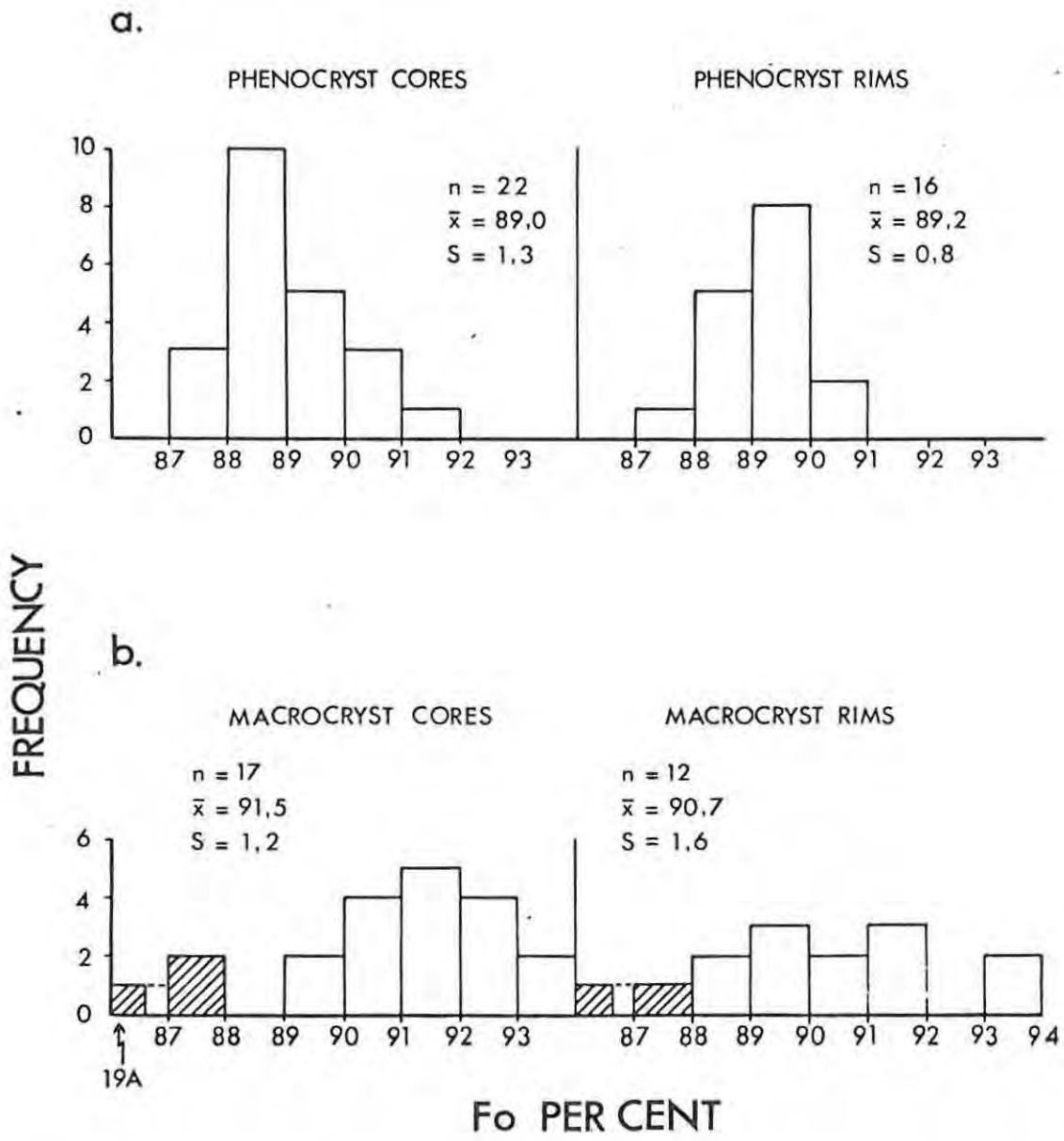

Fig. 4 Histograms showing Fo per cent in cores and rims of
a) Olivine phenocrysts
b) Olivine macrocrysts
from monticellite kimberlite. Statistics are presented for unshaded populations.

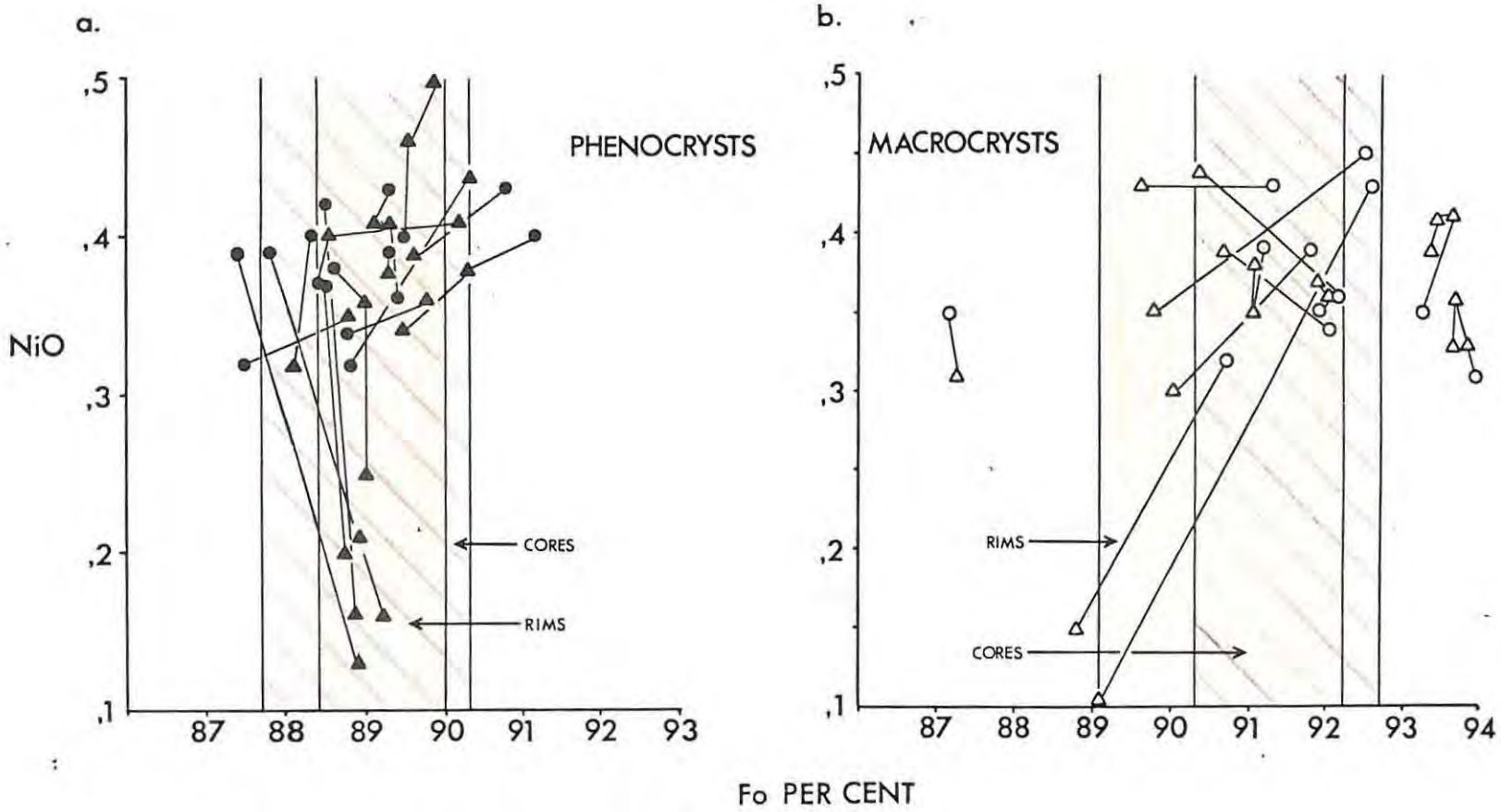

Fig. 5 Variation in NiO and Fo per cent from cores to rims of a) Olivine phenocrysts and b) Olivine macrocrysts in monticellite kimberlite. Bands mark the mean ± 1 standard deviation (statistics from Fig. 4) for core and rim compositions.

tendency for NiO to be depleted in the rims, several phenocrysts and macrocrysts show nickel enrichment in their rims. The variation of NiO, CaO and MnO in core to rim traverses from a selection of phenocrysts and macrocrysts is given in Fig. 6. Phenocrysts commonly show a sharp increase in CaO at their margins. Care was taken to ensure this was a real effect and not due to inadvertent analysis of alteration products or the influence of the matrix.

c) Olivine Granular Aggregates

Analyses from macrocrysts of olivine aggregates (olivine macrocrysts which are not single crystals) found in both kimberlite types, are given in Tables 4 and 5, and Fig. 7 gives the positions of the sub-grains analysed and represents the variation from their cores to rims with respect to NiO, CaO and Fo per cent. NiO content of cores ranges from 0,3 to 0,45 per cent and some grains had Ni-enriched margins while the rims of others are depleted in Ni. Calcium content, however, is always higher at the margins of grains than at their cores, whether the sub-grains are at the edge of macrocrysts (28_3) or internal (28_2). The composition of cores lies between Fo_{90-92} and zoning is towards less magnesian rims. Grain 29 is an unusual iron-and calcium-rich olivine, unique also in its morphology (Plate 4).

d) Discussion

Fig. 8a shows the Dutoitspan olivines in a plot of NiO against MgO, and allows a comparison with olivines of the Karoo Central Igneous Province. There is a broad trend from the low Mg-low Ni olivines of Drumbo Basalt through those of Insizwa, Southern Karoo Dolerites, Elephant's Head and finally the high Mg-high Ni kimberlitic olivines. Fig. 8b is a plot of NiO against Fo per cent, showing average Dutoitspan and average Wesselton and Ison Creek compositions (Mitchell, 1973b), relative to high-Ni olivine in peridotite inclusions and low-Ni olivine from kimberlite dykes and sheets (Emeleus and Andrews, 1975), and melilitites (McIver and Ferguson, 1979, and Moore and Erlank, in press). Also plotted are the compositions of olivine inclusions in diamond (Harris and

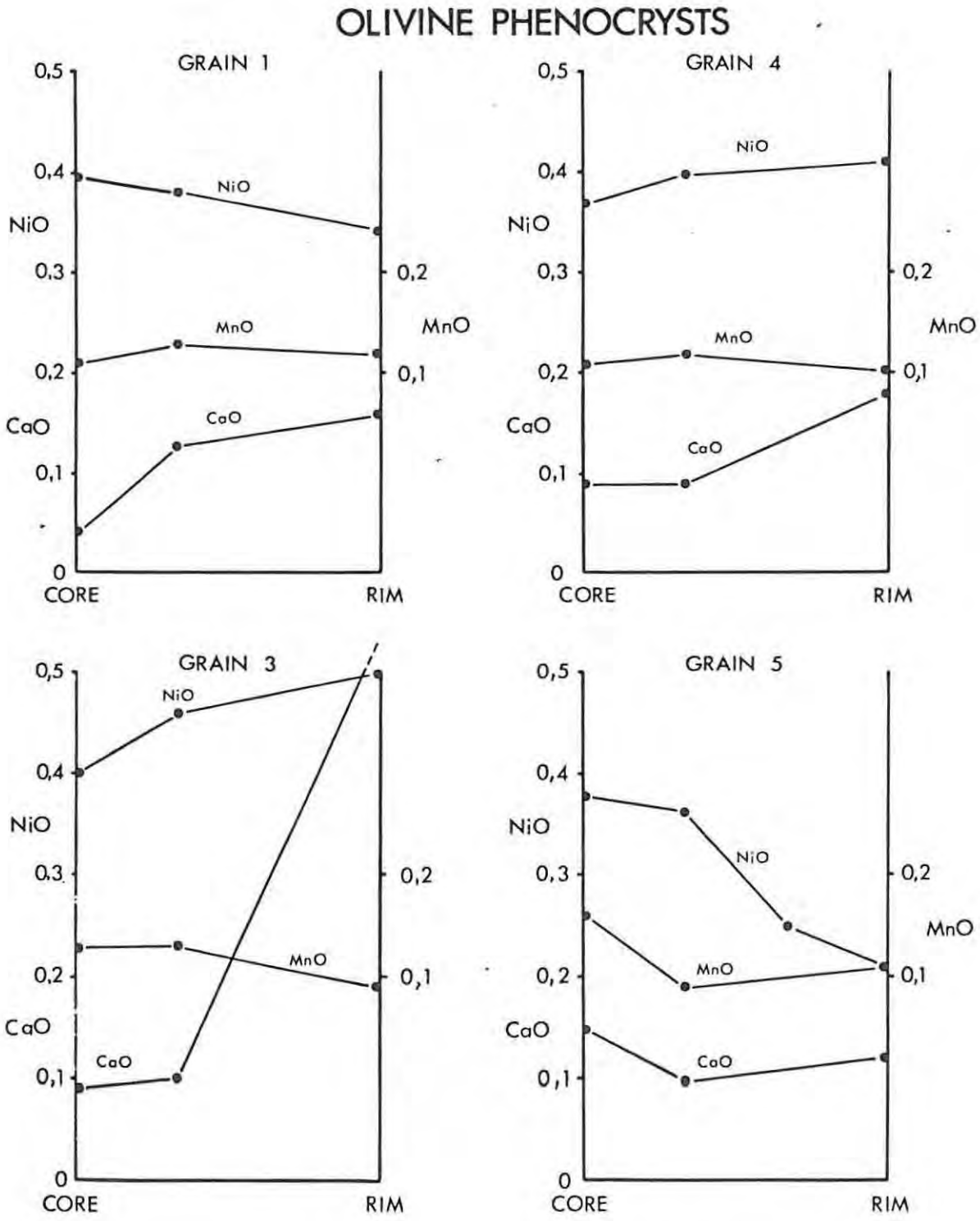

Fig. 6a Variation of NiO, CaO and MnO in core to rim traverses across olivine phenocrysts.

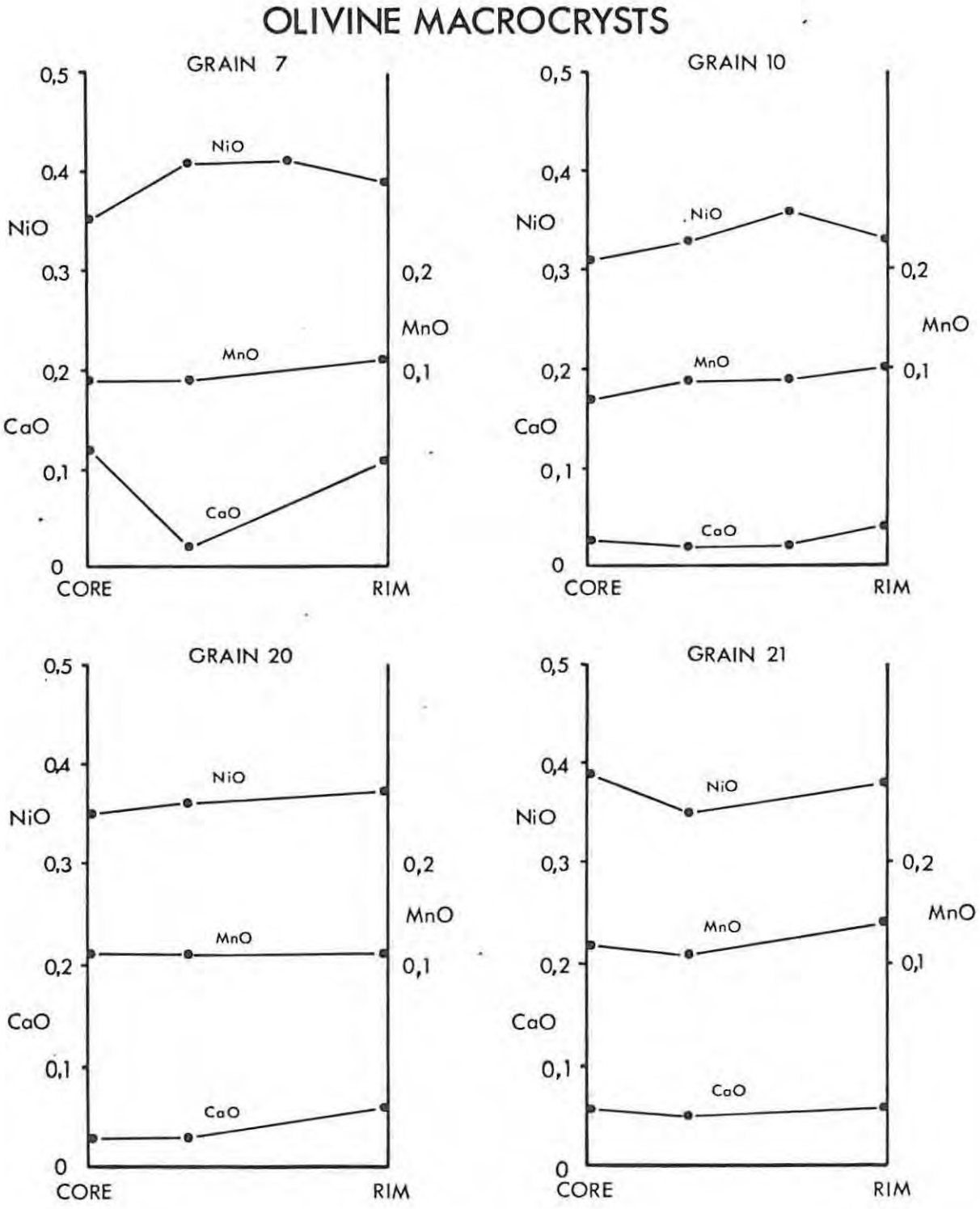

Fig. 6b Variation of NiO, CaO and MnO in core to rim traverses across olivine macrocrysts.

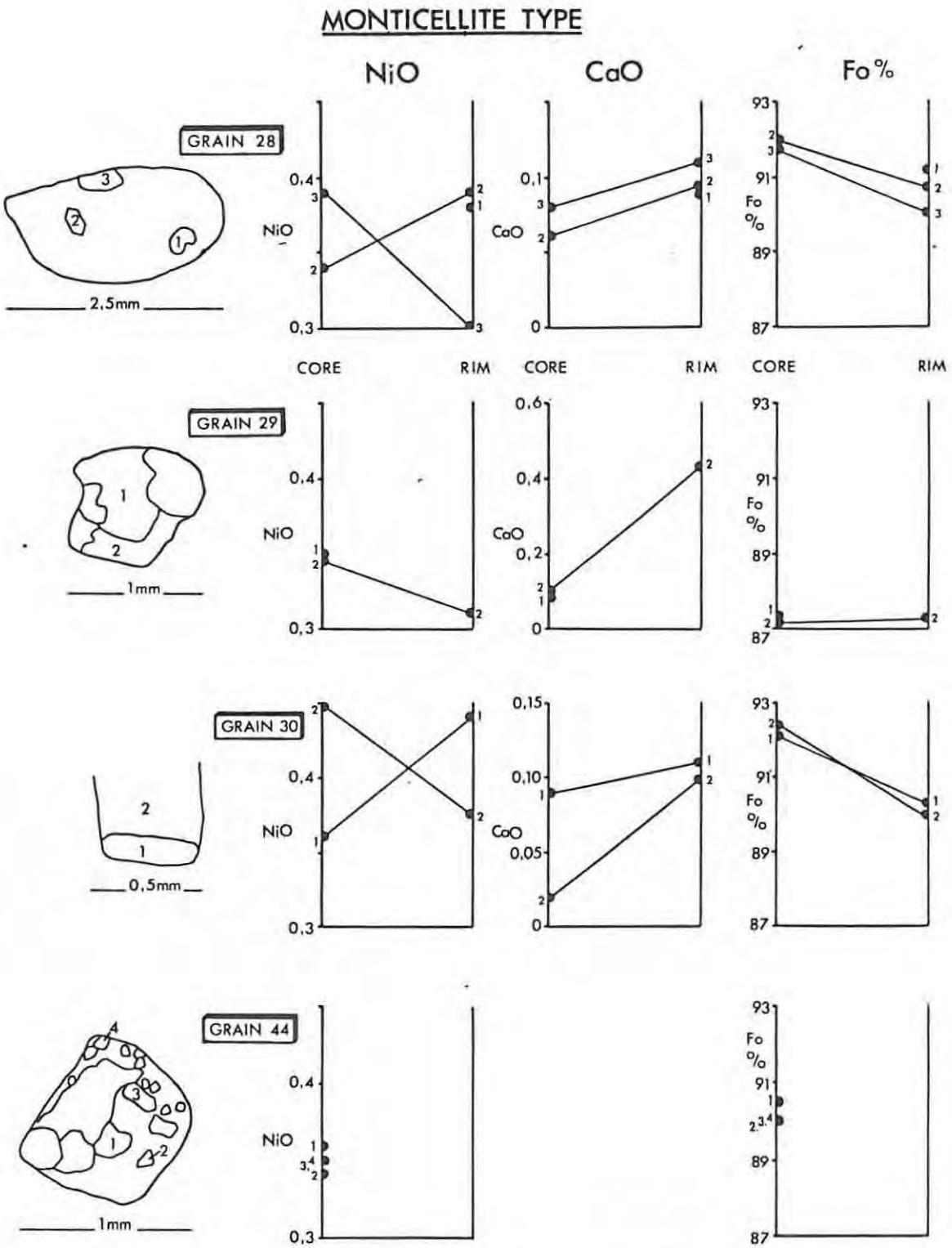

Fig. 7 Diagram illustrating the variation of NiO, CaO and Fo per cent from cores to rims of sub-grains analysed from granular olivine aggregates.

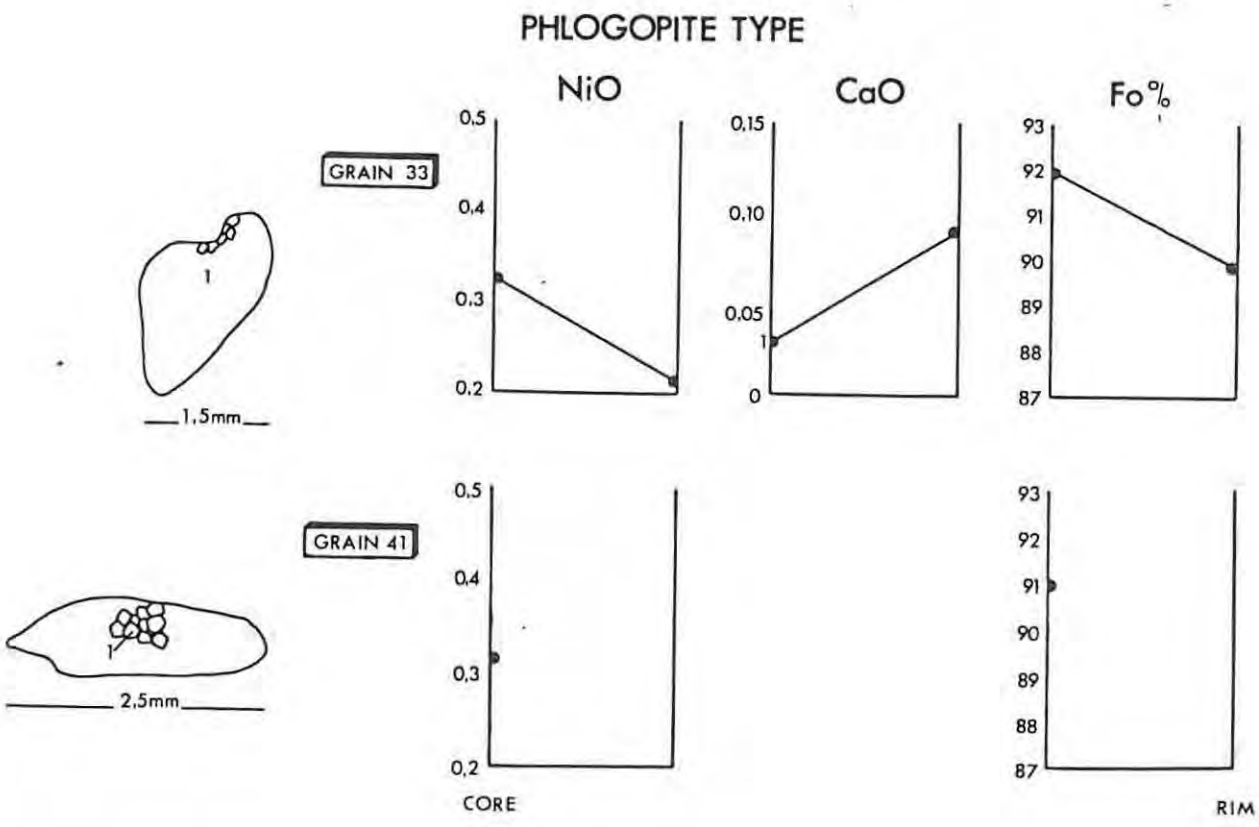

Fig. 7 (continued) Diagram illustrating the variation of NiO, CaO and Fo per cent from cores to rims of sub-grains analysed from granular olivine aggregates.

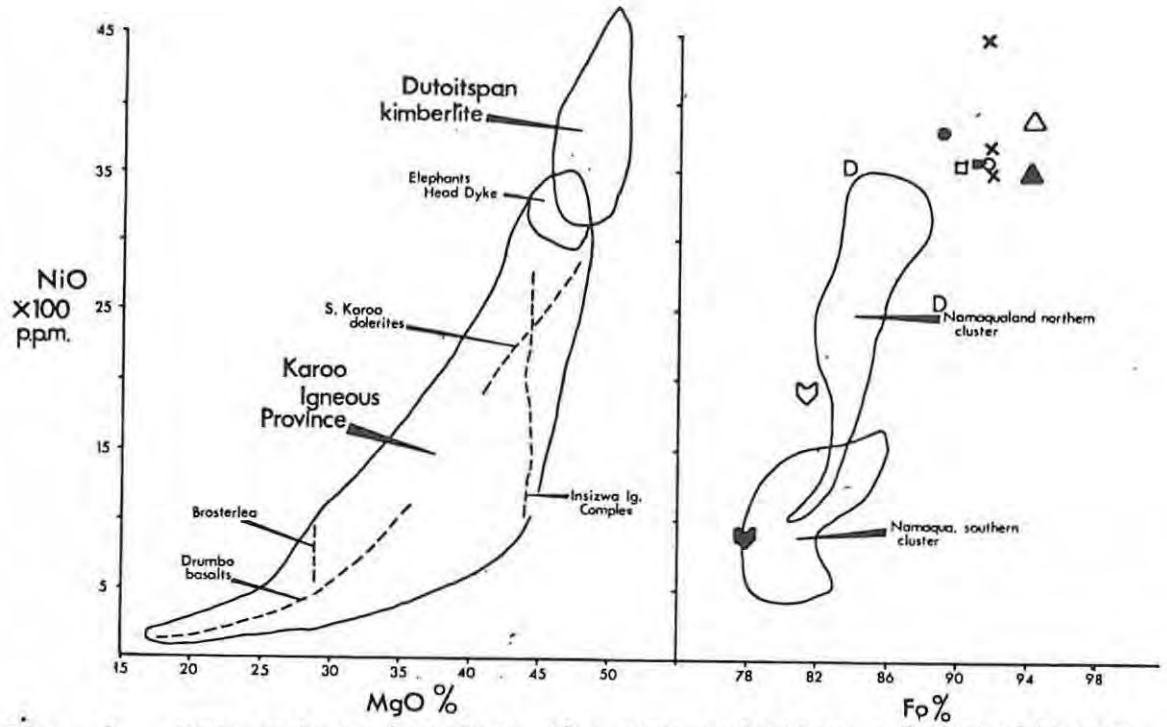

Fig. 8 Comparison between the compositions of Dutoitspan olivines with those from:

a) The Karoo Igneous Province (fields for Karoo data from Mitchell, 1979a).

b) Other kimberlites, average phenocryst compositions

■ Wesselton (Mitchell, 1973b)

□ Ison Creek, Kentucky (Mitchell, 1973b)

Kimberlite dykes and sheets

D W. Greenland (Emeleus and Andrews, 1975)

Olivine melilitites, average olivine compositions

♥ Sutherland, S.A., phenocrysts (McIver and

♡ Sutherland, S.A., megacrysts Ferguson, 1979)

Namaqualand, northern and southern clusters (Moore and Erlank, in press)

Peridotite Inclusions

✕ W. Greenland (Emeleus and Andrews, 1975)

Inclusions in diamond

▲ Finsh (Harris and Gurney, 1979)

△ Koffiefontein (Harris and Gurney, 1979).

Average Dutoitspan olivine phenocr. ● , macrocr. ○

Gurney, 1979). These are more magnesian than the average kimberlitic olivines and compare with the most magnesian olivines reported from peridotite nodules in the Bultfontein pipe (Fig. 9a after Boyd and Nixon, 1978).

The olivine compositions and zoning noted are in accord with observations made by several other workers. Elthon and Ridley (1979) report two groups of olivines, small unzoned grains (Fo_{88-89}) and large zoned grains (Fo_{91-94}) with rims of Fo_{88-89} in a Premier Mine kimberlite. Boyd and Clement (1977) present a detailed study on zoning and note that De Beers Mine kimberlite exhibits homogeneous cores (small grains of Fo_{93-87} and large grains of Fo_{94-84}) and thin zoned margins approaching Fo_{89-90} regardless of core composition. Both normal and reverse zoning are found. Emeleus and Andrews (1975), reporting on olivine from kimberlitic dykes and sheets in W. Greenland, find a range in composition from Mg_{74} to Mg_{92} and zoning which converges on a compositional band around Mg_{87-91}. Kimberlite from Wesselton Mine has phenocrysts of $Fo_{88,5-91}$ and macrocrysts of $Fo_{85,5-94}$ and no olivine less magnesian than Fo_{88} in the groundmass (Mitchell, 1973b). Mitchell (1979) presents histograms summarising data on two kimberlites, one of which is micaceous, from the Tunraq diatreme, and concludes that there is no difference in composition between the olivines from these bodies. The compositional ranges of phenocrysts (called groundmass olivine by Mitchell) and macrocrysts (called phenocrysts by Mitchell) are shown in Fig. 9b (from Mitchell, 1979). There is zoning from Fo_{92-90} cores to Fo_{90-88} rims in early olivine and Fo_{92-90} cores to Fo_{87} margins in groundmass olivine. Reverse zoning from Fo_{86} to Fo_{88} and Ni depletion in some rims is reported (Mitchell, 1979).

The composition of olivines in nodules from the Bultfontein Floors (which are dump areas primarily from the Bultfontein pipe but may include material from Dutoitspan) ranges from Fo_{86-90} in dunite and Fo_{91-94} (with a mode of $Fo_{93,5}$) in peridotite (Boyd and Nixon, 1978). The average olivine macrocryst composition from Dutoitspan ($Fo_{91,5}$) is

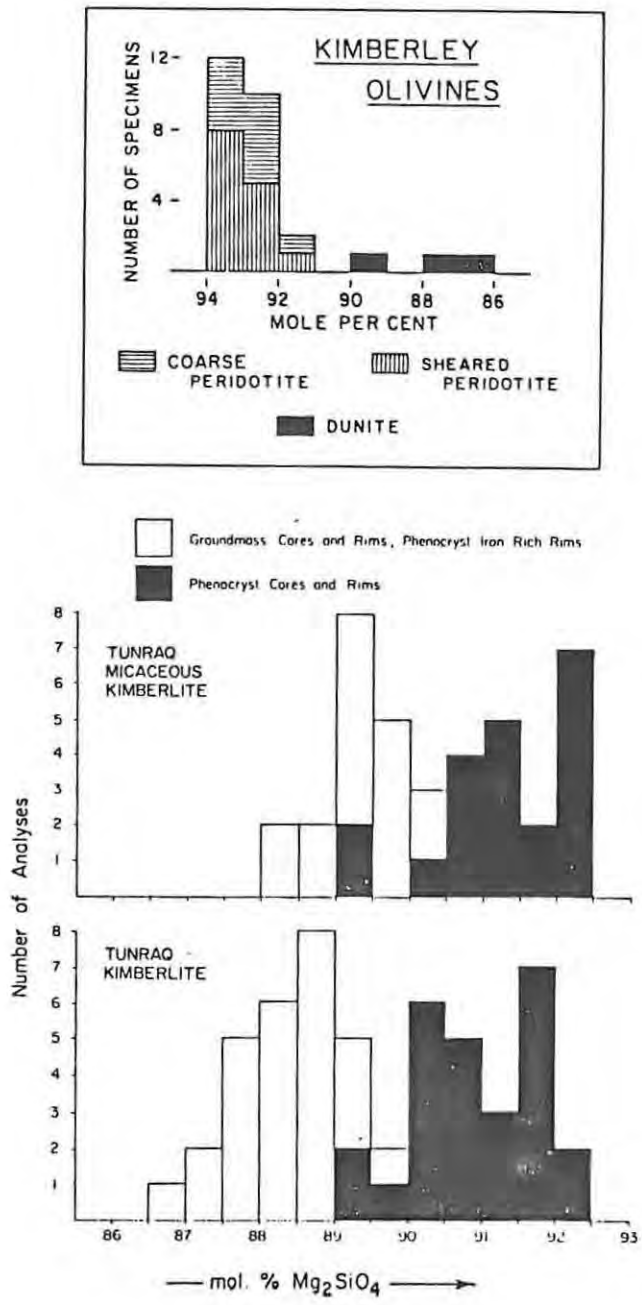

Fig. 9 Distribution of olivines in

a) peridotites and dunites from the Bultfontein Floors (from Boyd and Nixon, 1978).

b) Tunraq kimberlite (after Mitchell, 1979).

less than that of the mode for peridotite nodules. However, one of the iron rich "outliers" (Fo_{87-88} on Fig. 4b) is compositionally akin to the dunite olivine from Bultfontein (Fig. 9a). It is of note that the olivine aggregates described earlier from Dutoitspan have a restricted range of Fo_{90-92} which corresponds with the range of macrocryst compositions in the same kimberlite (Fig 4b) but coincides with the gap between the dunite and peridotite olivine compositions from the Bultfontein nodules (Fig. 9a) analysed by Boyd and Nixon (1978). It would normally be assumed that the mantle sample from adjoining pipes of similar age is very likely to have common characteristics and, indeed, some of the nodules may actually be from Dutoitspan itself. Thus, if the Dutoitspan olivine macrocrysts were derived from disaggregated peridotite nodules, they would be expected to have the same compositional distribution as the olivines from the Bultfontein nodules. But, based on the analyses available (and with the exception of the Fe-rich macrocryst which could be derived from disaggregated dunite) they do not show evidence for such a correlation.

e) Model for Olivine Generation

An understanding of the deformation of olivine in the macrocrysts and aggregates described should provide information on the structural evolution of the Dutoitspan kimberlites, which, together with compositional evidence in comparison with that of mantle xenoliths, can be used to formulate a model for the generation of the olivine.

In kimberlite, garnet lherzolite xenoliths are dominant (olivine = 60-70 per cent, enstatite = 20-25 per cent and diopside = 5-10 per cent) and are believed to represent fragments from depths of up to 200 km (Nicolas and Poirier, 1976). The tectonic or recrystallised textures they exhibit may result not from plate motion, but may be of local origin due to diapiric intrusions and are thought by Nicolas and Poirier (1976) not to be modified by intrusion processes.

Nicolas and Poirier (1976) describe three main textures

in these nodules. Coarse granular and coarse tabular textures with characteristic curvilinear grain boundaries, and porphyroclastic textures exhibiting large grains (8 x 2 mm) with numerous subgrains (0,5 mm) and later-formed polygonal, strain-free neoblasts (0,5 mm) are typical of the textures of granular lherzolites (Nixon and Boyd, 1973 a and b and Boyd and Nixon, 1978). The third texture described by Nicolas and Poirier (1976) is a mosaic texture where olivine is entirely crystallised into a mosaic of small polygonal grains (0,07 mm) and is equivalent to the flaser or submylonitic textures described by Nixon and Boyd (1973a) from sheared lherzolites. The mosaic texture is interpreted by Nicolas and Poirier (1976) as evidence of extensive plastic flow at 1400° C and 60 kbars (Boyd and Nixon, 1972 and MacGregor, 1974 in Nicolas and Poirier, 1976) resulting from increased deformation of porphyroclastic-textured material. The mosaic texture then grades progressively into a fluidal-mosaic texture where strain estimated at 800 to 900 per cent is believed to be attributable to super-plastic flow (Boullier and Nicolas, 1975).

Chemical differences between granular lherzolites and sheared lherzolites (sterile and fertile nodules respectively of Rogers, 1979) exist and these are outlined by Nixon and Boyd (1973a). Granular lherzolites are compositionally equivalent to upper mantle material which has been depleted in the constituents Na, Ti, Fe, Ca and Al. Sheared lherzolites correspond to the less depleted shear zones of the asthenosphere according to Boyd and Nixon (1972; 1973) and Boyd (1973, in Nixon and Boyd, 1973a). Boullier and Nicolas (1973) believe that the sheared lherzolites are derived from the granular lherzolites by deformation and explain chemical and mineralogical differences between the groups by mechanical disruption of interlayered granular peridotites and griquaites, clinopyroxene and garnet monomineralic beds

Nixon and Boyd (1973b) describe a discrete nodule association in Lesotho kimberlites. Olivine in this association occurs as monomineralic nodules with a mosaic texture

and is thought by these authors to have formed as phenocrysts in crystal-mush magmas in the Low Velocity Zone and subsequently become incorporated in kimberlites during eruption. According to Nixon and Boyd (1973b) the kimberlites of Northern Lesotho appear to have originated in the asthenosphere at depths of the order of 200 km. During the course of eruption they picked up mantle rocks including sheared lherzolites and phenocrysts from crystal-mush magmas in the Low Velocity Zone. They then acquired granular garnet lherzolites from the lithosphere and lastly granulites and other crustal rocks In effect discrete nodules are thus phenocrysts in kimberlite magma.

Nodules from the Kimberley mines do not appear to include Lesotho-type discrete nodules. Kimberley lherzolites have relatively low equilibration temperatures (less than 1100°C) and contain coarse phlogopite, a feature which contrasts with the absence of this mineral from high-temperature (greater than 1100°C) sheared peridotites from other areas (Boyd and Nixon, 1978).

Average olivine compositions and compositional ranges from the different nodules and other occurrences are ranked in the order of Fo per cent as follows.

Discrete nodule association	Fo_{87}	(Nixon and Boyd, 1973b)
Dutoitspan Fe-rich "outlier"	Fo_{87-88}	(this study)
Dutoitspan phenocrysts	Fo_{89}	(this study)
Sheared nodules	Fo_{90}	(Fo_{87-92}: Nixon and Boyd, 1973a)
	$Fo_{92,5}$	(Fo_{91-94}: Boyd and Nixon, 1978)
Dutoitspan granular aggregates	Fo_{91}	(Fo_{90-92}: this study)
Dutoitspan macrocrysts	$Fo_{91,5}$	(Fo_{90-94}: this study)
Granular nodules	Fo_{93}	(Fo_{92-94}: Nixon and Boyd, 1973a)
	$Fo_{92,5}$	(Fo_{91-94}: Boyd and Nixon, 1978)

The olivine granular aggregates at Dutoitspan (as illustrated in Plates 2 and 3) exhibit textures which appear to conform to the description of mosaic texture (Nicolas and Poirier, 1976), which implies that they are derived from sheared nodules. The composition of the observed aggregates is close to that of olivine reported from sheared nodules as listed above. The range of compositions of Dutoitspan macrocrysts (Fo_{90-94}) straddles compositions intermediate between sheared and granular nodules, whereas phenocrysts are less magnesian in general than any olivine of nodule origin. The Fe-rich "outlier" analysed (Fo_{87-88}) could represent part of a discrete nodule (Fo_{87} average) although the curvilinear grain boundaries do suggest a coarse granular texture (Nicolas and Poirier, 1976). It is possible that this grain is part of a granular-textured dunite, as olivine in dunite from the Bultfontein nodules ranges in composition from Fo_{86}-Fo_{90} (Boyd and Nixon, 1978).

Thus it is suggested here that the Dutoitspan olivine aggregates are derived from sheared mantle lherzolite and the single-crystal macrocrysts which have not undergone recrystallisation were formed at higher mantle levels in a kimberlitic crystal-mush magma which had incorporated the aggregates from greater depths. Some granular lherzolite or dunite could have been incorporated as the magma rose to higher levels still. Sudden, fluidized emplacement of the magma into the crust caused rounding of the olivine crystals already present and, unless they were deformed while at mantle levels, possibly gave rise to some of the strain textures evident as strain shadows and deformation lamellae in some of the macrocrysts. The second generation of kimberlitic olivine crystallised as euhedral phenocrysts at the lower crustal temperatures and pressures and lower overall magnesium concentration in the magma. Further cooling and changes in conditions led to the start of re-equilibration of all the olivine but, as indicated by the thin zoned margins, this process was quickly arrested. Local fluctuations in magma conditions caused reverse and oscillatory zoning. Depending on the amount of fluid present, secondary alteration of the olivine to serpentine proceeded and, in the case of the phlogopite kimberlite, caused extensive pseudomorphism of both phenocrysts and

macrocrysts.

2. Phlogopite

a) Variations in phlogopite chemistry

Microprobe analyses of phlogopites, mainly from the phlogopite kimberlite, but also from the monticellite kimberlite are presented in Tables 6 (phenocrysts) and 7 (macrocrysts). The phenocrysts are primary in texture that is there is no evidence of recrystallisation, except for grain 10 (an euhedral phlogopite lath in a mica cluster surrounding a rounded mauve garnet with a kelyphitic rim), and grains 25 and 26 (secondary flakes formed by the recrystallisation of a larger relict phlogopite plate). Grain 24 is a very fine-grained matrix phlogopite, not obviously secondary in texture, but chemically similar to the recrystallised material nearby (25 and 26). Most of the phenocrysts are euhedral to subhedral and undeformed. Macrocryst plates, also "primary textured", are frequently deformed and usually rounded. Zoning is of two types - more commonly from a dark brown core (2A and 2B) to a bleached rim (2C) but analyses of a bleached core (22A) and a dark-brown rim (22B) are also given (Table 7). In both cases, the rims are relatively TiO_2 enriched. Grain 17 (Table 7) has a dark core with reversed pleochroism and a bleached rim. The analyses of grains 17 and 22A require Fe^{3+} in tetrahedral co-ordination in order to satisfy the theoretical formula.

Variations in phlogopite composition are illustrated in Fig. 10. Fig. 10a shows a separation of the two fields - relatively Fe-enriched macrocrysts and low-Fe phenocrysts. The ratio Si/Al provides an efficient discriminator between most members of the two groups. Only two macrocrysts have a Si/Al ratio less than 3,25 and three phenocrysts have ratios greater than this. Note that the zoning of macrocrysts is towards the phenocryst compositions, that is macrocryst cores have more FeO than the rims.

Fig. 10b shows there is TiO_2 and Cr_2O_3 enrichment of

Table 6 Microprobe Analyses of Phlogopite Phenocrysts in Phlogopite and Monticellite Kimberlite

Oxide	5	6	7	10	11	12	13	16	18	19	21	23	24	25	26
SiO_2	42,05	40,78	41,63	39,90	39,35	39,98	39,28	43,36	40,19	40,54	39,65	40,08	40,59	39,23	39,10
TiO_2	1,23	0,37	2,13	2,02	2,77	3,57	4,08	3,04	3,11	2,98	2,98	0,80	0,13	0,30	n.d.
Al_2O_3	11,30	13,15	12,09	12,94	13,34	12,18	13,50	12,55	12,94	12,71	13,16	9,89	11,10	12,90	11,09
FeO_{total}	4,56	3,34	3,95	3,30	3,83	4,32	4,56	4,44	3,89	4,49	3,64	6,45	3,50	3,21	3,28
MgO	23,80	24,14	22,63	23,24	22,07	22,51	21,30	25,37	22,62	23,16	22,23	23,95	26,15	25,09	25,84
CaO	0,00	0,00	0,00	-	-	-	-	-	-	-	-	-	-	-	-
Na_2O	0,37	0,91	0,27	0,33	0,46	0,48	0,42	0,10	0,05	0,03	0,05	0,05	0,00	-	0,01
K_2O	10,23	9,16	10,08	10,11	10,08	9,62	10,07	7,74	10,05	10,00	9,94	9,24	10,20	10,04	9,39
Cr_2O_3	0,01	0,34	0,04	1,48	1,18	0,96	1,20	0,44	0,74	0,99	1,75	0,00	0,06	-	0,00
NiO	0,01	0,24	0,18	0,19	0,02	0,07	0,22	0,11	0,15	0,17	0,23	0,07	0,13	0,04	0,09
Total	93,73	92,42	93,35	93,49	93,29	93,68	94,62	97,15	93,74	95,07	93,63	90,53	91,86	90,81	88,80
Cations															
Si	6,16	5,96	6,16	5,85	5,85	5,90	5,80	5,93	5,89	5,86	5,83	6,00	5,92	5,79	5,85
Al	1,84	2,04	1,84	2,15	2,15	2,10	2,20	2,02	2,11	2,14	2,28	1,75	1,91	2,21	1,96
Fe^{3+}	0,00	0,00	0,00	0,00	0,00	0,00	0,00	0,00	0,00	0,00	0,00	0,16	0,15	0,00	0,19
Ti	0,00	0,00	0,00	0,00	0,00	0,00	0,00	0,05	0,00	0,00	0,00	0,09	0,02	0,00	0,00
Sum tet.	8,00	8,00	8,00	8,00	8,00	8,00	8,00	8,00	8,00	8,00	8,00	8,00	8,00	8,00	8,00
Al	0,12	0,23	0,28	0,09	0,19	0,01	0,14	0,00	0,13	0,03	0,11	0,00	0,00	0,05	0,00
Fe^{2+}	0,56	0,40	0,49	0,41	0,47	0,53	0,56	0,51	0,48	0,54	0,45	0,65	0,28	0,40	0,23
Mg	5,19	5,26	4,99	5,08	4,88	4,95	4,68	5,17	4,94	4,99	4,87	5,35	5,69	5,52	5,76
Ti	0,13	0,04	0,24	0,22	0,31	0,40	0,45	0,27	0,34	0,32	0,33	0,00	0,00	0,04	0,00
Cr	-	0,04	-	0,18	0,14	0,11	0,14	0,05	0,09	0,10	0,21	0,00	0,01	0,00	0,00
Ni	-	0,03	-	0,03	-	-	0,03	0,01	0,02	0,02	0,03	0,01	0,03	0,00	0,01
Sum oct.	6,00	6,00	6,00	6,01	5,99	6,00	6,00	6,01	6,00	6,00	6,00	6,01	6,01	6,01	6,00
Na	0,11	0,26	0,07	0,09	0,12	0,14	0,12	0,03	0,02	0,01	0,01	0,02	0,00	0,00	0,00
K	1,92	1,70	1,90	1,89	1,91	1,81	1,90	1,35	1,89	1,84	1,87	1,76	1,90	1,90	1,80
Sum int.	2,03	1,96	1,97	1,98	2,03	1,95	2,02	1,38	1,91	1,85	1,88	1,78	1,90	1,90	1,80
Si/Al	3,35	2,92	3,35	2,72	2,72	2,81	2,64	2,94	2,79	2,74	2,56	3,43	3,10	2,62	2,98
$Mg/Mg+Fe^{2+}$	0,90	0,93	0,91	0,93	0,91	0,90	0,89	0,91	0,91	0,90	0,92	0,89	0,95	0,93	0,96

Note: Phlogopite Kimberlite. Grains 5-7 are from sample 740/10, 10-13 from 580/18. 18,19 and 21 from 580/22 and grains 23-26 from 740/6. Monticellite Kimberlite. Grain 16 is from the contact phase, 580/1A. All are primary except grain 10, in the alteration rim around mauve garnet and grains 25 and 26, in relict phlogopite.

Table 7 Microprobe Analyses of Phlogopite Macrocrysts in Phlogopite and Monticellite Kimberlite

Oxide	1	14	2A	2B	2C	3	4	8	9	15	17	20	22A	22B
SiO_2	42,17	42,00	43,54	42,36	41,72	42,18	42,33	41,62	41,16	43,71	43,17	41,81	41,76	38,93
TiO_2	0,83	1,25	1,11	1,09	2,12	0,46	0,39	0,42	0,40	2,40	0,42	0,39	0,43	4,01
Al_2O_3	11,20	10,49	9,18	9,14	11,04	10,37	9,96	10,15	9,81	12,04	10,42	8,85	9,66	12,35
FeO_{total}	4,28	7,13	7,32	7,63	5,29	5,20	6,08	5,78	6,24	3,97	5,76	7,47	5,95	4,29
MgO	25,41	23,00	23,26	22,78	23,19	24,75	24,44	25,32	24,84	27,18	25,36	24,56	24,69	22,46
CaO	0,00	0,00	0,00	0,00	0,25	0,00	0,00	-	-	-	-	-	-	-
Na_2O	0,11	0,27	0,81	0,79	0,18	0,22	0,15	0,18	0,23	0,35	0,15	0,05	0,03	0,03
K_2O	10,46	10,35	10,22	10,19	10,21	10,33	10,45	10,37	10,46	7,29	10,38	10,09	10,18	10,11
Cr_2O_3	0,06	0,01	0,05	0,05	0,02	0,08	0,04	0,11	0,11	0,56	0,11	0,07	0,12	1,10
NiO	0,08	0,17	0,11	0,12	0,07	0,16	0,12	0,09	0,01	0,14	0,10	0,13	0,08	0,07
Total	94,59	94,74	95,59	94,14	94,08	93,76	93,97	94,02	93,36	97,64	95,91	93,42	92,90	93,35
Cations														
Si	6,06	6,15	6,35	6,29	6,13	6,15	6,17	6,03	6,05	5,88	6,13	6,13	6,13	5,76
Al	1,90	1,81	1,58	1,61	1,87	1,79	1,72	1,74	1,69	1,91	1,74	1,53	1,68	2,17
Fe^{3+}	0,00	0,00	0,00	0,00	0,00	0,00	0,07	0,19	0,22	0,00	0,09	0,30	0,16	0,00
Ti	0,04	0,04	0,07	0,10	0,00	0,05	0,04	0,04	0,04	0,21	0,04	0,04	0,04	0,07
Sum tet.	8,00	8,00	8,00	8,00	8,00	7,99	8,00	8,00	8,00	8,00	8,00	8,00	8,01	8,00
Al	0,00	0,00	0,00	0,00	0,04	0,00	0,00	0,00	0,00	0,00	0,00	0,00	0,00	0,00
Fe^{2+}	0,52	0,87	0,89	0,95	0,65	0,63	0,68	0,51	0,55	0,44	0,59	0,62	0,57	0,53
Mg	5,20	5,02	5,06	5,04	5,07	5,38	5,32	5,47	5,44	5,45	5,37	5,36	5,40	4,95
Ti	0,05	0,10	0,05	0,02	0,24	0,00	0,00	0,00	0,00	0,03	0,00	0,00	0,00	0,38
Cr	0,00	0,00	0,00	0,00	0,00	0,00	-	0,01	0,01	0,07	0,02	0,01	0,01	0,12
Ni	0,00	0,00	0,00	0,00	0,00	0,00	-	0,01	0,00	0,02	0,01	0,02	0,01	0,01
Sum oct.	6,01	5,99	6,00	6,01	6,00	6,01	6,00	6,00	6,00	6,01	5,99	6,01	5,99	5,99
Na	0,03	0,07	0,23	0,23	0,05	0,06	0,04	0,05	0,07	0,10	0,03	0,01	0,01	0,01
K	1,91	1,94	1,89	1,93	1,91	1,93	1,95	1,91	1,96	1,25	1,88	1,88	1,91	1,90
Sum int.	1,94	2,01	2,12	2,16	2,00*	1,99	1,99	1,96	2,03	1,35	1,91	1,89	1,92	1,91
Si/Al	3,20	3,40	4,02	3,91	3,28	3,44	3,59	3,47	3,58	3,08	3,52	4,00	3,65	2,65
$Mg/Mg+Fe^{2+}$	0,91	0,85	0,85	0,84	0,89	0,90	0,89	0,91	0,91	0,93	0,90	0,90	0,90	0,90

* Includes Ca = 0,04

Note: A, B and C denote analyses from the core (A) outwards to the rim of a given grain.
Phlogopite Kimberlite. Grains 1, 14, 2, 3, and 4 are from sample 740/10, grains 8 and 9 are from 580/18, and grains 20 and 22 from 580/22. Monticellite Kimberlite. Grains 15 and 17 are from the contact phase 580/1A.

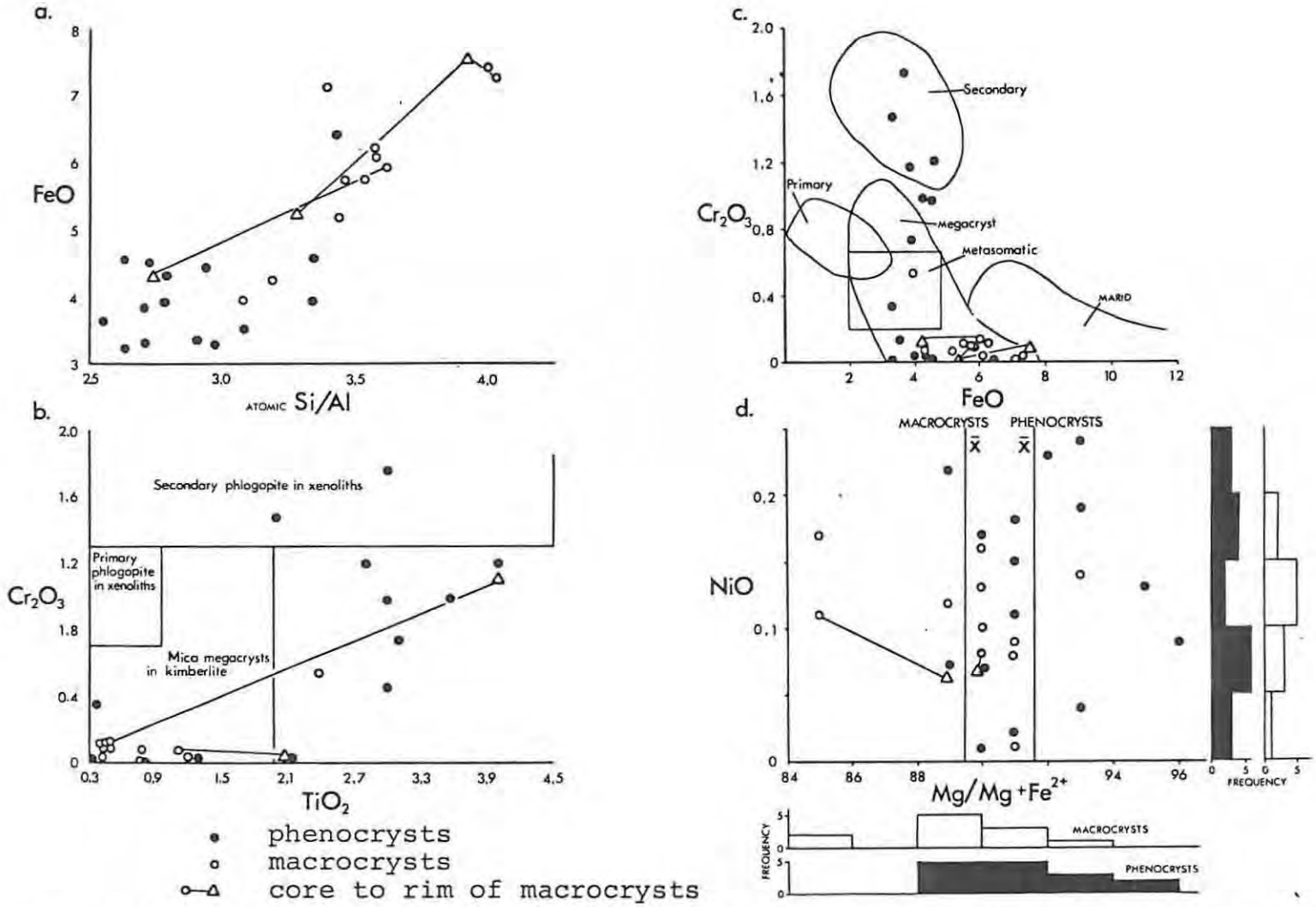

Fig. 10 Chemical variations in phlogopite. a) Total Fe as FeO (weight per cent) vs. atomic Si/Al. b) Cr_2O_3 vs. TiO_2 (weight per cent). Compositional fields after Dawson and Smith, and Carswell, both in Mitchell (1979). c) Cr_2O_3 vs. total Fe as FeO (weight per cent). Compositional fields from Dawson and Smith (1977). d) NiO (weight per cent) vs. atomic Mg/Mg+Fe, and histograms summarising the distribution of both parameters. Phenocrysts have the greater mean Mg/Mg+Fe ratio.

phenocrysts relative to macrocrysts, although there is some overlap in Ti content. Macrocrysts are depleted in Cr_2O_3, all except grain 15 from the monticellite type showing less than 0,2 per cent. The secondary phlogopite surrounding garnet is one of the two grains analysed that are highly enriched in Cr_2O_3 (Cr_2O_3 = 1,48 per cent, TiO_2 = 2,02 per cent).

Fig. 10c shows the separation of low Cr_2O_3 macrocrysts (over a range of FeO compositions) from phenocrysts, which show a wide spread in Cr_2O_3 content. The variation in NiO against $Mg/Mg+Fe^{2+}$ shows a considerable overlap between the two types of phlogopite. However, the frequency tables show that the macrocrysts have lower Mg/Mg+Fe ratios on average. There is no distinction on a basis of NiO content. The zoned macrocryst analysed (grain 2) has lower NiO and higher Mg/Mg+Fe in the rim.

The compositional fields superimposed on Figs. 10b and c are from other workers (Dawson and Smith, 1977; Mitchell, 1979). Most of the present analyses fall into the fields labelled 'macrocrysts'. The fields for primary and secondary phlogopite from xenoliths are shown on Figs. 10b and 10c. A few data points stray into the secondary phlogopite field but only grain 10 has the texture to support this classification. There are no analyses of primary phlogopite from xenoliths.

b) Discussion

Much work on phlogopite is quoted in the literature, starting with workers on nodules (including Carswell, 1975; Harte et al., 1975; Boettcher et al., 1977; Dawson and Smith, 1977; Boyd and Nixon, 1978; and Danchin, 1979) then workers on kimberlite matrix (Watson et al., 1978; Smith et al., 1978; Mitchell, 1978 and 1979. Elthon and Ridley, 1979 and Delaney et al., 1980). The consensus of opinion on the composition of phlogopite in nodules is that there are two types. These are termed primary and secondary textures by Delaney et al. 1980). Their primary phlogopite (FeO < 3,5 per cent, TiO_2 <

1,4 per cent) equates with the pale 'primary' phlogopite of Danchin (1979) and the 'mantle-derived' phlogopite of Boyd and Nixon (1978), which is coarse, deformed mica that has been sheared before incorporation in kimberlite magma. Secondary-textured phlogopite includes that found around the kelyphitic rims of garnets and in veinlets (Delaney et al., 1980). Secondary phlogopite around garnet is enriched in TiO_2 and/or Cr_2O_3 (Boyd and Nixon, 1978; Boettcher et al., 1977; Delaney et al., 1980 and Carswell, 1975). Boettcher et al. (1977) attribute such secondary material to pervasive metasomatism by fluids prior to or during anatexis leading to the generation of kimberlite magma. Veinlet phlogopite has low Cr_2O_3 and substantial Fe^{3+} in tetrahedral sites (Delaney et al., 1980). Harte and Gurney (1975) in Delaney et al. (1980) found, in addition to obviously secondary phlogopite, primary textured metasomatic phlogopite in veins and Delaney et al. (1980) interpret the texture in terms of "prolonged annealing following incursion of metasomatising fluid"; this type is distinct from the primary mantle-derived phlogopite.

Phlogopite which has crystallised from kimberlite magma is texturally classified by Mitchell (1979) and Elthon and Ridley (1979) in terms equivalent to macrocrysts and phenocrysts, as defined in the introduction of the present work, but no chemical distinction is given except that Mitchell (1979) reports an evolutionary trend towards lower TiO_2 and Cr_2O_3. The field labelled 'megacryst' on Figs. 10b and 10c generally embraces the compositions of published kimberlite-matrix phlogopites but Smith et al. (1978) and Mitchell (1979) have data reaching higher TiO_2 and Cr_2O_3 compositions. The present data also suggest that the megacryst field of Dawson and Smith (1977) should be enlarged to include higher levels of TiO_2 and Cr_2O_3. This field straddles the compositions of low-Cr_2O_3 macrocrysts and higher (more variable)-Cr_2O_3 phenocrysts. In terms of evolutionary trend, the data presented are somewhat surprising. The macrocrysts which are deformed and rounded (probably during fluidisation and emplacement of

kimberlite) pre-date the smaller, euhedral undeformed phenocrysts yet they are more Fe-rich than the phenocrysts and are zoned towards low-Fe, high-Ti, high-Cr rims, compositionally comparable with the second-generation mica. This contradicts the reference Mitchell (1979) makes of evolution towards lower TiO_2 and Cr_2O_3. He does not distinguish grains on a basis of textural differences so it is not possible to correlate his data with either the megacryst or phenocryst populations shown. However, Smith et al. (1978) present detailed information on three size classes of their so-called Type II micas. The largest grains (> 0,5 mm^2) can be correlated chemically with the macrocrysts on Figs. 10b and 10c because of their low Cr_2O_3 content - and the smaller size categories with the phenocryst trend, although the spread of data from Smith et al. (1978) suffices to stress the wide variability of micas. The Type I micas they identify as resulting from an intrusive precursor are more Fe-rich than any of the analyses from Dutoitspan.

c) Model for phlogopite generation

Smith et al., (1978) suggest that (a) the variations of Cr_2O_3 in the micas may result from competition with tiny euhedral chromite grains crystallising simultaneously with the mica, (b) ilmenite and perovskite affect Ti content and (c) serpentine affects Ni content. The same reasoning could be used to explain variations in FeO. Early phlogopite macrocrysts crystallising together with macrocrystic olivine would be in competition for Mg. It would appear that the partition coefficient is higher for Mg entering olivine. The phlogopite would be relatively depleted in Mg, and Fe^{2+} would enter the mica instead. At a later stage, after the abundant olivine macrocrysts have ceased crystallisation, there would be more Mg allowed into the mica phenocrysts and the rims around macrocrysts, hence the later crystallising phlogopite, although derived from the same kimberlite magma, would be more Mg-rich than the earlier generation of mica.

3. Monticellite

a) Monticellite Chemistry

Analyses of monticellite in Dutoitspan monticellite kimberlite (Table 8) are from a particularly carefully prepared polished sample. Except for grain 2, which is rounded, good to moderate crystal form is shown by all of the grains analysed.

No zoning is apparent, analyses 5A and 5B being virtually identical, and there is remarkably consistent agreement between grains, the only fluctuation being in the allocation of Fe^{2+} and Mg as shown in the cationic formulae in Table 6.

b) Discussion

Clement et al. (1975) have identified monticellite in the groundmass of two kimberlites from the De Beers Mine and present microprobe analyses, the mean of which is very comparable with (if slightly less calcic than) the Dutoitspan mean (see Table 8). They refer to increasing Fe content with decreasing grain size, suggestive of Fe-enrichment during monticellite crystallisation. This trend is not confirmed by the present data in which grains are ranked in size as follows:

1 = 5 > 2 > 4 > 3

Mitchell (1978) reports abundant monticellite, with some grains being zoned from Fe-rich cores to Fe-poor margins, in the Elwin Bay kimberlite and shows variation of up to 18 mole per cent $CaFeSiO_4$ and 10 per cent Mg_2SiO_4 among analyses of monticellite grains. Unlike Mitchell's (1978) data the Dutoitspan analyses in Table 8 have only negligible Mg_2SiO_4 and plot close to the base line of the triangular diagram, Mg_2SiO_4 - $CaFeSiO_4$ - $CaMgSiO_4$ (Fig. 11).

The results of Warner and Luth (1973) imply that there is limited mutual solution between $CaMgSiO_4$ and Mg_2SiO_4. The maximum amount of $CaMgSiO_4$ which may be dissolved in Mg_2SiO_4 (forsteritic olivine) is less than 5 mole per cent

Table 8 Microprobe Analyses of Monticellite

Oxides	1	2	3	4	5A	5B	Mean	6	7
SiO_2	37,41	37,93	36,92	37,31	37,07	37,15	37,29	37,61	36,48
Al_2O_3	-	-	-	-	-	-	-	0,03	0,02
FeO_{total}	5,88	3,76	4,43	3,36	3,80	3,88	4,19	3,99	8,96
MnO	0,27	0,29	0,22	0,28	0,13	0,13	0,22	-	-
MgO	22,16	23,03	22,72	23,73	22,98	23,00	22,94	23,91	20,70
CaO	34,92	35,24	35,04	34,93	35,14	35,09	35,06	34,12	32,96
Total	100,64	100,25	99,33	99,61	99,12	99,24	99,70	99,66	99,12
Cations (on the basis of 4 O)									
Si	0,99	1,00	0,99	0,99	0,99	0,99	0,99	1,00	0,99
Al	-	-	-	-	-	-	-	0,00	0,00
Fe	0,13	0,08	0,10	0,07	0,08	0,09	0,09	0,09	0,20
Mn	0,00	0,01	0,00	0,00	0,00	0,00	0,00	-	-
Mg	0,88	0,91	0,91	0,94	0,92	0,92	0,91	0,95	0,84
Ca	1,00	1,00	1,01	1,00	1,01	1,00	1,00	0,97	0,96
Total	3,00	3,00	3,01	3,00	3,00	3,00	2,99	3,01	2,99
Mol.% end members									
$CaFeSiO_4$	13,0	8,4	10,0	7,5	8,5	8,7	9,4	8,8	20,0
$CaMgSiO_4$	86,3	91,6	89,2	91,7	91,1	90,8	90,1	87,9	76,0
Mg_2SiO_4	0,7	0,0	0,9	0,8	0,4	0,5	0,5	3,3	4,0

Note: Grains 1-5 are from Dutoitspan Monticellite kimberlite, 580/9. The mean composition for this sample is given. Analysis 6 is the average of 4 analyses of a De Beers Mine kimberlite and analysis 7 is for the "Blue Hills" Monticellite Peridotite from the Gros Brukkaros Complex. 6 and 7 are from Clement et al. (1975).

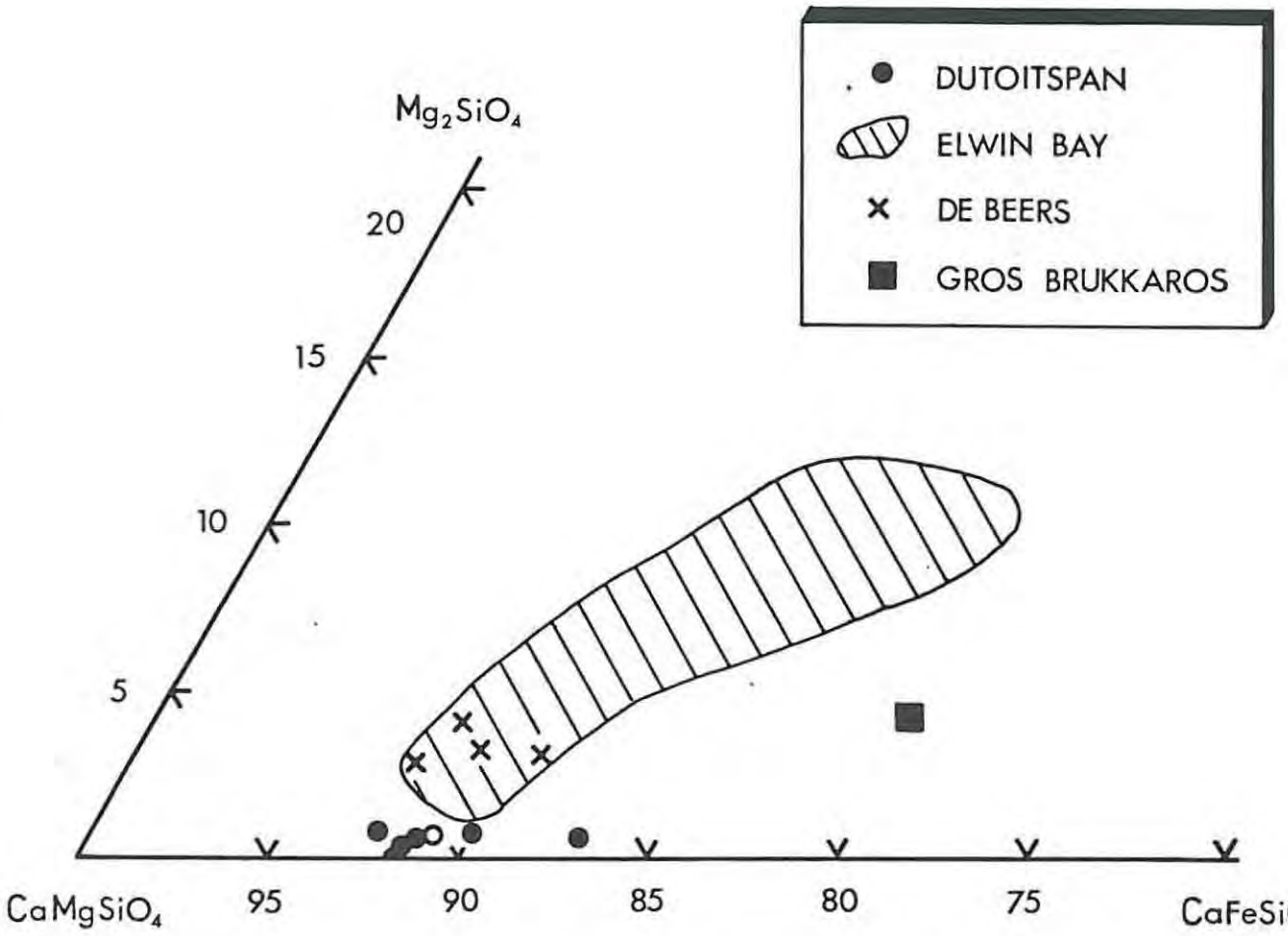

Fig. 11 Composition of monticellite expressed as molecular percentage of Mg_2SiO_4, $CaMgSiO_4$ and $CaFeSiO_4$. Data for Elwin Bay from Mitchell (1978), for De Beers and Gros Brukkaros (see also Table 6) from Clement et al. (1975). The mean value for Dutoitspan is plotted as an open circle.

under physico-chemical conditions likely to exist in natural systems, and where monticellite occurs in reaction relationship with early formed Mg-rich olivine, monticellite would be expected to dissolve 5-10 mole percent Mg_2SiO_4 (Warner and Luth, 1973). There is no indication that the Dutoitspan monticellite is secondary in origin, so the fact that it is deficient in Mg_2SiO_4 is not surprising, particularly as Warner and Luth (1973) stress that there is partial immiscibility between the end-member phases of the $CaMgSiO_4$ - Mg_2SiO_4 join. There is no need to invoke more extensive solid solution than is suggested by Warner and Luth's (1973) study of the Fe-free system to account for the plotted Dutoitspan monticellite compositions.

4. Oxide Minerals

a) Ilmenite

Analyses from the ilmenite grains described in section II are given in Table 9 and plotted on Fig. 12. There is no evidence of zoning in grains 1 and 2 but grain 5, a sub-grain from a macrocryst in phlogopite kimberlite (580/21) has a TiO_2- and MgO-enriched margin, similar in composition to the relict ilmenite aggregate (grains 2 and 3, Table 9) in the nodule shown in Plates 21 and 22. There is substantial compositional variation both within macrocrysts (note the difference in MgO content between the sub-grains 6 and 7) and between macrocrysts.

The available data do not provide any criteria for distinguishing between the compositions of the ilmenite grains from the two different kimberlite types. However, the phlogopite type has the highest frequency of occurrence of ilmenite macrocrysts (Appendix 5). Grain 1 contains a markedly higher content of Fe_2O_3 and lower MgO than the other ilmenites tabulated in Table 9. It is doubtful whether this analysis represents an ilmenite as it plots at an improbably low temperature (about 550°C) on Lindsley's (1976) estimate of the hematite-ilmenite miscibility gap. Furthermore the totals are high. This grain is probably a mixture

Table 9 Microprobe Analyses of Ilmenite Macrocrysts

Oxides	1A	1B	1C	Mean	2A	2B	3	4	5A	5B	6	7
TiO_2	42,93	43,27	42,83	43,01	53,10	53,40	53,23	47,84	49,44	52,17	46,42	45,74
Al_2O_3	0,18	0,03	0,20	0,14	0,40	0,33	0,33	0,17	0,26	0,28	0,16	0,18
Fe_2O_3	21,48	20,66	21,42	21,19	4,28	3,66	3,52	13,10	9,27	4,30	14,92	15,50
Cr_2O_3	1,95	1,94	1,96	1,95	2,51	2,39	2,12	2,42	2,53	2,60	2,01	1,93
FeO	31,03	29,82	31,03	30,63	28,18	28,47	27,54	29,34	27,83	28,85	28,67	30,95
MgO	4,83	5,63	4,80	5,09	11,57	11,45	11,89	8,23	9,90	10,66	7,68	6,09
MnO	-	-	-	-	0,41	0,50	0,45	0,27	0,36	0,48	0,45	0,37
Total	102,40	101,35	102,24	102,00	100,60	100,20	99,14	101,37	99,59	99,34	100,30	100,76
Cations (on the basis of 6 O)												
Al	0,006	0,001	0,007	0,005	0,011	0,009	0,013	0,005	0,008	0,008	0,005	0,006
Fe^{3+}	0,436	0,419	0,436	0,430	0,084	0,066	0,064	0,251	0,175	0,079	0,292	0,307
Cr^{3+}	0,042	0,042	0,042	0,042	0,048	0,045	0,040	0,049	0,050	0,050	0,041	0,040
Ti	1,743	1,755	1,742	1,747	1,909	1,922	1,924	1,830	1,865	1,912	1,816	1,808
Mg	0,389	0,452	0,387	0,409	0,824	0,817	0,852	0,624	0,740	0,774	0,595	0,477
Fe^{2+}	1,401	1,345	1,403	1,383	1,127	1,139	1,107	1,248	1,167	1,176	1,247	1,361
Mn	-	-	-	-	0,017	0,020	0,018	0,012	0,015	0,020	0,020	0,016
Mole % end members												
$MgTiO_3$	16,3	19,3	17,5	17,7	39,6	39,6	41,3	28,4	34,8	37,3	27,3	21,5
$FeTiO_3$	63,9	61,5	63,0	62,8	56,5	57,1	55,5	59,6	56,7	58,8	58,9	64,0
Fe_2O_3	19,9	19,2	19,5	19,5	3,9	3,3	3,2	12,0	8,5	3,9	13,8	14,4

Note: A, B and C denote analyses from core(A) to rim.

1. Ilmenite mixture (see text) in phlogopite kimberlite, 740/16 (Plate 24).
2,3. Sub-grains of relict ilmenite nodule in phlogopite kimberlite, 580/26 (Plates 21 and 22).
4,5. Sub-grains of an ilmenite macrocryst in phlogopite kimberlite 580/21 (Plate 23).
6,7. Sub-grains of ilmenite macrocryst in monticellite kimberlite, 580/6 (Plate 11).

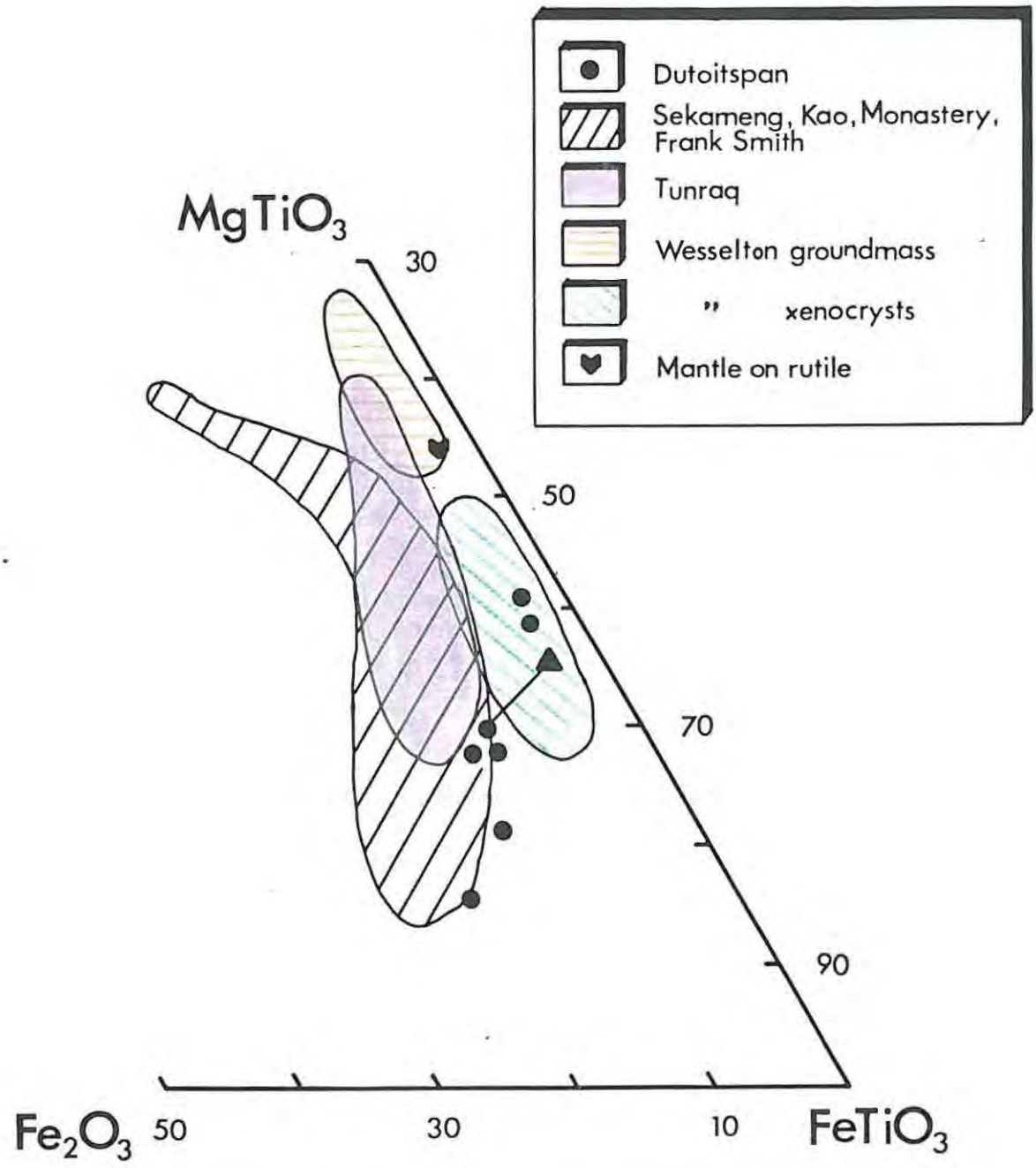

Fig. 12 Composition of ilmenite expressed as molecular percentage of $MgTiO_3$, FeO_3 and $FeTiO_3$. Data for southern African kimberlites from Mitchell (1979a), for Tunraq from Mitchell (1979), and for Wesselton from Shee (1979a). Line joins core (closed circle) to rim (closed triangle).

of ilmenite and hematite, the highly reflective patches shown in Plate 24 testifying to the presence of an oxidation/exsolution phase.

b) Perovskite

Partial microprobe analyses of perovskite grains are given in Table 10. All the totals are low, as rare earth elements, strontium, and niobium were not determined due to lack of suitable standards. The deviation from 100 per cent is considered to be an indication of the amounts of these elements substituting for calcium (Mitchell, 1972).

The CaO content of grain 5 (27,54 per cent) is much less than the range 35,95-40,15 per cent found by Mitchell, (1972) (see Table 10). This grain also contains substantial Cr_2O_3 (7,74 per cent), so the analysis is likely to represent interference by another phase, possibly spinel. There are no substantial differences in the main oxides CaO, TiO_2 and Na_2O between the groundmass perovskite grain (2) and the reaction material surrounding an ilmenite macrocryst (1). The phlogopite kimberlite contains perovskite (grains 1 and 2) slightly enriched in CaO and TiO_2 in comparison with that from the monticellite type (grains 3 and 4). The rim of grain 3 is slightly enriched in FeO and depleted in Al_2O_3, Cr_2O_3 and MgO, in comparison with the core of the grain. This grain is intergrown with a phase rich in FeO as indicated by analysis 6, which is of an area of fine-scale intergrowth in grain 3.

c) Spinels

Microprobe analyses of spinels from the contact phase of the monticellite-kimberlite type are given in Table 11. The first three analyses represent the cores of euhedral to subhedral spinel grains which are surrounded by a spinel-free silicate gap, in turn mantled by a thin idiomorphic opaque rim. This texture was noted only in the contact phase. A single chromite analysis (grain 4, Table 11) represents the core of a euhedral reddish-brown grain. The small size of the grains has, in general, adversely affected the quality

Table 10 Partial Microprobe Analyses of Perovskite and Other Phases Associated with Ilmenite and Perovskite Grains

Oxides	1	2	3A	3B	4	5	6	7	Range*
TiO_2	54,34	54,06	52,60	53,91	50,15	51,89	20,75	47,85	52,42-55,85
Al_2O_3	0,22	0,17	0,17	0,12	0,19	0,21	0,84	0,16	0,15- 0,38
Cr_2O_3	0,49	0,50	0,47	0,05	0,46	7,74	0,89	2,03	-
FeO_{total}	0,91	0,00	0,00	0,48	0,74	0,75	61,43	34,75	1,00- 2,05
MgO	0,08	0,06	0,26	0,09	0,11	-	8,72	11,14	0,07- 0,22
CaO	38,85	38,98	35,81	35,52	34,89	27,54	9,98	-	35,95-40,15
Na_2O	0,59	0,73	0,94	1,03	0,49	-	0,07	-	0,37- 0,88
Total	95,48	94,50	90,25	91,20	87,03	88,12	102,68	96,57	

1. Perovskite rim surrounding ilmenite macrocryst in phlogopite kimberlite, 580/21 (Plate 23).
2. Euhedral groundmass perovskite grain near the ilmenite grain above.
3. Large grain of secondary perovskite in monticellite kimberlite, 580/10 (Plate 12).
4. Primary overgrowth of perovskite surrounding grain 3.
5. Euhedral groundmass perovskite grain near ilmenite macrocryst in phlogopite kimberlite, 740/16 (top right in Plate 24).
6. Intergrowth area in grain 3.
7. Intergrowth lamellae in the ilmenite macrocryst of the monticellite kimberlite, 580/6 (Plate 11).

* Range found by Mitchell (1972) in 21 analyses of groundmass and reaction-rim perovskite grains.

Table 11 Microprobe Analyses of Spinels from the Contact Phase of the Monticellite-Kimberlite Type

Oxide		1	2	3	4
TiO_2		16,81	19,77	14,55	3,11
Al_2O_3		5,87	6,08	8,04	5,85
Cr_2O_3		0,07	0,08	0,05	48,67
Fe_2O_3		35,88	33,28	38,82	11,18
FeO		22,96	27,48	20,69	15,47
MgO		15,38	15,35	16,07	13,39
Total		96,97	102,04	98,22	97,67
					MnO = 1,00
Cations					
Ti^{4+}	B	3,401	3,837	2,888	0,633
Fe^{2+}	B	2,273	2,558	1,925	0,249
Mg^{2+}	B	1,128	1,279	0,963	0,384
Fe^{3+}	B	7,308	6,464	7,711	2,276
Al^{3+}	B	1,873	1,849	2,503	1,867
Cr^{3+}	B	0,016	0,016	0,010	10,413
Fe^{2+}	A	2,925	3,374	2,643	3,252
Mg^{2+}	A	5,076	4,625	5,359	5,016
Mole % end members					
$MgAl_2O_4$		11,7	11,6	15,6	-
$MgCr_2O_4$		0,1	0,1	0,1	-
Mg_2TiO_4		32,9	31,1	31,7	-
Fe_2TiO_4		9,9	16,9	4,4	-
Fe_3O_4		45,4	40,4	48,2	-

1,2,3 Cores of euhedral to subhedral composite grains comprising spinel cores surrounded by a spinel-free silicate gap, in turn mantled by a thin opaque idiomorphic rim.

4 Reddish brown chromite.

of the analyses.

d) Discussion

Ilmenite grains in kimberlite exhibit a wide range in composition as is illustrated in Fig. 12 where Dutoitspan ilmenite compositions are plotted together with fields from other kimberlites for comparison. The most magnesian ilmenite grains occur in the groundmass at Wesselton and are comparable in composition with groundmass ilmenite in the Lighobong kimberlite (Boctor and Boyd, 1980). Ilmenite in a reaction mantle around rutile is more magnesian than the xenocrystic ilmenite from Wesselton kimberlite (Shee, 1979b). This is in accord with Mitchell's (1973b) observation that the Wesselton ilmenite xenocrysts contain less MgO than do mantles upon rutile. Compositional trends are interpreted here to be from low to high MgO contents because of the high MgO content of ilmenite groundmass grains; this contradicts the statement by Mitchell (1979) who, without groundmass grain analyses, interprets trends to be from "high to low MgO contents with increasing Fe_2O_3 contents". The presence of perovskite reaction rims demonstrates that magnesian ilmenite was not in equilibrium with the magma which eventually formed the groundmass (Mitchell, 1979). Haggerty (1976) describes progressive decomposition of picroilmenite resulting in the marginal formation of Mg-rich Mt_{ss} and perovskite and with more intense decomposition Hem_{ss} and rutile are associated phases. He favours the probability of a subsolidus reduction mechanism related to $CO:CO_2$ equilibria although he does not rule out the possibility that the formation of Mt_{ss} could be related to a process of low-temperature chemical weathering.

The core compositions of the mantled spinel grains (1-3, Table 11) are similar to magnesian ulvöspinel-ulvöspinel-magnetite solid solutions (MUM) analysed by Mitchell (1979) and Mitchell and Clarke (1976), who describe a similar texture of spinel-gap-rim (Phase C, p. 163). The chromite analysis (grain 4, Table 11) is similar to that of the Phase B titan-magnesian aluminous chromites of Mitchell and Clarke (1976) also called TIMAC spinels by Mitchell (1979). Among

the analyses presented by Shee (1979b) from Wesselton mine are chromites and Ti-magnetites similar in composition to the Dutoitspan analyses. Among Shee's analyses it is of note that the chrome spinels enclosed in olivine are understandably higher in Cr_2O_3 content and unzoned whereas groundmass chromites have cores lower in Cr_2O_3 and rims further depleted in Cr_2O_3 and enriched in MgO.

Spinel crystallisation in the Tunraq kimberlites commenced with relatively uncommon Al_2O_3-poor aluminous-magnesian-chromites and evolved via rare TIMAC chromites to large titaniferous-magnesian chromite. Increasing Fe^{3+} and Ti led to the development of the MUM series (Mitchell, 1979). According to Pasteris (1979) there are two main trends represented by De Beers spinels, firstly that common to many kimberlites - chromite-rich cores and titanomagnetite-rich rims, and secondly titanomagnetite cores to magnesian pleonaste rims (only in areas in direct contact with wallrock). Although such rims are common among De Beers spinels, Pasteris (1979) also finds zoned spinels with only partial pleonaste rims or atoll spinels. Typical zonation and texture of the atoll spinels is a subhedral titanomagnetite core, sometimes with a central chromite nucleus, a gap (no spinel), and a narrow rim rich in magnetite. Only in those cases where part or all of the pleonaste rim is missing does one see a narrow magnetite rim (Pasteris, 1979).

Pasteris (1979) reports a positive correlation between the preservation of Mg-pleonaste rims and phenocryst phlogopite, which is also the situation found at Dutoitspan where the contact phase,bearing atoll spinels,is rich in phlogopite compared with samples away from the contact. Progressive breakdown/resorption of pleonaste rims and large phlogopite phenocrysts suggests interaction with some third Mg-Al-phase, possibley garnet (Pasteris, 1979). Thus the titanomagnetites are a pre-fluidization phase which underwent physical attrition and/or chemical reaction during fluidization. The breakdown of garnet would account for the presence of Mg-enriched rims on some olivines (as described in Section II)

as well as the Mg-pleonaste rims on spinels. Except at wall-rock contacts where phlogopite phenocrysts and Mg-pleonastes could be quenched in, there would be eventual breakdown of these phases during typical magmatic processes (laté-stage increases in fO_2 causing oxidation of the Fe^{2+} to a magnetite component as rims on the atoll spinels, and redissolution of Mg-Al-species by the remaining melt).

5. Garnet

The following analysis is for a rounded mauve garnet from the phlogopite-kimberlite type. The garnet grain has a narrow kelyphitic rim and is surrounded by dark brown laths of phlogopite, one of which was analysed (grain 10, Table 6). If the analysis in Table 12 is classified using the discriminant indices published by Dawson and Stephens (1975) it has the highest probability of belonging to group 9. This is confirmed by using the flow sheet method (Fig. 5, Dawson and Stephens, 1975). In the addendum to their paper the authors suggest the name 'chrome-pyprope' for this group of garnet compositions. The occurrences of garnet grains belonging to this group include kimberlite, garnet lherzolite, garnet olivine websterite, garnet harzburgite, eclogite and diamond inclusions.

V WHOLE ROCK CHEMISTRY

Six samples from the monticellite kimberlite, including one from the contact rock, and six from the phlogopite kimberlite have been analysed using X-ray fluorescence spectroscopy (see Appendix 3). Major elements for all samples and trace elements for all but 3 phlogopite kimberlites are listed in Table 13 and recalculated H_2O^- and L.O.I.-free data are presented in Table 14.

In order to try to overcome the problem of contamination, whole rock samples were hand-sorted (see section II) and crustal inclusions were removed before analysis.

There is a marked contrast in the major and trace

Table 12 Microprobe Analysis of Garnet

Oxide	Weight %	Mean*	Range*
SiO_2	41,93		
TiO_2	0,02	0,17	0,00 - 0,45
Al_2O_3	19,89		
FeO	6,93	8,01	5,42 -11,80
MnO	0,44		
MgO	20,60	20,01	13,60 -24,20
CaO	5,25	5,17	3,67 - 8,36
Na_2O	0,05		
Cr_2O_3	4,24	3,47	0,24 - 9,15
NiO	0,03		
Total	99,37		

* Mean value and range of oxides for cluster group 9, used in discriminant analysis for the classification of garnets from kimberlite and associated xenoliths (Dawson and Stephens, 1975).

Discriminant scores calculated using the indices from Dawson and Stephens (1975) are as follows:

$R_1 = 755$	$R_4 = 754$	$R_7 = 723$	$R_{10} = 763$
$R_2 = 721$	$R_5 = 695$	$R_8 = 703$	$R_{11} = 752$
$R_3 = 750$	$R_6 = 746$	$R_9 = 765$**	$R_{12} = 742$

** The highest score, which implies that group 9 has the highest probability of being the right classification for the analysis. The garnet analysis above is thus likely to be that of chrome-pyrope.

Table 13 Dutoitspan Major and Trace Element Analyses

Oxide %	Contact	Monticellite-Kimberlite Type					Phlogopite-Kimberlite Type					
	740/C	740/2	740/11	580/3	580/5	580/9	740/8	740/10	740/16	580/15	580/20	580/26
SiO_2	28,08	30,89	27,67	31,88	32,14	33,23	35,25	30,94	33,69	36,81	34,67	37,82
TiO_2	1,34	1,53	1,34	1,42	1,32	1,29	0,98	1,12	1,07	1,07	1,28	0,98
Al_2O_3	2,78	2,51	1,87	2,54	3,85	2,57	4,49	3,05	3,87	5,08	3,74	4,89
$Fe_2O_{3\,total}$	7,93	9,01	7,68	8,13	8,03	8,04	6,91	7,12	7,13	7,00	7,75	6,78
MnO	0,17	0,16	0,14	0,15	0,15	0,15	0,13	0,13	0,12	0,13	0,13	0,12
MgO	27,10	32,68	30,68	32,41	30,71	32,08	26,47	28,29	27,82	27,51	29,29	26,94
CaO	13,61	10,23	10,95	6,48	8,42	8,76	8,46	9,60	7,78	6,38	8,98	7,09
Na_2O	0,30	0,17	0,41	0,60	0,39	0,64	1,56	0,45	0,17	1,06	1,17	1,51
K_2O	1,71	1,71	0,69	1,18	2,36	1,61	3,03	2,44	3,16	3,18	1,97	3,14
P_2O_5	1,72	1,27	2,28	1,79	1,80	1,86	1,80	1,79	2,79	1,45	1,97	1,37
LOI	13,83	9,39	7,20	11,02	9,33	7,67	9,72	13,32	9,56	6,62	7,28	6,77
H_2O^-	0,86	0,75	9,50	1,01	1,19	0,96	1,01	1,39	2,09	2,22	1,18	1,46
Total	99,43	100,30	100,40	98,61	99,69	98,86	99,81	99,64	99,27	98,51	99,41	98,87
ppm												
Co	75	86	85	89	80	72	77	85	75	-	-	-
Cr	1334	1660	1911	1754	1538	1310	1514	1689	1369	-	-	-
V	146	95	124	111	93	189	142	126	219	-	-	-
Sr	2338	1559	1601	1327	1236	1538	1040	1434	1625	-	-	-
Rb	131	88	64	73	103	93	131	152	145	-	-	-
Y	21	18	18	16	15	15	13	14	12	-	-	-
Zr	245	315	342	303	293	291	219	264	232	-	-	-
Nb	172	155	151	141	132	131	104	119	112	-	-	-
Ba	4887	1340	1439	1191	1098	1517	2617	2288	2762	-	-	-
La	152	139	134	111	117	114	77	105	100	-	-	-
Ce	212	203	188	166	170	165	109	146	139	-	-	-
Nd	87	82	76	70	77	69	52	65	58	-	-	-
C.I.*	1.01	1,16	1,34	1,43	1,37	1,94	1,69	1,25	1,25	1,66	1,84	1,75

* Contamination index as defined by Clement (personal communication, see text),

Note: Major element analyses by J. Misiewicz.

Table 14 Dutoitspan Major Element Analyses Recalculated on H_2O^- and L.O.I.-free basis to 100%

Oxide	740/C	740/2	740/11	580/3	580/5	580/9	740/8	740/10	740/16	580/15	580/21	580/26
SiO_2	33,14	34,26	33,06	36,82	36,04	36,83	39,57	36,43	38,45	41,05	38,12	41,73
TiO_2	1,58	1,70	1,60	1,64	1,48	1,43	1,10	1,32	1,22	1,19	1,41	1,08
Al_2O_3	3,28	2,78	2,23	2,93	4,32	2,85	5,04	3,59	4,42	5,67	4,11	5,39
Fe_2O_3 total	9,36	9,99	9,18	9,39	9,01	8,91	7,76	8,38	8,14	7,81	8,52	7,48
MnO	0,20	0,18	0,17	0,17	0,17	0,17	0,15	0,15	0,14	0,14	0,14	0,13
MgO	31,98	36,25	36,65	37,43	34,44	35,55	29,71	33,31	31,75	30,68	32,20	29,72
CaO	16,06	11,35	13,08	7,48	9,44	9,71	9,50	11,30	8,88	7,11	9,87	7,82
Na_2O	0,35	0,19	0,49	0,69	0,44	0,71	1,75	0,53	0,19	1,18	1,29	1,67
K_2O	2,01	1,90	0,82	1,36	2,65	1,78	3,40	2,87	3,61	3,55	2,17	3,46
P_2O_5	2,03	1,41	2,72	2,07	2,02	2,06	2,02	2,11	3,18	1,62	2,17	1,51

element composition of the peripheral monticellite kimberlite and its core of phlogopite kimberlite. The monticellite contact rock has chemical characteristics which, like its petrography, set it apart from the main body of monticellite kimberlite.

1. Contamination

The Dutoitspan kimberlites contain carbonatised xenoliths of unknown crustal origin as well as various mantle nodules. There is no possibility of quantifying this multi-contaminant situation in the manner described by Kruger (1978). He uses a correction procedure which takes into account the concentration of major and trace elements in the contaminant. Although perfect de-contamination could not be achieved by the physical method used here, because of partial resorbtion of large xenoliths and the effect of manysmaller inclusions which could not be removed at all (problems also mentioned by Fesq et al., 1975) a fair measure of success was nevertheless achieved as judged by the contamination index (C.I.) of Clement (personal communication), presented in Table 13. Over half the analyses score in C.I. under 1,5 which according to Clement is the figure above which the sample concerned is taken to be contaminated. Uncontaminated analyses are scored 1,0 by the formula which follows:

$$C.I. = \frac{SiO_2 + (Al_2O_3 \times 10) + (Na_2O \times 10)}{MgO + (K_2O \times 10)}$$

An olivine basalt has a C.I. of about 17 and a phorphyritic granite scores about 5. The C.I.'s for analyses presented by other workers are calculated in Table 15 for comparison. The Dutoitspan samples which have C.I.'s closest to 1,0 are the contact phase 740/C and the neighbouring sample 8 metres from the contact, 740/2. The matrix in both these samples is fine grained. Carbonate material is abundant in the contact rock 740/C and the presence of carbonates in the matrix of 740/2 suggests that this sample also lies within a zone exhibiting chill effects.

There is no simple linear relationship between either SiO_2 or Al_2O_3 and C.I. (Figs. 13a and 13b), which is taken to

Table 15 Some Other Southern African Kimberlite Analyses

Oxide	1	2	3	4	5	6	7	8
SiO_2	26,11	30,47	32,77	33,21	44,67	-	48,46	-
TiO_2	2,33	1,69	1,45	1,97	1,70	-	1,76	-
Al_2O_3	2,81	1,88	3,76	4,45	4,46	-	4,12	-
Fe_2O_3	8,61	9,12	7,78	10,59	8,64	-	8,52	-
MnO	0,25	0,23	0,13	0,17	0,14	-	0,15	-
MgO	27,63	33,75	25,96	22,78	22,42	-	23,04	-
CaO	16,68	10,70	8,48	9,36	6,63	-	4,46	-
Na_2O	0,37	0,53	0,71	0,19	0,85	-	0,57	-
K_2O	0,18	0,95	2,25	0,79	1,31	-	0,74	-
P_2O_5	3,04	1,78	1,18	0,65	0,28	-	0,18	-
L.O.I.	11,82	8,82	11,44	12,62	5,22	-	5,35	-
H_2O^-	-	-	3,11	2,66	3,01	-	2,21	-
Total	99,83	99,92	99,02	99,44	99,33	-	99,56	-
ppm								
Co	72	89	75	--	72	-	73	-
Cr	1894	1501	1179	1160	890	920	1060	1120
V	126	110	80	-	-	-	-	-
Sr	1403	1196	888	-	401	-	-	-
Rb	28	65	95	-	104	-	-	-
Y	24	14	13	-	-	12	-	5
Zr	390	257	223	-	-	107	-	121
Nb	152	113	92	-	-	77	-	64
Ba	-	-	-	-	507	-	-	-
La	114	69	43	-	38	-	-	-
Ce	174	113	84	-	59	-	-	-
Nd	75	52	35	-	<25	-	-	-
C.I.	1,97	1,26	1,60	2,59	2,75	-	3,13	-

1 De Beers, DB/P5 (monticellite contact rock)
2 De Beers, peripheral monticellite kimberlite] Kruger (1978)
3 De Beers, core phlogopite kimberlite]
4 Lesotho kimberlite average. Gurney and Ebrahim (1973).
5 Premier brown kimberlite average. Fesq et al. (1975).
6 Premier brown kimberlite (t.e. only). Kable et al. (1975).
7 Premier grey kimberlite average. Fesq et al. (1975).
8 Premier grey kimberlite (t.e. only). Kable et al. (1975).

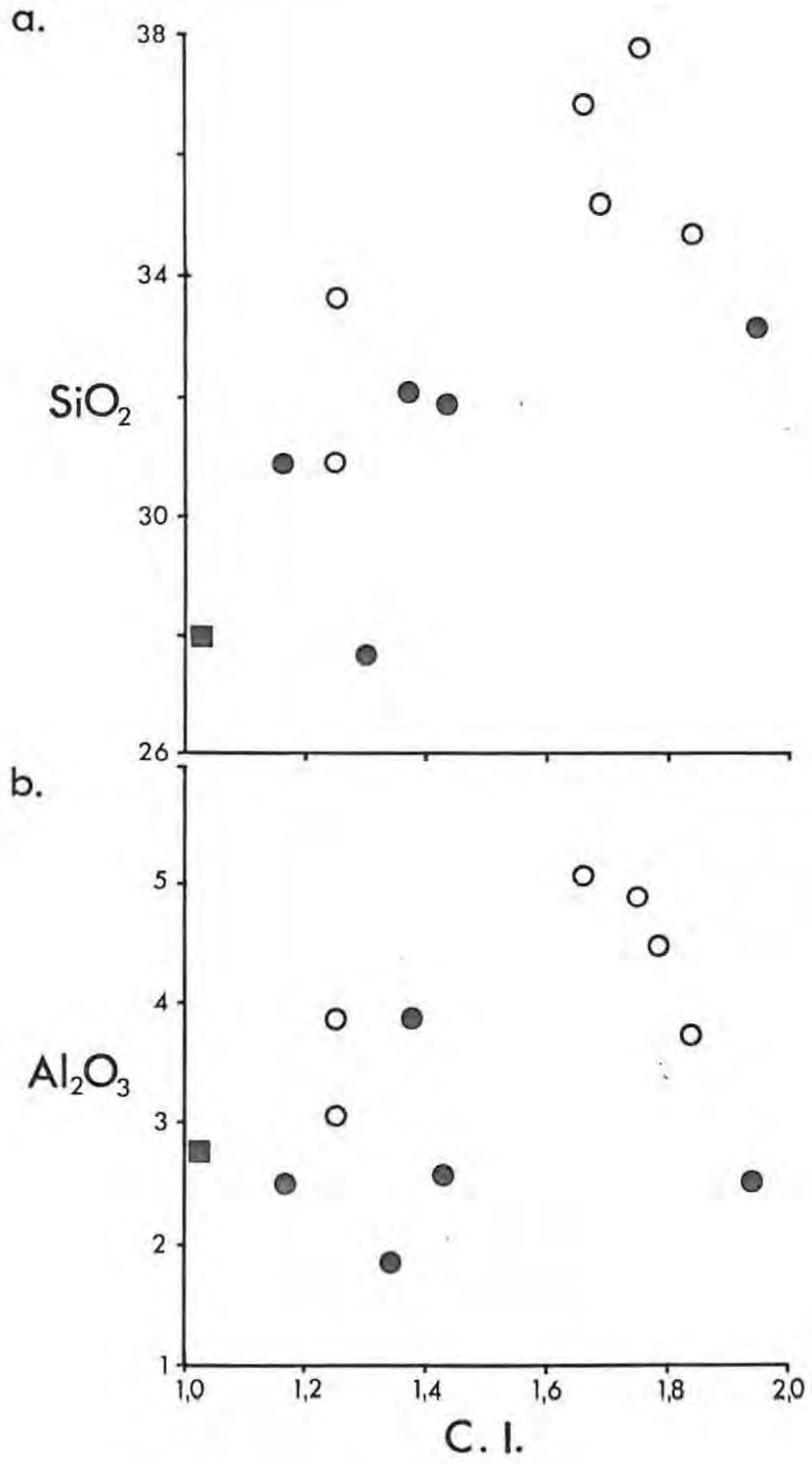

Fig. 13 Plot of a) SiO_2 and b) Al_2O_3 against contamination index, C.I. (see text) for the monticellite kimberlite (closed circles), the monticellite contact rock (closed square) and phlogopite kimberlite (open circles).

imply that potential systematic contamination effects have been eliminated by the sorting method used. Despite the apparent variation in contamination according to the C.I.'s presented, there is no graphical evidence in the figures described below to suggest that any of the points represent unreliable analyses. The obvious outlier, 740/C, is taken to be uncontaminated (C.I. = 1,01) and thus represents a true kimberlite magma composition. Most of the other monticellite kimberlite samples are reasonably uncontaminated (C.I.'s less than 1,50). Only the phlogopite kimberlites are affected by the original xenoliths and still exhibit fairly marked contamination (C.I.'s range from 1,25 to 1,84). In all, it is believed that these analyses are the best possible to represent the natures of the two kimberlite magmas concerned.

2. Major Element Geochemistry

The data plotted on the triangular diagram, Fig. 14a show variation in MgO, total FeO and Al_2O_3 for the Dutoitspan kimberlites as compared with the kimberlite and melilite basalt fields defined by Ferguson (1980). The main variation in the plotted data is in their Al_2O_3 content which is higher in the phlogopite-kimberlite type. Figures 14b, c and d illustrate major-element variations which serve to distinguish the high-Al_2O_3, high-K_2O phlogopite type from the high-MgO monticellite type, yet both types exhibit the same correlations. A strong positive correlation exists between K_2O and Al_2O_3 (Fig. 14b) and the contact phase plots on the trend. There is a strong negative correlation between K_2O and MgO, but in this case the contact phase is depleted in MgO and K_2O relative to the main trend (Fig. 14c). In Figs. 14b and c the two kimberlite types fall into two obviously separate chemical populations. The scatter of points in Fig. 14d is greater than in Figs. 14b and 14c and both kimberlites show a similar range in CaO except for the contact phase which is highly enriched in CaO. The major element chemistry thus accurately reflects mineral abundances in that the higher olivine content of the monticellite kimberlite gives rise to MgO enrichment and the higher phlogopite content of the phlogopite type is endorsed by Al_2O_3- and K_2O-enrichment. The CaO content of the contact phase, which sets it apart from the other analyses, is due to

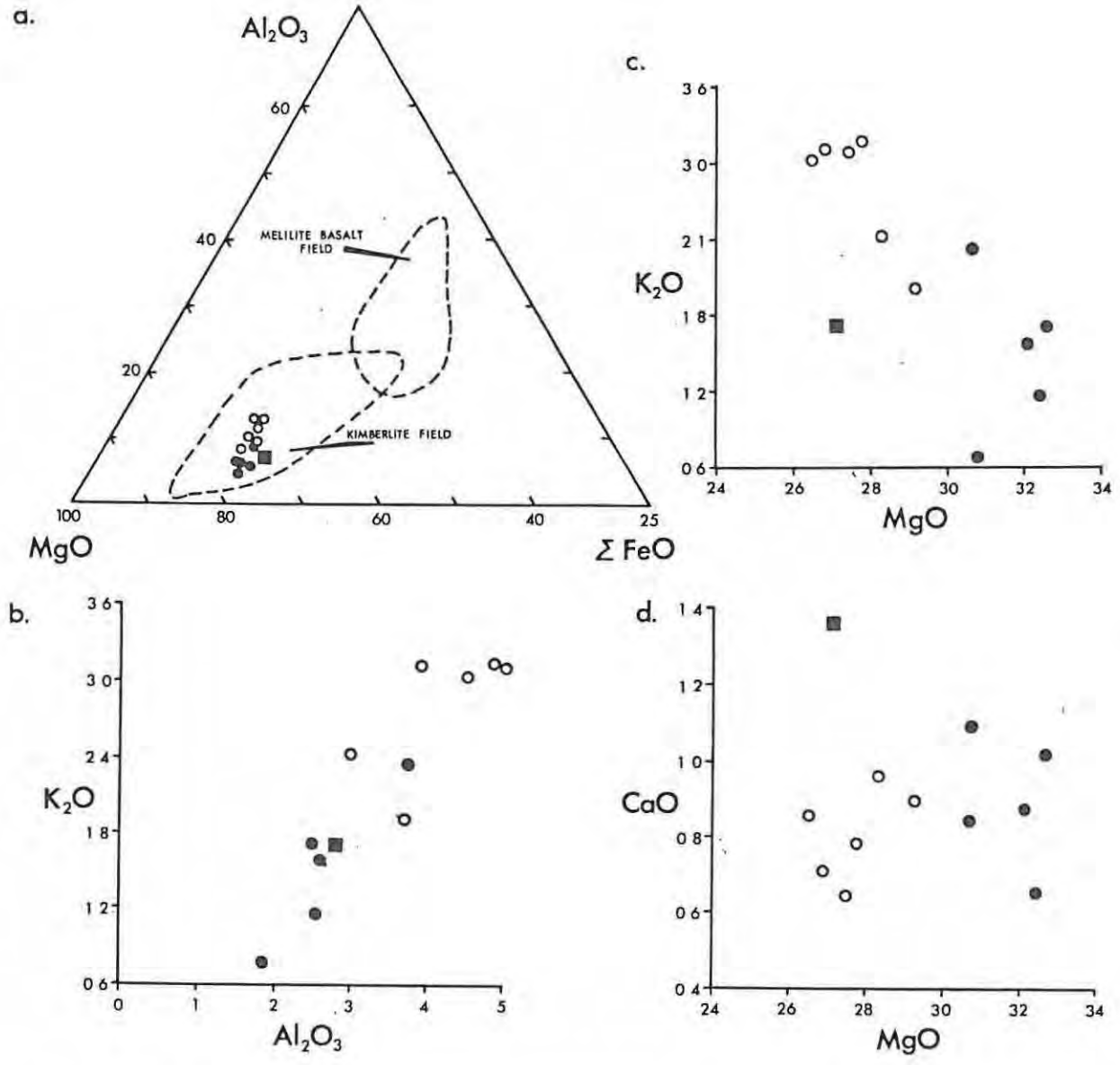

Fig. 14 Major element oxide (weight per cent) variation diagrams for 5 monticellite kimberlites (closed circles), the monticellite contact (closed square) and 6 phlogopite kimberlites (open circles). Fields in a) are from Ferguson (1980).

the abundant calcite in the matrix.

3. Minor and Trace Element Geochemistry

The mobile elements, K and Rb, are positively correlated with each other (Fig. 15a) but there is a fair spread of points lying between K/Rb ratios of 100 to 250. The two kimberlite types exhibit the same range in Sr content (Fig. 15c and d) except for marked Sr enrichment of the contact phase. This confirms that the observed contact phase is indeed likely to be a chilled margin as the calcite has apparently captured the Sr at the expense of the later crystallising kimberlite since Sr is preferentially incorporated into carbonate rather than silicate phases (Koster van Groos, 1975). Ba, too, has been highly enriched in the contact phase and the phlogopite kimberlite has higher Ba contents than that of the monticellite kimberlite (Fig. 15c). Figs 15d and 15f show that the two types of kimberlites cannot be discriminated in terms of Cr content. Very good positive correlations between Nb and Zr (Fig. 15b) and TiO_2 and MnO (Fig. 15e) are observed, the monticellite type having the relatively higher concentrations of Nb (probably in ilmenite, titanomagnetite and perovskite), Zr (probably in perovskite), TiO_2 (in perovskite and titanomagnetite) and MnO (in olivine and ilmenite). The regression fitted by eye to the data excluding the contact phase in Fig. 15b, has a slope of 0,47. The contact phase, however, has a much higher Nb/Zr ratio of 0,70. Fig. 15g illustrates the increase in V and decrease in Co from the monticellite to the phlogopite type. The contact phase contains higher V and lower Co than the other samples of monticellite kimberlite. The plot of Rb/MgO suggests a useful discriminant between the two kimberlite types (Fig. 15h). The Rb-enriched monticellite contact rock plots among the phlogopite kimberlite points.

The abundances of light rare earth elements La, Ce and Nd, and Y which, according to Frey et al. (1968) has geochemical characteristics similar to heavy rare earth elements, are plotted on Fig. 15i as the chondrite normalised value versus atomic number (as for example Haskin et al., 1968;

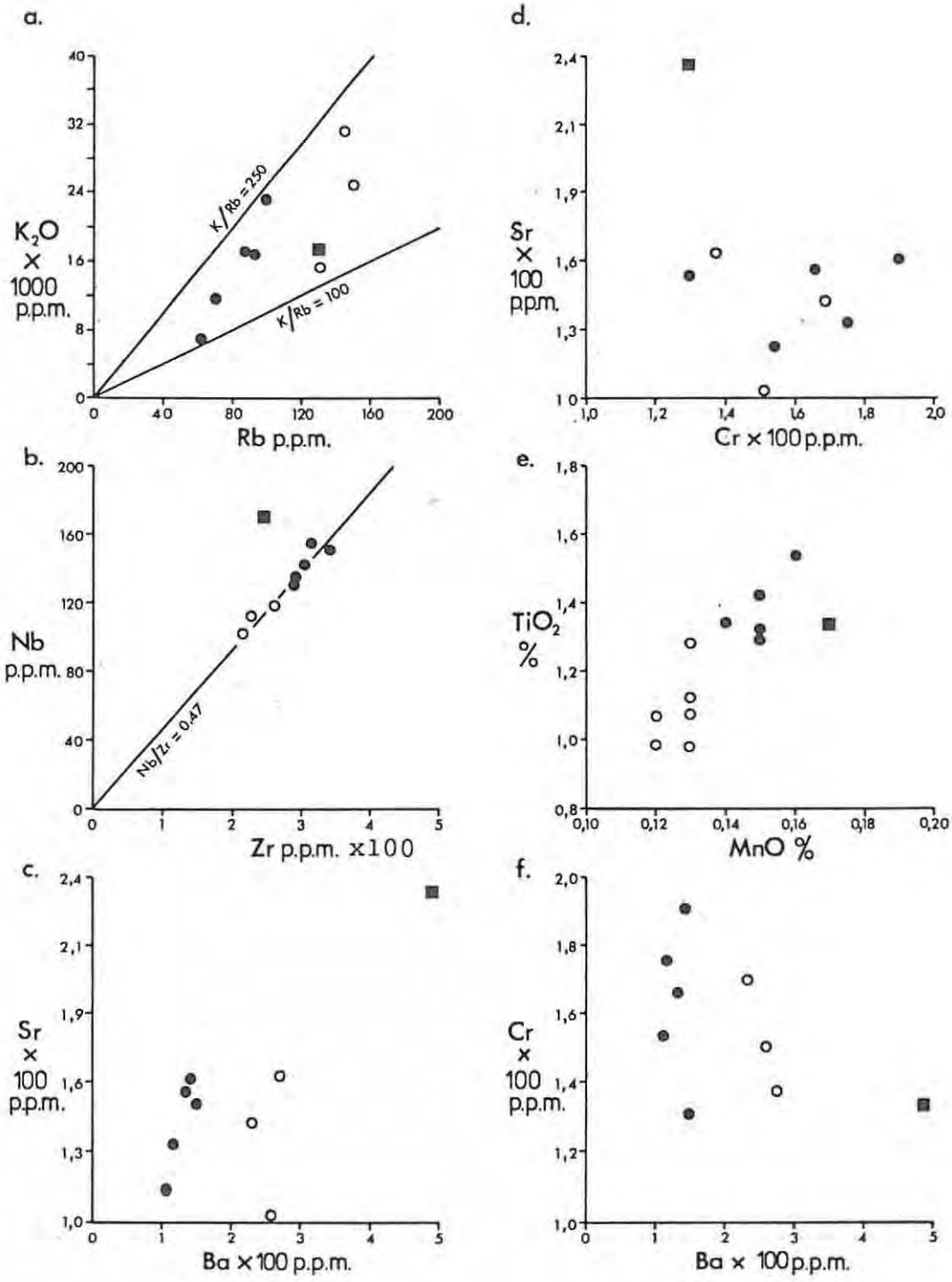

Fig. 15 a) to f) inclusive. Minor oxide and trace element (ppm or weight per cent) variation diagrams for 5 monticellite kimberlites (closed circles), the monticellite contact (closed square) and 3 (or in the case of 15 e), 6) phlogopite kimberlites (open circles).

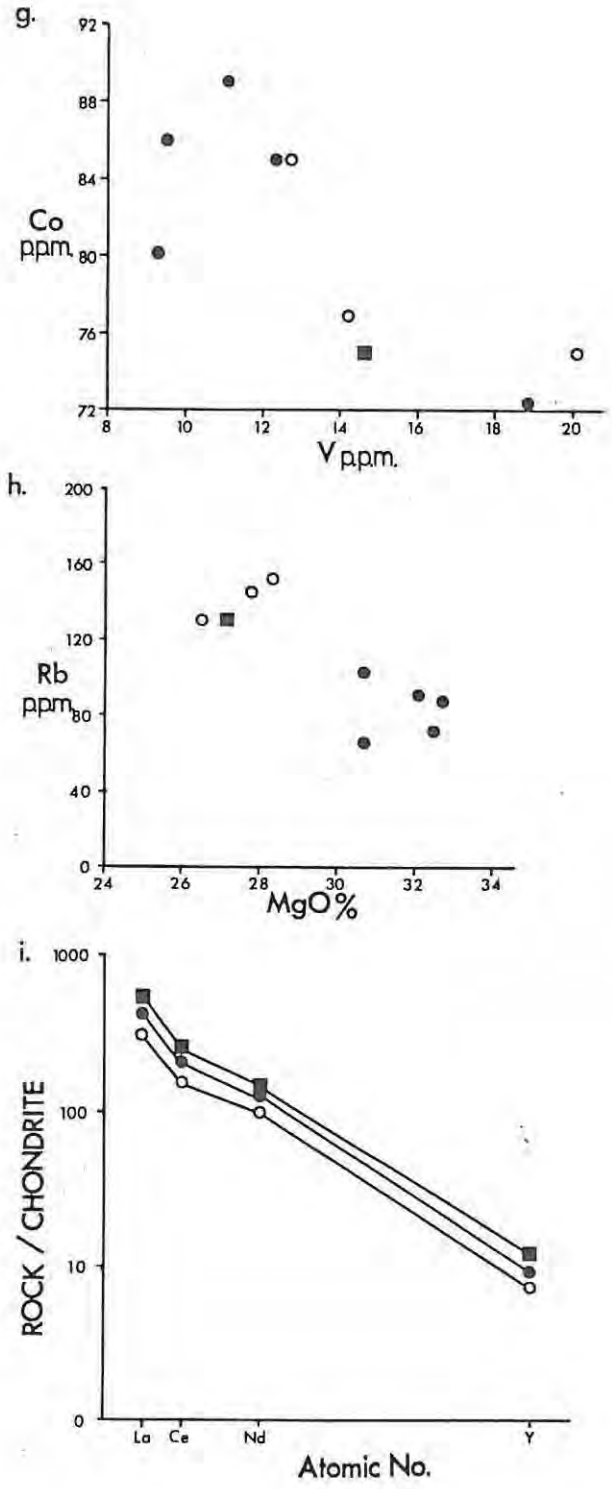

Fig. 15 (continued) g) and h). Trace element ppm and major element oxide weight per cent variation diagrams for 5 monticellite kimberlites (closed circles), the contact rock (closed square) and 3 phlogopite kimberlites (open circles).

i) Average chondrite normalised LREE and Y content against atomic number. Symbols as in g).

Mitchell and Brunfelt, 1975; Kruger, 1978; Rogers 1979 and others). There is strong enrichment in the light REE for each of the kimberlite types. The contact phase has the highest abundance of REE, followed by the monticellite type, and the phlogopite type has the lowest abundance of REE. The REE distribution patterns exhibited on Fig. 15i are identical in all three cases, suggesting a close genetic relationship between the kimberlites because they all have the same amount of fractionation between light- and heavy-REE. The contact phase exhibits the greatest amount of absolute enrichment of REE, followed by the monticellite type, then the phlogopite type.

Data from various kimberlites are plotted with the Dutoitspan data on Figs. 16a and 16b. The trends displayed by the Dutoitspan data conform to general trends in both the K_2O/MgO and the Nb/Zr plots.

4. Discussion

There are striking similarities between the chemical characteristics of the two Dutoitspan kimberlites and the De Beers Mine kimberlites analysed by Kruger (1978). Firstly, both studies involve a peripheral monticellite-rich kimberlite intruded by a core of phlogopite kimberlite and in both cases the contact of the monticellite kimberlite with the country rock into which it intruded is a finer-grained phase with a more carbonate-rich matrix. The De Beers Mine so called chill-phase (DB/P5) of Kruger (1978) is less olivine-rich than the coarser grained samples but there is no noticeable difference in olivine content of the Dutoitspan contact phase compared with other samples of the monticellite-kimberlite type. There are distinct differences between the core and peripheral kimberlites common to both the Dutoitspan and the De Beers situations. These characteristics include higher contents of MgO, CaO, Fe_2O_3, TiO, P_2O_5, Cr, Co, Nb, Zr and REE in the peripheral kimberlite and a higher Rb content in the core kimberlite. REE patterns are virtually identical for both studies. The oxides K_2O and Al_2O_3

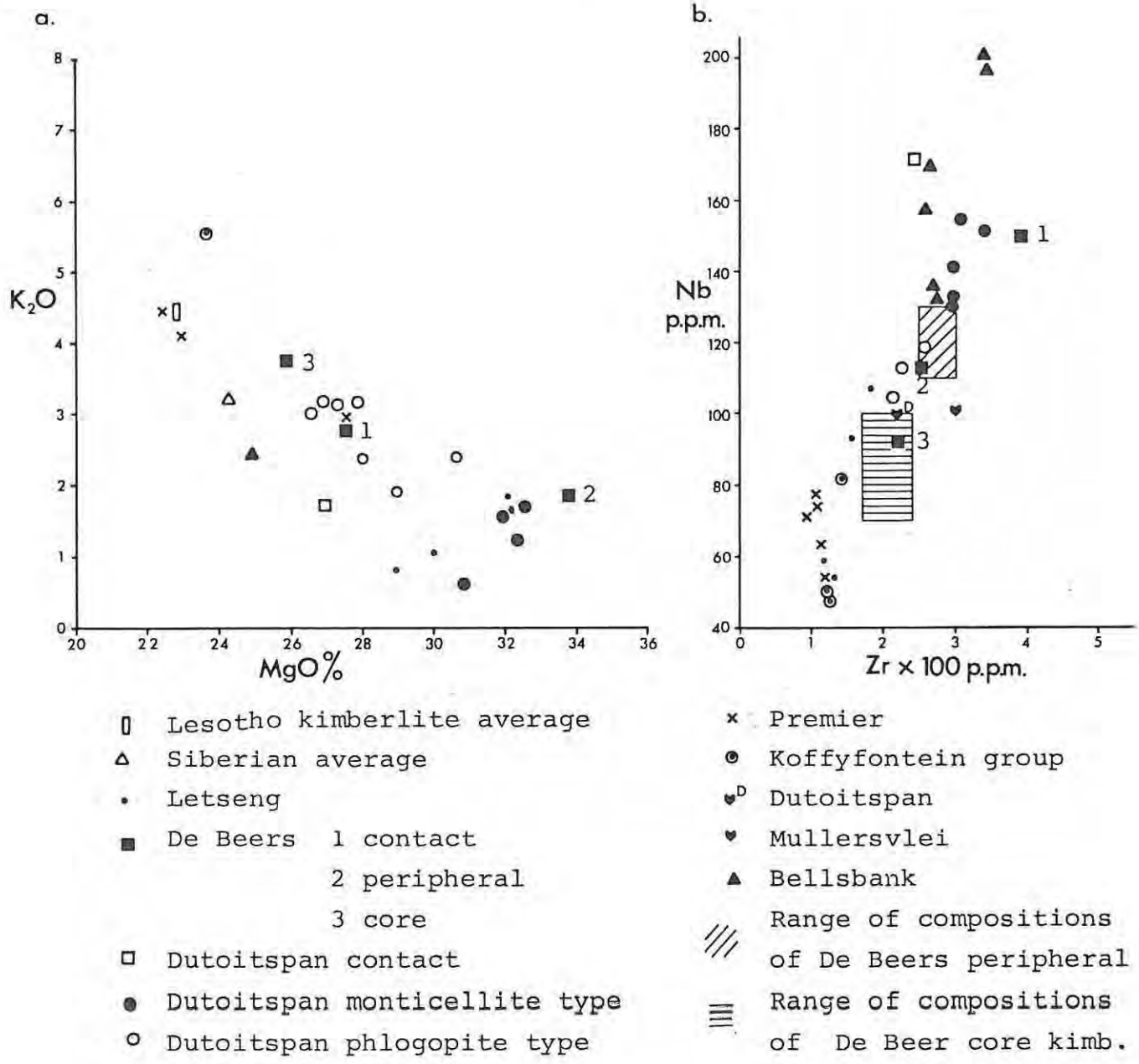

Fig. 16 Variation in a) K_2O against MgO weight per cent and b) Nb against Zr among various kimberlite whole rock analyses, as a comparison with the trends displayed by Dutoitspan analyses. Data from Gurney and Ebrahim (1973), Ilupin and Lutz (1971) in Fesq et al. (1975), Kruger (1978), Kable et al. (1975).

are well correlated in each case, with the K_2O/Al_2O_3 ratio of 0,65 at Dutoitspan being comparable with the ratio of 0,50 for De Beers Mine (Kruger, 1978), and good separation of the high-K-Al phlogopite type from the monticellite type exists. There is also good correlation between Nb and Zr except for the contact phase which is Nb-enriched at Dutoitspan (compared with the main trend at a Nb/Zr ratio of 0,47) and slightly Nb-depleted at De Beers compared with the Nb/Zr ratio of 0,43 (Kruger, 1978). Both at De Beers and at Dutoitspan does the peripheral kimberlite display higher Nb and Zr concentrations than the core kimberlite. The range from 64 to 295 of K/Rb ratios among De Beers Mine kimberlites (Kruger, 1978) is comparable with the Dutoitspan K/Rb ratio range of 100 to 250.

Niobium and zirconium are among the elements listed by Kable et al. (1975) as not being affected by contamination and are thus regarded as useful trace elements in understanding the geochemistry of kimberlites. The Nb/Zr relationship appears to be sensitive to carbonate content and by implication may have a bearing on the influence of volatile content of kimberlite magmas. Low-carbonate kimberlites have Nb/Zr ratios around 0,50 and CO_2-rich kimberlites have Nb/Zr about 0,70, as reported by Ferguson et al. (1973) who give Nb/Zr ratios of 0,49 and 0,53 respectively for kimberlite material host to autoliths and average kimberlite, and Nb/Zr = 0,69 for two high-CO_2, low-MgO autoliths. Wedepohl and Muramatsu (1979) report an average Nb/Zr ratio of 0,44 for South African kimberlites. The De Beers kimberlites analysed by Kruger (1978) have Nb/Zr ratios ranging from 0,40 to 0,47. Harris and Middlemost (1969) report a Nb/Zr ratio of 0,53 and Kable et al. (1975) a range from 0,42 to 0,71 (excluding the information for the Water Fissure, thought by them to have been sampled together with the calcrete capping in the area by mistake). The higher ratios represent enrichment of Nb in micaceous types (Kable et al., 1975). It is not clear whether these types contain more carbonate material in the matrix. If this is the case they would conform to the characteristics of the Dutoitspan contact phase which has a

Nb/Zr ratio of 0,70.

The implication is that the Nb/Zr ratio is thus important in that it distinguishes kimberlites of obviously different cooling history (contact phase against the rest), as shown in Fig. 15b, yet the correlation is good enough to support a genetic relationship between two kimberlites whose Nb/Zr contents fall on a common trend. At the same time the difference in absolute abundances of both trace elements allows separation of kimberlite types within a given diatreme (Dutoitspan, Fig. 15b; Kruger, 1978, Fig. 3.8, p. 59).

The K/Rb ratio in kimberlite lies between 100 and 300, being usually less than 200 (Ferguson et al., 1973; Wedepohl and Muramatsu 1979; Kruger, 1978; Harris and Middlemost, 1969 and Fesq et al., 1975). The wide spread in this ratio is no doubt caused, to some extent, by contamination, which affects K_2O content. According to Kruger (1978) the K/Rb ratio should decrease in subsequent liquids derived from partial melting of the same mantle source if there is residual phlogopite because residual phlogopite is enriched in Rb relative to K (Beswick, 1976).

The high REE content and LREE enrichment of kimberlites has been documented by several workers. Mitchell and Brunfelt (1975) and Rogers (1979) present chondrite normalised REE distribution patterns showing extreme fractionation among South African kimberlites. Mitchell and Brunfelt (1975) suggest that apatite, perovskite and carbonate are sites of the REE. Where Eu anomalies occur they are thought to be due to the presence of perovskite or mica (Mitchell and Brunfelt, 1975). The abundance of REE in kimberlite is possibly achieved by substantial REE entering micas crystallising from REE-enriched liquid because of the complexing affinity of REE and other incompatible elements with volatiles (Schilling and Winchester, 1969 in Fesq et al. 1975). The REE distribution patterns reported by Kruger (1978) are similar to those of Dutoitspan in showing greatest enrichment of the contact phase, followed by the peripheral (monticellite) then the core

(phlogopite) kimberlite.

The trace elements Rb, Ba, Zr and Nb are the most useful discriminators in distinguishing the two main types of Dutoitspan kimberlites. The Nb/Zr ratio appears to be a sensitive petrogenetic indicator.

VI. SUMMARY AND CONCLUSIONS

The following points summarise the main characteristics of the monticellite- and phlogopite-kimberlite types studied at Dutoitspan and highlight the mineralogical, petrological and petrochemical similarities and differences between the two types. These facts need to be taken into account in discussing the genesis and crystallisation history of the Dutoitspan kimberlites.

a) The peripheral monticellite kimberlite has a chilled contact where it is intrusive into gneissic granite wallrock and it is, in turn, intruded by a core of phlogopite kimberlite.

b) The monticellite type contains abundant, relatively unaltered macrocrysts and phenocrysts of olivine as well as macrocrysts of ilmenite and perovskite (altered from ilmenite), and some altered angular crustal inclusions, in a matrix comprising perovskite and spinel microphenocrysts, and fine-grained monticellite, serpentine, phlogopite, calcite and apatite. Heavy mineral concentrates contain far fewer ilmenite, garnet and chrome diopside grains than those of the phlogopite type (see Appendix 5) and the diamond grade of the monticellite kimberlite is also lower (Hawthorne, personal communication).

c) The mineralogy of the monticellite contact rock differs from the main body of this kimberlite type in that it contains phlogopite macrocrysts, substantial amounts of primary groundmass calcite, and monticellite is virtually absent.

d) The phlogopite type is characterised by macrocrysts of phlogopite and olivine, which are often extensively serpentinised, phenocrysts of phlogopite and serpentinised phenocrysts of olivine. Abundant altered fragmental inclusions

of crustal rocks are found. Heavy minerals include substantial amounts of ilmenite, garnet and chrome diopside, and there is a higher diamond grade than in the monticellite type. The matrix contains small amounts of perovskite and spinel micro-phenocrysts with fine grained phlogopite, serpentine, apatite, calcite and cebollite.

e) Mineral chemistry. Olivine compositions range from Fo = 91,5 $\pm$ 1,2 (1 σ) for macrocrysts to Fo = 89,0 $\pm$ 1,3 for phenocrysts. Zoning of rims tends towards a compositional band of Fo_{89-90} irrespective of whether cores are more Fe-rich or more Mg-rich. Phlogopite compositon is similar in both kimberlite types. Phenocrysts in the phlogopite-kimberlite type are more Fe-rich than macrocrysts. Bleached rims on phlogopite macrocrysts are Ti-enriched. Contact rock- spinel compositions include titan-magnesian-aluminous chromite (TIMAC) and magnesian-ulvöspinel-ulvöspinel-magnetite (MUM), which are atoll-textured spinels. Picroilmenite macrocrysts have reaction mantles of perovskite and titanomagnetite with overgrowths of perovskite. Garnet is chrome-pyrope in composition and monticellite is relatively Ca-poor.

f) Whole Rock Chemistry. The two kimberlite types have similar Nb/Zr, K_2O/Al_2O_3 and K_2O/Rb ratios, similar LREE enrichment and REE distribution patterns, but good separation of the low-Nb-Zr, high-K-Al phlogopite type from the monticellite type exists. The monticellite kimberlite has higher levels of MgO, CaO, Fe_2O_3, TiO_2, P_2O_5, Cr, Co, REE, Sr, Y, Zr and Nb, and less Al_2O_3, Na_2O, K_2O, Rb and Ba than the phlogopite type. The contact rock is highly enriched in CaO, Sr, Nb, Ba and enriched in LREE compared with the average monticellite kimberlite.

g) There are striking similarities between these Dutoitspan kimberlites and the two De Beers kimberlites studied by Kruger (1978).

h) Of the common mantle-nodule assemblage minerals (Boyd and Nixon, 1978), only olivine, garnet and chrome diopside are observed in heavy mineral concentrates in any abundance.

1. Petrogenesis of Kimberlite Magmas

In the most recent publication by Perchuk and Vaganov (1980) on the origin of kimberlites it is established experimentally that "kimberlite magma is the product of complete mantle melting under the action of alkalic (K_2O) water-carbonate-silicate fluid, supersaturated with volatiles having low density and a high migration ability". Their data imply that kimberlite magma immiscibility at high CO_2 fugacity, $T = 1300^{\circ}C$ and $P = 60-70$ kbars, allows separation of a carbonate magma. This can account for the presence of primary carbonate material in kimberlite matrix. According to Ringwood (1975) the temperature of kimberlite magma, prior to explosive eruption and adiabatic cooling, is about $1000^{\circ}C$ and a minimum pressure of 45 kbars is required for the stable synthesis of diamond from graphite. This implies a minimum depth of 140 km (and up to 300 km) for the generation of kimberlite magma.

In terms of the hypothesis that kimberlite is derived by melting of the mantle, it is imporant to consider the composition of kimberlites relative to peridotites. Kimberlites are enriched in TiO_2, Al_2O_3, Fe_2O_3, Cr_2O_3, MnO, CaO, K_2O, P_2O_5, H_2O and CO_2 and are poorer in SiO_2 and MgO; $K_2O > Na_2O$ and there are lower Mg:Fe ratios in kimberlites (Dawson, 1971). Trace element studies on kimberlites indicate high concentrations of LREE, P, Nb, Th, U and Ta (Mitchell and Brunfelt, 1975; Rogers, 1979; Wedepohl and Muramatsu, 1979; Fesq et al., 1975). There is greater fractionation in terms of La/Yb vs. Sm in kimberlites than in basalts (Rogers, 1979). The difference in La/Lu ratios between sterile nodules, where $(La/Lu)_N = 30-100$, and fertile nodules, where $(La/Lu)_N < 5$, is interpreted by Rogers (1979) as evidence for contamination of the mantle by fluid with kimberlitic trace elements, that is metasomatic enrichment, which, followed by subsolidus re-equilibration, gives the composition of the sterile nodules.

Thus any model proposed for kimberlite genesis must take into account the extreme enrichment in lithophile elements in the low-SiO_2, magnesian kimberlite magma. Harris and Middlemost (1970) proposed that a process of zone refining

(explained by Cox, 1979) and wall rock reaction after a small degree of partial melting leads to enrichment of incompatible elements. In a favourable structural environment the volatile-rich kimberlite magma may rise to lower pressure regimes and further emplacement is then dominated by gas fluidisation; final emplacement is at a low temperature (Harris and Middlemost, 1979). In order to explain observed lithophile element enrichment in kimberlites, Dawson (1971) gives as alternatives a "residual hypothesis" (with kimberlite as the final product of the basalt extrusion cycle, as also supported by Mitchell and Brunfelt, 1975) and an "incipient melting hypothesis", with partial melting in those parts containinga hydrous, potassic phase, this being in support of conditions for diamond formation which require an accumulation of volatiles under mantle conditions.

Other alternatives include firstly the suggestion that magmas co-existing with garnet can be highly enriched in LREE (Gast, 1968 in Carmichael et al., 1974), and secondly that a source rock containing phlogopite, apatite and rutile could take account of typical kimberlite element enrichment (Kable et al., 1975).

Gurney (1974) reviews hypotheses for the origin of kimberlite and suggests that in the low velocity zone of the mantle there exists an interstitial fluid containing dissolved water, CO_2, other volatiles and incompatible elements. The presence of this fluid and the rise in termperature accompanying plate movement causes partial melting of the mantle and thus gives rise to kimberlite magma. Emplacement above 140 km below the earth's surface must be rapid in order to preserve diamonds and transport dense xenoliths (Gurney, 1974). The ultimate depth of origin is thought by Gurney (1974) to be greater than 200 km, the deepest assigned xenolith depth.

Fesq et al. (1975) agree that the concentration of, for example, K, Ti, P and REE is not adequately explained by simple-melting of garnet peridotite source rock and they support a possible association between kimberlites, carbonatites

and possibly melilitites, but Mitchell (1979) presents persuasive arguments denying that there can be any relationship between the generation of kimberlites and carbonatites. Deans (1966) notes that although both carbonatites and kimberlites contain high levels of Nb and REE, there is no Cr in carbonatites nor are there inclusions or kimberlite indicator minerals.

2. Crystallisation Relationships among Kimberlite Minerals

The order of crystallisation of kimberlite minerals is interpreted from textural features, according to their temporal relationship to the event of fluidisation, which is imprinted on early crystallised phases by the observed rounding, deformation, partial resorbtion or zoning. Spinels provide information on changes in oxygen fugacity, temperature and contain evidence for the breakdown of earlier phases such as garnet.

Pasteris (1979) working on the De Beers kimberlite presents information on spinel compositions, from which certain conditions of emplacement are inferred. Early formed titanomagnetites were partially resorbed or rounded during fluidisation. Thereafter the breakdown of garnet is thought by Pasteris (1979) to have allowed the formation of Mg-pleonaste rims on spinels, and Mg-enriched rims on olivine. With rapid pressure release, as the kimberlite rose, phlogopite and Mg-pleonaste were particularly sensitive to changes in fO_2. The Mg-(Fe)-pleonaste broke down under late-stage increase in fO_2 during oxidation of the Fe^{2+} to magnetite, and re-dissolution of the Mg-Al-species by the melt. Only at contacts are the phlogopite phenocrysts and Mg-pleonastes quenched in. The spinel grains in the Peuyuk kimberlite are thought by Mitchell and Clarke (1976) to have crystallised after fluidisation, and trends reflect decreasing oxygen fugacities (10^{-19} to 10^{-22} bars) in response to falling temperatures (800-600°C) along the quartz-fayalite-magnetite buffer.

The origin of magnesian ilmenite and its relationship to kimberlite has been described by Mitchell (1977a) as some-

thing of an enigma. Is magnesian ilmenite a mantle xenocryst or a kimberlite phenocryst? Trace element studies and factor analysis led Mitchell (1977a) to conclude that the geochemistry of ilmenites cannot be interpreted in terms of a differentiation hypothesis. Each pipe he studied is characterised by a particular suite of discrete ilmenite nodules which are considered to be phenocrysts in a proto-kimberlite magma. Elthon and Ridley (1979) also present arguments to support the origin of picroilmenite by direct crystallisation from the kimberlite melt.

The lack of iron substitution in kimberlite perovskite crystals might be an indication that they formed under reducing conditions and fO_2 is estimated by Mitchell (1977a) at 10^{-20} bars in the final stages of crystallisation of the magma. Boctor and Boyd (in preparation) report that perovskite from kimberlite dykes and sills is more enriched in REE relative to perovskite from diatremes. In carbonate-depleted diatremes the REE content of perovskite is lower than in carbonate-rich diatremes.

Olivine compositions of Fo_{93-87} for phenocrysts and Fo_{94-84} for rounded macrocrysts from the De Beers "Peripheral" kimberlite are reported by Boyd and Clement (1977) who interpret marginal zoning, which approaches Fo_{89-90} regardless of core composition, to be metasomatic in origin rather than by growth zoning.

Phlogopite chemistry shows variations which, according to Elthon and Ridley (1979), can be related to changing conditions in the kimberlitic magma and the failure of early crystallising phlogopite grains to re-equilibrate with the magma. Smith et al.(1978) suggest that local effects on the scale of 1 mm can cause variations in composition. They consider that groundmass micas must have crystallised either during the final stages of emplacement and consolidation, or after emplacement, with an average increase in oxidation state as crystallisation proceeds, probably by loss of volatiles from the kimberlite. There are characteristic differences

between the Type II micas of Smith et al. (1978) and the primary micas in peridotite xenoliths (Carswell, 1975; Smith and Dawson, 1975 in Smith et al., 1978).

Elthon and Ridley (1979) observe that kimberlites, unlike most other silicate magmas, can initially, at high pressures, dissove large quantities of both CO_2 and H_2O if the degree of partial melting is very small. Large volumes of Co_2 de-gas from the melt during ascent (Wyllie, 1977 in Elthon and Ridley, 1979) and thus different phases crystallise at depth and from the near-surface melt. The early phases described for a Premier Mine phlogopite kimberlite by Elthon and Ridley (1979) include picroilmenite, rutile, olivine, phlogopite, ortho- and clino-pyroxene, garnet, spinel and armalcolite. Following the reaction of picroilmenite with the magma to form perovskite and magnetite, the later crystallisation period involved perovskite, magnetite, olivine, phlogopite, carbonate, apatite and sulphides. Mitchell (1978) presents a pre- and post-fluidisation crystallisation history for the Elwin Bay (monticellite bearing) kimberlite whereby olivine, pyrope garnet, aluminous-magnesian chromite and mica are early phases. Titan-magnesian chromite crystallised before, during and after fluidisation. Later spinels are titan-magnesian aluminous chromites and the last spinel phase to crystallise is magnetite. Other post-fluidisation phases include pyrite, mica, perovskite, rutile, monticellite, calcite and serpentine. The crystallisation relationships described by Elthon and Ridley (1979) and Mitchell (1978) have much in common eith the Dutoitspan phlogopite and monticellite kimberlite relationships respectively as discussed in the last part of this section.

3. Petrogenesis of the Dutoitspan Monticellite and Phlogopite Kimberlites

The striking similarities between the Dutoitspan and De Beers core and peripheral kimberlites mentioned are unlikely to be coincidental and it is difficult to accept mantle heterogeneity (as proposed by Kruger, 1978, for the De Beers kimberlite described) as the explanation for the observed geo-

chemistry. There must surely be an underlying process which has created a repetition of similar spatial, mineralogical, and chemical relationships in two separate diatremes.

The relationships between the monticellite and phlogopite kimberlites at Dutoitspan appear to support derivation of the kimberlites as partial melts of garnet lherzolite mantle material in the presence of a suitable fluid (as perhaps described by Perchuk and Vaganov, 1980) which would allow the enrichment of lithophile elements as observed. The greater enrichment of these elements in the monticellite type is possibly due to a smaller degree of partial melting. The high K, Ba and Rb concentrations in the phlogopite type are due to the high distribution coefficients (as given by Cox, 1978) of these elements for mica. Mitchell and Brunfelt (1975) show that the ratio La/Yb and La abundance in the melt decreases as the percentage of partial melting increases, and suggest different degrees of partial melting to account for the differences between the REE contents of different kimberlite types.

Thus a small degree of partial melting (in the presence of suitable fluids) will give a liquid highly enriched in LREE, Nb and Sr, as indeed they are in the monticellite kimberlite. Further partial melting will reduce concentrations of these elements relative to the initial liquid, but lithophile elements will still be enriched relative to peridotite as in the phlogopite kimberlite. The rapid freezing of the perovskite-enriched chilled margin would have caused entrapment of REE, Nb and Sr, giving the extreme enrichment observed. The matching REE distribution patterns of the contact-phase, monticellite, and phlogopite kimberlites reinforces the suggested genetic relationship between them. The earlier monticellite kimberlite, derived from the initial partial melt, has the greater abundances of REE, particularly at the contact.

The extensive alteration of crustal inclusions in both kimberlite types is evidence for rapid gas streaming during their emplacement. Based on the abundance of crustal

inclusions in the core phlogopite type, this kimberlite was emplaced faster than the earlier peripheral monticellite kimberlite. The fragments were held in suspension and frozen in before they could settle or be resorbed. The later magma seems to have been associated with more volatiles as shown by greater degrees of serpentinisation of olivine in the phlogopite type. This extra volatile content, as well as rapid emplacement, which would prevent oxidation of diamonds, could contribute both to the greater quantity of heavy minerals and the enhanced diamond grade of the phlogopite type. The higher volatile content of the phlogopite type is perhaps anomalous in terms of this type being a higher melting fraction, as is the fact that the lower-melting monticellite type is the more abundant of the two kimberlites.

4. Crystallisation History of the Dutoitspan Kimberlites

The early minerals which crystallised in the monticellite-kimberlite type include olivine, picroilmenite, phlogopite, garnet, chromite, perovskite and spinels. Some small euhedral spinel inclusions in olivine, large chromite grains, and perovskite euhedra with spinel inclusions were among the first minerals to crystallise.

Early phases were then rounded and/or deformed during ascent of the magma. Olivine aggregates are thought to be derived from highly sheared parts of the fertile upper mantle from which the kimberlite magma was generated; the aggregates are also rounded. The post fluidisation phases include euhedral olivine phenocrysts, subhedral phlogopite phenocrysts, and euhedral spinel and perovskite microphenocrysts, then granular monticellite and finally anhedral calcite and serpentine. Second-generation perovskite formed mantles on earlier perovskite grains which were rounded or broken during fluidisation Serpentinisation of olivine phenocrysts is related to perovskite and spinel crystallising in clusters around the edges of the phenocrysts. Late perovskite and magnetite forms in the reaction mantles around ilmenite macrocrysts, with smaller macrocrysts being totally altered to perovskite. Perovskite then forms euhedral overgrowths on all these grains. Large

pre-fluidisation phlogopite macrocrysts were resorbed as were pleonaste rims on spinels. The thin magnetite rims around atoll spinels were formed at the time of resorption of the pleonaste (Pasteris, 1979). Only at the contact were phlogopite macrocrysts quenched in. The atoll texture of spinels in the Dutoitspan samples is the only evidence suggesting pleonaste existed, none having survived resorption, unlike the De Beers spinels described by Pasteris (1979).

At the contact, due to a rapid decrease in temperature, an immiscible carbonate melt separated to give primary groundmass calcite. Trace elements such as Nb, Sr and REE were enriched by crystallisation of perovskite and titanomagnetite.

Pre-fluidisation phases which crystallised in the phlogopite-kimberlite type include macrocrysts of olivine, phlogopite and picroilmenite with garnet, diamond, spinel, ortho- and clino-pyroxene. Fluidisation resulted in rounding of olivine, deformation and rounding of phlogopite and re-equilibration of picroilmenite. Subsequent crystallisation included more Fe-rich phlogopite, olivine, perovskite overgrowths and euhedral groundmass grains, spinels, serpentine, calcite, apatite and cebollite. The high volatile content of the residual magma in the final stages of crystallisation caused extensive serpentinisation of olivine and phlogopite phenocrysts and macrocrysts.

APPENDICES

Appendix 1 Microprobe Analytical Conditions

a) Olivine

Element	Crystal	Standard	Range in Std. Counts
Si	KAP	St.J.Is. Ol	33000 - 34500
Ti	LiF(220)	Rutile	52000 - 53000
Fe	LiF(220)	St.J.Is. Ol	7300 - 7400
Mn	LiF(220)	Rhodonite	26500 - 27500
Mg	KAP	St.J.Is. Ol	28000 - 29800
Ca	LiF(220)	Wollastonite	33000 - 34000
Ni	LiF(220)	Ni-Magnetite	1100 - 1200

b) Phlogopite

Element	Crytal	Standard	Range in Std. Counts
Si	KAP	St.J.Is. Ol	33000 - 35000
Ti	LiF(220)	Rutile	52000 - 53000
Cr	Qtz	Chromite	42000 - 44000
Fe	LiF(220)	St.J.Is. Ol	7500 - 7600
Mg	KAP	St.J.Is. Ol	31000 - 32000
Ca	LiF(220)	Wollastonite	19500 - 21000
Na	KAP	Jadeite	3300 - 3400
K	Qtz	Orthocl. JVPL	6800 - 7100
Ni	LiF(220)	Ni-magnetite	1100 - 1200
Al	KAP	KK-Hornbl.	11700 - 12300

c) Monticellite

Element	Crystal	Standard	Standard Counts
Si	KAP	St.J.Is. Ol	38514
Fe	LiF(220)	St.J.Is. Ol	7211
Mn	LiF(220)	Rhodonite	33365
Mg	KAP	St.J.Is. Ol	33685
Ca	LiF(220)	Wollastonite	31389

d) Ilmenite and Perovskite

Element	Crystal	Standard	Range in Std. Counts
Si	KAP	Wollastonite	63799
Ti	LiF(220)	Ilmenite	32000 - 33000
Al	KAP	Spinel	67000 - 70000
Cr	LiF(220)	Chromite	38000 - 39000
Fe	LiF(220)	Ilmenite	21500 - 22000
Mn	LiF(220)	Rhodonite	33615
Mg	KAP	Ilmenite	7300 - 7500
Ca	LiF(220)	Wollastonite	31000 - 31500
Ni	LiF(220)	Ni-magnetite	1100 - 1200

e) Garnet

Element	Crystal	Standard	Range in Std. Counts
Si	KAP	St.J.Is. Ol	33000 - 35000
Ti	LiF(220)	Rutile	52000 - 53000
Al	KAP	KK-Hornbl.	11700 - 12300
Cr	Qtz	Chromite	42000 - 44000
Fe	LiF(220)	St.J.Is. Ol	7500 - 7600
Mn	LiF(220)	Rhodonite	26000 - 27000
Mg	KAP	St.J.Is. Ol	31000 - 32000
Ca	LiF(220)	Wollastonite	19500 - 21000
Na	KAP	Jadeite	3300 - 3400
Ni	LiF(220)	Ni-magnetite	1100 - 1200

Appendix 2 Program To Calculate Olivine Mineral Formula And Example of Output

a) Listing of Program 'FORM'

```
10  LET C=0
15
55  PRINT "TYPE IN SAMPLE NAME"
60  INPUT IE
65  PRINT "TYPE IN NUMBER OF OXYGENS IN MINERAL FORMULA"
66  INPUT B
80  DIM A(12),AE(12),B(12),C(12),D(12),M(12),X(12),Y(12)
90  LET T=0
110  DATA SIO2,60.09,2,1,TIO2,79,90,2,1,AL2O3,101,96,2,3
120  DATA FE2O3,159,70,2,3,FEO,71,85,1,1,MNO,70,94,1,1
130  DATA MGO,40.32,1,1,CAO,56,08,1,1,NIO,74,41,1,1
135  DATA NA2O,61,99,2,1,K2O,94,21,2,1,H2O,18,2,1
140  FOR I=0 TO 11
150  READ AE(I),M(I),X(I),Y(I)
160  NEXT I
165  PRINT "TYPE IN ORDER SIO2,TIO2,AL2O3,FE2O3,FEO,MNO"
166  PRINT "               MGO,CAO,NIO,NA2O,K2O,H2O"
167
168
169
170  FOR I=0 TO 11
171
180  INPUT A(I)
190  LET B(I)=A(I)*X(I)/M(I)
200  LET T=T+B(I)
210  NEXT I
220  PRINT "MINERAL FORMULA FOR: ",IE
230  PRINT
240  PRINT "              OXIDE","FORMULA"
245  PRINT "        ----------------------------"
246  LET Z=0
250  FOR I=0 TO 11
255  LET C(I)=B(I)*B/T
260  LET D(I)=C(I)*Y(I)/X(I)
265  LET Z=Z+D(I)
270  LET C=C+C(I)
280  PRINT AE(I),A(I),D(I)
290  NEXT I
295  PRINT "           TOTAL CATIONS= ",Z
296  LET F=D(8)/D(5)+D(8)*100
297  PRINT
298  PRINT "MG/MG+FE % = ",F
300  IF C=B THEN 320
310  REM ERROR
320  STOP
330  END
```

b) Sample Output

```
TYPE IN SAMPLE NAME
TYPE IN NUMBER OF OXYGENS IN MINERAL FORMULA
TYPE IN ORDER SIO2,TIO2,AL2O3,FE2O3,FEO,MNO
             MGO,CAO,NIO,NA2O,K2O,H2O
MINERAL FORMULA FOR:          2/11/A

          OXIDE                FORMULA
        ---------------------------------
SIO2          40.92            0.99931
TIO2          0.1E-1           0.183662E-3
AL2O3         0                0
FE2O3         0                0
FEO           7.25             0.148074
MNO           0.1              0.20686E-2
MGO           50.6             1.84161
CAO           0.3E-1           0.785019E-3
NIO           0.43             0.848016E-2
NA2O          0                0
K2O           0                0
H2O           0                0
        TOTAL CATIONS=         3.00051
```

Appendix 3 X-Ray Fluorescence Analytical Information

a. Trace element values for International and In-house Standards used

Trace element	KRF-13B	CAR-08A	S-12	S-9	PRO-11	S-15
Rb	10,1	18,5	11,1	56,6	-	-
Sr	205,0	297,0	4,0	53,4	-	-
Y	26,2	23,7	76,0	15,3	-	-
Zr	110,0	129,8	441,0	144,0	-	-
Nb	4,3	14,1	90,5	6,3	-	-
Co	44,7	-	8,4	16,6	21,3	69,0
Cr	293,0	-	385,0	114,0	62,0	1998,0
V	244,0	-	402,0	133,0	95,0	16,0
Ba	205,0	243,0	29,0	-	736,0	-

	GSP	AGV	NIMG	BCR	G-2
La	191,0	35,0	105,0	25,0	96,0
Ce	394,0	65,0	195,0	54,0	165,0
Nd	188,0	39,0	73,0	29,0	55,0
Ba	1300,0	-	-	-	-

b. Instrumental Conditions

	Major elements	Trace elements
voltage	55 kV	
amperage	40 mA	
tube	chromium	tungsten
counter	flow	flow (Co, Cr, V, La Ce, Nd, Ba) scint (Rb, Sr, Y, Zr)
crystal	TLAP (Na, Mg) LiF200 (Mn, Fe, Ti, Ca, K) PET (Si, Al) Germanium (P)	LiF200

c. Average Lower Limits of Determination and Absolute Errors for Trace Element Analyses

Element	L.L.D.	Abs. Error
Sr	1,83	1,93
Rb	1,98	0,80
Y	1,73	0,53
Zr	1,82	0,88
Nb	1,82	0,70
Ba	1,54	9,30
La	7,20	2,21
Ce	12,89	3,63
Nd	3,92	1,93
Co	2,79	0,77
Cr	4,24	3,61
V	3,62	1,06

Appendix 4 X- Ray Diffraction Results

A Phillips Cobalt X-Ray tube with an Fe filter and a Debye-Sherrer camera (5,73 cm diameter) were used for the powder diffraction work. A voltage of 40 kV and an amperage of 40 mA were employed. Powder samples, about 0,5 mm in diameter, prepared as described in Section II, were exposed for about 2 hours using slit collimators.

The results of the X-Ray diffraction mineral identifications are tabulated below. Olivine composition was determined by careful replicated measurement of the back reflection line 174 and the equation of Jambor and Smith (1966) given below was used to calculate Fo per cent. An average olivine composition of $Fo_{89,52}$ was obtained.

$$Fo = 4151,46 - 3976,45\ d_{174}$$

1. Olivine

Line	Intensity	$d_{meas.}$	$d_{theor.}$	$hkl_{theor.}$
1	40	5,14	5,10	020
2	80	3,90	3,88	021
3	30	3,73	3,72	101
4	40	3,50	3,50	111
5	35	3,00	3,01	121
6	80	2,78	2,764	130
7 α_1	100	2,52	2,509	131
7 α_2^2	100	2,46	2,457	112, 200
8	70	2,26	2,267	122
9	30	2,16	2,160	211
10	100	1,75		
11 α_1	50	1,50		
11 α_2	50	1,48		
back reflection				
12	30	1,04	Fo %	
12'	30	1,020566	93,23	
		1,021050	87,66	Line 174
		1,021050	87,66	
13 α_1	10	0,94	89,52 mean	
13 α_2	10	0,94		
14 α_1	15	0,93		
14 α_2	10	0,93		
15 α_1	15	0,91		
15 α_2	10	0,90		

2. Ilmenite

Reynolds (1978) reports that the combined effect of the presence of MgO and Fe_2O_3 in kimberlite ilmenites is to decrease the unit cell dimensions of such ilmenites compared with the unit cell dimensions of ilmenites from other igneous rocks. The d-spacings calculated by Reynolds for kimberlitic ilmenite in K3-Kaal Vallei sample material are comparable with those below (personal communication). Note that the geikielite end-member has d-spacings lower than those of kimberlitic ilmenite.

Line	Intensity	Calculated d-spacings		Theoretical values geikielite	
		grain 1	grain 2	d-spacing	hkl
1	80	3,71	3,73	3,70	012
2	100	2,73	2,73	2,72	104
3	85	2,53	2,54	2,53	110
4	80	2,22	2,23	2,22	113
5	80	1,86	1,86	1,85	024
6	90	1,71	1,72	1,71	116
7	30	1,62	1,62	1,62	018
8	80	1,50	1,50	1,49	214
9	85	1,46	1,47	1,46	030
10	40	1,33	1,33	1,32	1.0.10

Note: Theoretical values from the
Fink and ASTM powder diffraction files

Appendix 5 Numbers of grains in heavy mineral concentrates from 5 kg samples

	Size (mm)	Monticellite Type	Phlogopite Type		
		740/3	740/9	740/16	740/8
Garnet	2,0	0	11	10	1
	1,0	1	271	325	17
	0,5	7	599	638	35
	Total	8	881	973	53
Non-magnetic Ilmenite	2,0	8	33	30	27
	1,0	42	862	558	554
	0,5	310	2360	2744	1096
	Total	360	3255	3332	1650
Magnetic Ilmenite	2,0	0	0	0	0
	1,0	54	0	0	0
	0,5	0	0	0	0
	Total	54	0	0	0

	Size (mm)	Monticellite Type	Phlogopite Type		
		740/3	740/9	740/16	740/8
Chrome diopside					
	2,0	2	2	4	6
	1,0	11	92	80	55
	0,5	44	174	163	145
	Total	57	268	247	206
Spinel	2,0	0	0	0	0
	1,0	0	2	0	7
	0,5	4	4	4	12
	Total	4	6	4	19

REFERENCES

Albee A.L. and Ray L. (1970). Correction factors for electron probe microanalysis. Analytical Chemistry, 42, 1408 - 1414.

Allsopp H.L. and Kramers J.D. (1977). Rb-Sr and U-Pb age determinations on southern African kimberlite pipes. 2nd International Kimberlite Conference, Santa Fé. Extended Abstracts.

_____, Kramers J.D., Miller J.A., and Hutchinson G. (1979). A review of the application of the Rb-Sr, U-Pb and K-Ar methods to the dating of kimberlite pipes, with special reference to the occurrence of anomalously old ages. Kimberlite Symposium, Cambridge. Abstracts.

Arndt N.T. (1977). Partitioning of nickel between olivine and ultrabasic and basic komatiite liquids. Carnegie Institution of Washington Yearbook, 76, 553 - 557.

Basu A.R. and MacGregor I.D. (proof print). Chromite spinels from ultramafic xenoliths. Geochemica Cosmochemica Acta.

Bence A.E. and Albee A.L. (1968). Empirical correction factors for the electron microanalysis of silicates and oxides. Journal of Geology, 76, 382 - 403.

Beswick A.E. (1976). K and Rb relations in basalts and other mantle derived materials. Is phlogopite the key? Geochemica Cosmochemica Acta , 40, 1166 - 1183.

Bishop F.C., Smith J.V. and Dawson J.B. (1978). Na, K, P and Ti in garnet, pyroxene and olivine from peridotite and eclogite xenoliths from African kimberlites. Lithos, 11(2), 155 - 173.

Bobrievich A.P., Bondarenko M.N., Gnevlishev M.A., Krasov L.M., Smirnov G.I., and Yurkevich R.K. (1957). Diamonds of Siberia. Gosgeoltekhizdat, Moscow. 159pp. (in Russian).

_____, _____, _____, _____, _____, _____. (1959) The diamond deposits of Yakutia. Nedra. Moscow. 527 pp.

Boctor N.Z. and Boyd F.R. (1980). Oxide minerals in the Liqhobong kimberlite, Lesotho. American Mineralogist, 65, 631 - 638.

_____ and _____ (In Press). Distribution of R.E.E. in perovskite from kimberlites.

_____ and Meyer H.O.A. (1979). Oxide and sulphide minerals in kimberlite from Green Mountain, Colorado. Proceedings of the 2nd International Kimberlite Conference, 1, 217 - 228. Ed. F.R. Boyd and H.O.A. Meyer. American Geophysical Union.

Boettcher A.L., O'Neil J.R., Windom K.E., Stewart D.C. and Wilshire H.G. (1977). Metasomatism and the genesis of kimberlites and alkali basalts. 2nd International Kimberlite Conference. Extended Abstracts.

Boullier A.M. and Nicolas A. (1975). Classification of textures and fabrics of peridotite xenoliths from South African Kimberlites. Physics and Chemistry of the Earth, 9, 467 - 476. Ed. L.H. Ahrens, J.B. Dawson, A.R. Duncan, and A.J. Erlank. Pergamon Press. 940pp.

Boyd F.R. (1973). A pyroxene geotherm. Geochemica Cosmochemica Acta, 37, 2533 - 2546.

_____(1975). Ultramafic xenoliths from the Frank Smith mine and the Kimberley Area. Kimberlite Symposium, Cambridge. Abstracts.

_____(1976). Inflected and non inflected geotherms. Carnegie Institution of Washington Yearbook, 75, 523 - 531.

_____ and Clement C.R. (1977). Compositional zoning of olivines in kimberlite from the de Beers Mine, Kimberley, South Africa. Carnegie Institution of Washington Yearbook, 76, 485 - 493.

Boyd F.R. and Nixon P.H. (1973). Origin of the ilmenite-silicate nodules in kimberlites from Lesotho and South Africa. Lesotho Kimberlites, 254 - 268. Ed. P.H. Nixon, Cape and Transvaal Printers, Cape Town. 350 pp.

_____ and Nixon (1978). Ultramafic nodules from kimberlite pipes. Geochemica Cosmochemica Acta, 42(9), 1367 - 1382.

_____ and Pasteris J.D. (1977). Ilmenite association at the Frank Smith kimberlite pipe, S. Africa. Carnegie Institution of Washington Yearbook, 77, 866 - 870.

Carmichael I.S.E. (1967). The iron-titanium oxides of salic volcanic rocks and their associated ferromagnesian silicates. Contributions to Mineralogy and Petrology, 14, 36 - 64.

_____, Turner F.J. and Verhoogen J. (1974). Igneous Petrology. McGraw Hill, 739 pp.

Carswell D.A. (1975). Primary and secondary phlogopites and clinopyroxene in garnet lherzolite xenoliths. Physics and Chemistry of the Earth, 9, 417 - 429 .

Clarke D.B. and Mitchell R.H. (1975). Mineralogy and petrology of the Somerset Island kimberlite, N.W.T., Canada. Physics and Chemistry of the Earth, 9, 123 - 135.

Clement C.R., Gurney J.J. and Skinner E.M.W. (1975). Monticellite - an abundant groundmass mineral in some kimberlites. Kimberlite Symposium, Cambridge. Abstract.

_____ , Skinner E.M.W., Hawthorne J.B. and Kleinjan L. (1977a). Precambrian ultramafic dykes with kimberlite affinities in the Kimberley area. 2nd International Kimberlite Conference, Santa Fé. Extended Abstracts.

_____, Skinner E.M.W. and Scott B.H. (1977). Kimberlite redefined. 2nd International Kimberlite Conference, Santa Fé. Extended Abstracts.

Clement C.R. and Skinner E.M.W. (1979). A textural-genetic classification of kimberlite rocks. Kimberlite Symposium, Cambridge. Poster Session.

Cohen L.H. and Rosenfeld J.L. (1979). Diamond depth of crystallisation inferred from compressed included garnet. Journal of Geology, 87, 333 - 340.

Cox K.G., Bell J.D. and Pankhurst R.J. (1979). The Interpretation of Igneous Rocks. Allen and Unwin. 450 pp.

Czamanske G.K., Wones D.R. and Eichelberger J.C. (1977). Mineralogy and Petrology of the intrusive complex of the Pliny range, New Hampshire, American Journal of Science, 277, 1073 - 1123.

Danchin R.V. (1979). Mineral and bulk chemistry of garnet lherzolite and garnet harzburgite xenoliths from the Premier Mine, South Africa. Proceedings of the 2nd International Kimberlite Conference, 2, 104 - 126.

Dawson J.B. (1971). Advances in kimberlite geology. Earth Science Reviews, 7, 187 - 214.

_____ and Hawthorne J.B. (1973). Magmatic sedimentation and carbonatitic differentiation. Journal of the Geological Society London, 129, 61 - 85

_____ and Smith J.V. (1977). The MARID (mica - amphibole - rutile - ilmenite - diopside) suite of xenoliths in kimberlite. Geochemica Cosmochemica Acta, 41, 309 - 323.

_____ and Stephens W.E. (1975). Statistical classification of garnets from kimberlites and associated xenoliths. Journal of Geology, 83, 589 - 607.

Deans T. (1966). Economic Mineralogy of African Carbonatites. Carbonatites, 385 - 413. Ed. O.F. Tuttle and J. Gittins. 591 pp.

Deer W.A., Howie R.A., and Zussman Z. (1962). Rock-forming minerals. Longmans.

_____, _____, and _____. (1967). An Introduction to the Rock-forming Minerals. Longmans. 528pp.

Delaney J.S., Smith J.V., Carswell, D.A. and Dawson J.B. (1980). Chemistry of micas from kimberlites and xenoliths - II. Primary and secondary-textured micas from peridotite xenoliths. Geochemica Cosmochemica Acta, 44, 857 - 872.

Elthon D. and Ridley W.I. (1979). The oxide and silicate mineral chemistry of a kimberlite from the Premier Mine: implications for the evolution of kimberlitic magma. Proceedings 2nd International Conference, 1, 206 - 216.

Emeleus C.H. and Andrews J.R. (1975). Mineralogy and Petrology of kimberlite dyke and sheet intrusions and included peridotite xenoliths from S.W. Greenland. Physics and Chemistry of the Earth, 9, 179 - 197.

Ferguson A.K. (1978). Ca-enrichment in olivines from volcanic rocks. Lithos, 11, 189 - 194

Ferguson J. (1980). Kimberlite and kimberlitic intrusives of southeastern Australia. Mineralogical Magazine, 43, 727 - 731.

_____, Danchin R.V. and Nixon P.H. (1973). Petrochemistry of kimberlite autoliths. Lesotho Kimberlites, 285 - 293. Ed. P.H. Nixon. Lesotho National Development Corporation. Cape and Transvaal Printers Ltd. Cape Town. 350 pp.

Fesq H.W., Kable E.J.D. and Gurney J.J. (1975). Aspects of the geochemistry of kimberlites from the Premier Mine and other selected South African occurrences with particular reference to the rare earth elements. Physics and Chemistry of the Earth, 9, 687 - 708.

Finnerty A.A. and Boyd F.R. (1977). Pressure dependent solubility of Ca in forsterite co-existing with diopside and enstatite. Carnegie Institution of Washinton Yearbook, 77, 713 - 717.

Forbes W.C. and Flower M.F.J. (1974). Phase relations of titan phlogopite. Earth and Planetary Science Letters, 22, 60 - 66.

Foster M.D. (1960). Interpretation of the composition of tri-octahedral micas. U.S. Geological Survey Professional Paper, 354-B, 48 pp.

Frey F.A., Haskin M.A., Poetz J.A. and Haskin J.A. (1968). Rare earth abundances in some basic rocks. Journal of Geophysical Research, 73, 6085 - 6098.

_____, Ferguson J. and Chappell B.W. (1977). Petrogenesis of S. African and Australian kimberlitic suites. 2nd International Kimberlite Conference, Santa Fé. Extended Abstracts.

Gurney J.J. (1974). The origin of kimberlite: modern concepts. Transactions of the Geological Society of South Africa, 77, 353 - 361.

_____ and Ebrahim S. (1973). Chemical composition of Lesotho Kimberlites. Lesotho Kimberlites, 280 - 284.

_____, Harris J.W. and Rickard R.S. (1979). Inclusions in southern African diamonds and their relationship to the xenoliths. Kimberlite Symposium, Cambridge. Abstracts.

Haggerty S.E. (1973). Spinels of unique composition associated with ilmenite reactions in the Liqhobong kimberlite pipe, Lesotho. Lesotho Kimberlites, 149 - 158.

_____ (1975). The chemistry and genesis of opaque minerals in kimberlites. Physics and Chemistry of the Earth, 9, 295 - 307.

_____ (1976). Opaque mineral oxides in terrestrial igneous rocks. Oxide Minerals. Mineralogical Society of America Short Course Notes. Ed. Douglas Rumble III. Southern Printing Company, Blacksburg, Virginia.

Harris J.W. and Gurney J.J. (1979). A study of the mineralogy and chemistry of sulphide inclusions in diamonds. Kimberlite Symposium, Cambridge. Abstracts.

Harris P.G. and Middlemost E.A.K. (1969). The evolution of kimberlites. Lithos, 3, 77 - 78.

Hart S.R. and Davis K.E. (1978). Nickel partitioning between olivine and silicate melts. Earth and Planetary Science Letters, 40, 203 - 219.

Harte B., Cox K.G. and Gurney J.J. (1975). Petrography and geological history of upper mantle xenoliths from the Matsoku Kimberlite Pipe. Physics and Chemistry of the Earth, 9, 477 - 506.

Haskin L.A., Haskin M.A., Frey F.A. and Wildeman J.R. (1968). Relative and absolute terrestrial abundances of the rare earths. Origin and Distribution of the Elements. International Series of Monographs in Earth Sciences, Vol. 30. Ed. L.H. Ahrens.

Hawthorne J.B. (1975). Model of a kimberlite pipe. Physics and Chemistry of the Earth, 9, 1 - 16.

Hazen R.M. and Finger L.W. (1978). The crystal structures and compressibilities of layer minerals at high pressure; II, Phlogopite and chlorite. American Mineralogist, 63, 3 and 4, 289 - 292.

Jambor J.L. and Smith C.H. (1964). Olivine composition determination with small diameter X-ray powder cameras. Mineralogical Magazine, 33, 730 - 741.

Kable E.J.D., Fesq H.W. and Gurney J.J. (1975). The significance of the inter-element relationships of some minor and trace elements in southern African kimberlites. Physics and Chemistry of the Earth, 9, 709 - 734.

Koster van Groos A.F. (1975). The distribution of Sr between co-existing silicate and carbonate liquids at elevated pressures and temperatures. Geochemica Cosmochemica Acta, 39, 27 - 34.

Kruger F.J. (1978). A contribution to the petrology of kimberlites. Unpublished M.Sc. thesis, Rhodes University.

_____ (1980). The occurrence of cebollite in kimberlite and included zeolitized crustal xenoliths. Mineralogical Magazine, 43, 583 - 586.

Lindsley D.H. (1976). Experimental studies of oxide minerals. Oxide Minerals.

Meyer H.O.A. (1977). Mineralogy of the upper mantle-review. Earth Science Reviews, 13, 251 - 281.

Mitchell A.A. (1979a). The extrusive and intrusive rocks of the Molteno - Jamestown area. Unpublished M.Sc. thesis, Rhodes University.

Mitchell R.H. (1972). Composition of perovskite in kimberlite. American Mineralogist, 57, 1748 - 1753.

_____ (1973a). Magnesian ilmenite and its role in kimberlite petrogenesis. Journal of Geology, 81, 301 - 311.

_____ (1973b). Composition of olivine, silica activity and oxygen fugacity in kimberlite. Lithos, 6, 65 - 81.

_____ (1977a). Geochemistry of magnesian ilmenite from kimberlites in Africa and Lesotho. Lithos, 10, 29 - 37.

_____ (1977b). Ultramafic xenoliths from the Elwin Bay kimberlite, the first Canadian Palaeogeotherm. Canadian Journal of Earth Science, 14, 1202 - 1210.

_____ (1978). Mineralogy of the Elwin Bay kimberlite, Somerset Island, N.W.T., Canada. American Mineralogist, 63, 47 - 57.

_____ (1979). Mineralogy of the Tunraq kimberlite, Somerset Island, N.W.T., Canada. Proceedings of the Second International Kimberlite Conference, 1, 161 - 171.

_____ and Brunfelt A.O. (1975). Rare earth element geochemistry of kimberlite. Physics and Chemistry of the Earth, 9, 671 - 686.

_____ and Clarke D.B. (1976). Oxide and sulphide mineralogy of the Peuyuk kimberlite, Somerset Island, N.W.T., Canada. Contributions to Mineralogy and Petrology, 56, 157 - 172.

Modreski P.J. (1977). The melting of phlogopite in the presence of enstatite, aluminous enstatite, diopside, spinel, corundum and pyrope. Carnegie Institution of Washington Yearbook, 77, 392 - 396.

Moore A.E. and Erlank A.J. (in press). Unusual olivine zoning - evidence for complex physico-chemical changes

during the evolution of olivine melilitite and kimberlite magmas. Contributions to Mineralogy and Petrology.

McIver J.R. and Ferguson J. (1979). Kimberlitic, melilitic, trachytic and carbonatite eruptives at Saltpetre Kop, Sutherland, South Africa. Proceeding of the Second International Kimberlite Conference, 1, 111 - 128.

McMahon B.M., Haggerty S.E. and Bence R.J. (1979). Oxide mineral chemistry and oxygen fugacities of the Benfontein sills, South Africa. Kimberlite Symposium, Cambridge. Abstracts.

Neuerburg G.J. (1975). A procedure, using hydrofluoric acid, for quantitative mineral separations from silicate rocks. Journal of Research, U.S. Geological Survey, 3, no 3, 377 - 378.

Nicolas A. and Poirier J.P. (1976). Crystalline Plasticity and Solid State Flow in Metamorphic Rocks. Wiley and Sons. 444 pp.

Nixon P.H. and Boyd F.R. (1973a). Petrogenesis of the granular and sheared ultrabasic nodule suite in kimberlite. Lesotho Kimberlites. 48 - 56. Ed. P.H. Nixon.

_____ and _____ (1973b). The discrete nodule (megacryst) association in kimberlites from Northern Lesotho. Lesotho Kimberlites. 67 - 75. Ed. P.H. Nixon.

_____ and _____ (1975). Mantle evolution based on studies of kimberlitic nodules from southern Africa. Kimberlite Symposium, Cambridge. Abstracts.

Norrish K. and Hutton J.T. (1969). An accurate X-ray spectrographic method for the analysis of a wide range of geologic samples. Geochemica Cosmochemica Acta, 33, 431 - 453.

O'Hara M.J., Saunders M.J. and Mercy E.L.P. (1975). Garnet-peridotite, primary ultrabasic magma and eclogite; interpretation of upper mantle processes in kimberlite. Physics and Chemistry of the Earth, 9, 571 - 604.

Pasteris J.D. (1979). Aluminous spinels and spinel silicate interactions in the De Beers Kimberlite, R.S.A. Kimberlite Symposium II, Cambridge. Abstracts.

Perchuk L.L. and Vaganov V.I. (1980). Petrochemical and thermodynamic evidence on the origin of kimberlites. Contributions to Mineralogy and Petrology, 72, 219 - 228.

Pokhilenko N.P., Sobolev N.V. and Lavrentiev Yu.G. (1979). Xenoliths of peridotites from Udachnaya Kimberlite Pipe Yakutia. Kimberlite Symposium II, Cambridge. Abstracts.

Reid A.M., Brown R.W., Dawson J.B., Whitfield G.G. and Siebert J.C. (1976). Garnet and pyroxene compositions in some diamondiferous eclogites. Contributions to Mineralogy and Petrology, 58, 203 - 220.

Reynolds I.M. (1978). A mineralogical investigation of co-existing iron - titanium oxides from various igneous rocks with special reference to some South African titaniferous ores. Ph.D. thesis. Rhodes University. (Unpublished).

Ringwood A.E. (1975). Composition and Petrology of the Earth's Mantle. McGraw Hill. 618 pp.

Rogers N.W. (1979). Trace elements in kimberlites and ultra-basic xenoliths. University of London Reactor Centre.

Shee S.R. (1979a). The petrography and oxide mineral chemistry of the W3 kimberlite, 930 metre level, Wesselton Mine. De Beers Internal Report, DBG/PI/87 and 90.

_____ (1979b). The opaque oxides of the Wesselton Mine. Kimberlite Symposium II, Cambridge. Poster Session.

Simkin T. and Smith J.V. (1970). Minor element distribution in olivine. Journal of Geology, 78, 304 - 325.

Skinner E.M.W. and Clement C.R. (1979). Mineralogical classification of southern African kimberlites. Proceedings of the 2nd International Kimberlite Conference, 1, 129 - 139.

_____ and Scott B.H. (1979). Petrography, mineral chemistry and geochemistry of kimberlite and associated lamprophyre dykes near Swartruggens, W. Transvaal, R.S.A. Kimberlite Symposium II, Cambridge. Abstracts.

Smith D. and Zientek M. (1979). Mineral chemistry and zoning in eclogite inclusions from Colorado Plateau diatremes. Contributions to Mineralogy and Petrology, 69, 119 - 131.

Smith J.V. and Dawson J.B. (1975). Chemistry of Ti-poor spinels, ilmenites and rutiles from peridotite and eclogite xenoliths. Physics and Chemistry of the Earth, 9, 309 - 322.

_____, Brennesholtz R. and Dawson J.B. (1978). Chemistry of micas from kimberlites and xenoliths. 1. Micaceous kimberlites. Geochemica Cosmochemica Acta, 42, 959 - 971.

_____, Hervig R.L., Ackermand D. and Dawson J.B. (1979). K, Rb and Ba in micas from kimberlitic and peridotitic xenoliths, and implications for origin of basaltic rocks. Proceedings of the 2nd International Kimberlite Conference, 1, 241 - 251.

Stephens W.E. and Dawson J.B. (1976). Statistical comparison between pyroxenes from kimberlites and their associated xenoliths. Journal of Geology, 85, 433 - 449.

Stephenson D. (1974). Mn and Ca enriched olivines from nepheline syenites. Lithos, 7, 35 - 41.

Stormer J.C.Jr.(1973). Ca zoning in olivine and its relationship to silica activity and pressure. Geochemica Cosmochemica Acta, 37, 1815 - 1821.

Warner R.D. and Luth W.C. (1973). Two-phase data for the join Monticellite ($CaMgSiO_4$) - Forsterite (Mg_2SiO_4); Experimental results and numerical analysis. American Mineralogist, 58, 998 - 1008.

Watson E.B. (1979). Calcium content of forsterite co-existing with silicate liquid in the system Na_2O-CaO-MgO-Al_2O_3-SiO_2. American Mineralogist, 64, 824 - 829.

Watson K.D., Bruce G.S.W. and Halladay L.B. (1978). Kimberlitic dyke in Keith township, Ontario. Canadian Mineralogist, 16, 97 - 102.

Wedepohl K.H. and Muramatsu Y. (1979). The chemical composition of kimberlites compared with the average composition of three basaltic magma types. Proceedings of the 2nd International Kimberlite Conference, 1, 300 - 312

Williams A.F. (1932). The Genesis of the Diamond. 2 vols. E. Benn. London.

Wyatt B. (1979). Manganoan ilmenite from the Premier Kimberlite. Kimberlite Symposium II, Cambridge. Abstracts.

Wyllie P.J. (1979). Compositions of liquids and vapours in the regions of kimberlite magma generation and crystallisation. Kimberlite Symposium II, Cambridge. Abstracts.